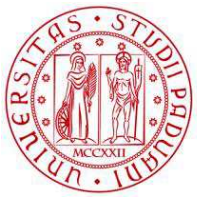

UNIVERSITÀ
DEGLI STUDI
DI PADOVA

Sede Amministrativa: Università degli Studi di Padova
Dipartimento di Salute della Donna e del Bambino

CORSO DI DOTTORATO DI RICERCA IN:
Medicina dello Sviluppo e Scienze della Programmazione Sanitaria
CURRICULUM: Emato-oncologia, Genetica, Malattie rare e Medicina predittiva
CICLO 29°

Deregulated FGF signaling substantially contributes to early osteogenic defects in Mucopolysaccharidosis type II

Alterazioni nella regolazione della via di segnale FGF contribuiscono allo sviluppo dei difetti osteogenici precoci nella Mucopolisaccaridosi di tipo II

Coordinatore: Ch.mo Prof. Carlo Giaquinto

Supervisore: Ch.mo Prof. Maurizio Scarpa

Dottorando: Dott.ssa Stefania Bellesso

TABLE OF CONTENT

ABSTRACT

FGF signaling is a key pathway strictly involved in many stages of ossification and gain of function mutations of many FGF pathway components have been associated with bone diseases like craniosynostosis and chondrodysplasia. The fine-tuning of the FGF signaling pathway is achieved at different levels, both intracellularly and by extracellular glycosaminoglycans (GAGs), which play a critical role in ligand and receptor binding. In this work, I show that the deficiency of iduronate 2-sulfatase (IDS), which is involved in GAGs catabolism, perturbs FGF signaling leading to early bone defects before the onset of evident massive GAGs storage.

A defective IDS activity causes a rare lysosomal storage disease called Mucopolysaccharidosis type II, in which skeletal abnormalities represent one of the major disabling aspects. Enzyme replacement therapy (ERT) is the currently available therapeutic option, which, however, suffer from limited efficacy.

To better elucidate early alterations of bone development occurring in MPSII, I took advantage of the zebrafish model, given its easy genetic manipulation and the evolutionary conserved mechanisms and signaling pathways regulating bone formation. In particular, I generated zebrafish models for MPSII, using a morpholino-based knock down technology and CRISPR/Cas9 technique, respectively. Using different approaches, including *in situ* hybridization and transgenesis, I demonstrated that the altered IDS function affects the expression of key FGF signaling markers and bone differentiation markers at early life stages, before any massive glycosaminoglycans accumulation is detectable.

The involvement of the FGF signaling downstream to the IDS loss of function was also detected in cranial and appendicular bones of IDS knockout mice and in Hunter patient fibroblasts. Therefore, the results of this study suggest that in MPSII an early FGF signaling impairment, due to IDS deficit, may cause a dysregulated expression of genes involved in bone development before the occurrence of lysosomal GAGs accumulation.

RIASSUNTO

La via di segnale FGF è una importante *pathway* coinvolta in diverse fasi dell'osteogenesi e mutazioni che colpiscono componenti di questa via sono associate a diverse malattie umane come le craniosinostosi e le condrodisplasie. La regolazione della via di segnale FGF avviene a diversi livelli, sia con meccanismi intracellulari che tramite l'interazione con i glicosaminoglicani (GAGs) presenti nella matrice extracellulare, i quali possiedono un ruolo critico nell'interazione fra ligando e recettore.

In questo lavoro viene dimostrato che alterazioni nella funzionalità dell'enzima iduronato 2-sulfatasi (IDS), coinvolto nel catabolismo dei GAGs, sono responsabili dell'alterazione della via di segnale FGF.

La mancata o deficitaria attività dell'enzima IDS è causa dell'insorgenza di una rara patologia da accumulo lisosomiale chiamata Mucopolisaccaridosi di tipo II, nella quale uno degli aspetti più disabilitanti è rappresentato da manifestazioni patologiche dell'apparato scheletrico. La terapia comunemente impiegata è la somministrazione dell'enzima ricombinante (Enzyme Replacement Therapy, ERT) che, pur determinando un miglioramento di una parte della sintomatologia, non risulta efficace, o comunque risulta scarsamente efficace, in distretti importanti come cuore e sistema scheletrico.

Per lo studio della patogenesi molecolare della MPSII e la comprensione dei meccanismi patogenetici che inducono alterazioni precoci nello sviluppo osseo, è stato utilizzato lo zebrafish come modello. Zebrafish risulta infatti un buon modello perché semplice da manipolare geneticamente; inoltre, in esso, il controllo delle principali vie di segnale che regolano il suo sviluppo osseo è altamente conservato.

Sono stati generati sia modelli transienti con l'utilizzo della tecnica oligo morfolino, sia un mutante stabile applicando il metodo Crispr/Cas9. Utilizzando diversi approcci sperimentali, comprese tecniche di ibridazione *in situ* e transgenesi, è stato dimostrato che la mancata funzionalità dell'IDS determina alterazioni nell'espressione di marcatori chiave della via di segnale FGF e della differenziazione ossea a stadi molto precoci, prima di un evidente accumulo di glicosaminoglicani nei tessuti.

L'alterazione di questa *pathway* è stata osservata anche in campioni di ossa craniche e appendicolari di topi IDS-KO e in fibroblasti di pazienti Hunter.

I risultati di questo studio suggeriscono dunque che nella MPSII disfunzioni dell'enzima IDS inducano, in fasi precoci, alterazioni nella regolazione della via di segnale FGF, che a loro volta possono essere responsabili dell'alterata espressione di geni coinvolti nello sviluppo osseo, prima che si verifichi l'accumulo dei GAGs nei lisosomi.

ABBREVIATIONS

4S: N-actylgalactosamine-4-sulfatase
ASA: Arylsulfatase A
B2M: beta-2-microglobulin
BGLAP: Bone Gamma-Carboxyglutamate Protein
BMPs: Bone morphogenic proteins
BSP: Bone sialoprotein
Cas: CRISPR associated proteins
CNS: Central nervous system
Col2: collagen II
ColX: collagen X
CRISPR: Clustered regularly interspaced short palindromic repeats
crRNA: CRISPR RNA
CS: chondroitin sulfate
dpf: days post fertilization
DS: dermatan sulfate
Dusp6: dual specificity phosphatase 6
ECM: Extracellular matrix
ENU: N-ethyl-N-nitrosourea
Erk: Extracellular signal-regulated kinase
ERM: ETS-related molecule
ERT: Enzyme Replacement Theraphy
FGE: FGly generating enzymes
FGF: Fibroblast growth factor
FGFr: Fibroblast growth factor receptor
FGly: Formyglycine
GAG: Glicosaminoglycan
GAPDH: glyceraldehyde-3-phosphate dehydrogenase
gRNA: guide RNA
HS: Heparan sulfate
HSCT: Hematopoietic Stem Cells Transplantation
ids: iduronate 2-sulfatase gene
IDS: Iduronate 2-sulfatase enzyme
IDSP1: iduronate 2-sulfatase pseudo gene
IHH: Indian hedgehog
IL1β: interluchine 1 β
ISH: *in situ* hybridization
KS: keratan sulfate
LSD: Lysosomal Storage Disorder
MAP: Mitogen-Activating Protein
MPS: Mucopolysaccharidosis
NCC: cranial neural crest
NHEJ: Non-Homologous End Joining
nls: nuclear localization signals
OCN: Osteocalcin

Osx: Osterix
PAM: Protospacer Adjacent Motif
Pea3: Polyoma enhanceractivator 3
PI3: Phosphoinositide 3
PLCγ: Phospholipase C gamma
PPR: Parathyroid hormone related peptide receptor
PTC: Patched
PTHrP: Parathyroid hormone related peptide
PTU: Phenylthiourea
Runx: Runt domain-containing transcription factor
SMO: Smoothened
Spry: Protein sprouty homolog
TNFα: tumor necrosis factor α
tracrRNA: transacting RNA
WT: wild type

1 INTRODUCTION

1.1 Lysosomal storage disorders

Lysosomal storage disorders (LSDs) are a family of hereditary diseases caused by abnormal accumulation of macromolecules into lysosomes, leading to impaired organelle homeostasis. More than 50 different LSDs have been classified and their overall incidence is almost 1 to 5000 live births (Wraith, 2011).

Most LSDs are inherited in an autosomal recessive way, while there are only three LSDs with an X-linked inheritance: Fabry disease, Danon disease and Mucopolysaccharidosis type II.

LSDs are due to different mutations occurring in genes encoding for lysosomal enzymes or proteins important in lysosomal biogenesis or trafficking. The loss of lysosomal protein function or enzymatic activity is responsible for a progressive accumulation of different kind of substrates (Boustany et al., 2013). Traditionally, LSDs are classified according to the type of substrate. However, in most lysosomal storage disorders the stored material can be heterogeneous (Ballabio et al., 2009).

LSDs are generally divided into:

-Sphingolipidoses

-Mucopolysaccharidoses

-Glycogen storage disease

-Oligosaccharidoses

-Integral membrane protein disorders.

Although lysosomal storage disorders can share common basic pathogenetic defects, among different LSDs there is a high phenotypic variability, depending on the different stored substrates, affected cell types and organ involvement.

All LSDs display a marked phenotypic heterogeneity, considering the onset of symptoms, which can be during pregnancy, at postnatal stages or in late adulthood. Also the progression is variable and patients affected by the same LSD or carrying the same disease-related-mutations can display very different disease manifestations (Wraith et al., 2011).

The most recurrent pathological alterations in LSDs are dimorphism, cardiac disease, hepatosplenomegaly, skeletal disease with dysostosis multiplex and neurological abnormalities.

1.2 Mucopolysaccharidosis

Mucopolysaccharidoses (MPSs) are an heterogeneous group of rare genetic disorders caused by the deficiency of specific lysosomal enzymes that are involved in the breakdown of glycosaminoglycans (GAGs) dermatan sulfate (DS), heparan sulfate (HS), keratan sulfate (KS), chondroitin sulfate (CS) or hyaluronan. In these disorders the direct effect of mutations occurring in lysosomal-related genes is the progressive accumulation of undegraded or partially degraded GAGs into the lysosomes. Glycosaminoglycans storage leads to progressive cell dysfunction, that in turn causes multiorgan and multisystem defects, thus reducing life expectancy.

There are eleven different types of MPSs that are categorized by the specific altered enzyme and the types of stored molecules (Table 1) and their overall incidence is 1 every 25.000 live births (Gökdoğan et al., 2016).

MPSII is the only mucopolysaccharidosis with an X-linked inheritance. The other mucopolysaccharidoses are inherited in an autosomal recessive manner and there are no differences in their frequency between males and females. All MPSs present with very different pathological features, which can be characterized by a variable degree of severity. However, some clinical features, such as musculo-skeletal alterations, are common to all MPSs.

Historically, the pathogenesis of MPSs has been attributed to the progressive intracellular accumulation of undegraded glycosaminoglycans, however it is now clear that more complex pathogenic mechanisms may contribute to the pathological manifestations.

MPS animal models show that the progressive worsening of symptoms is not associated with a progressive tissue GAGs accumulation. Furthermore, in MPSI mouse models it has been demonstrated that alterations in the skeletal development occur very early, before any histological change (Heppner et al., 2015).

Since glycosaminoglycans are involved in key cell regulations, such as signal transduction and growth factors sequestering, undegraded or partially degraded GAGs may lead to cellular homeostasis perturbations, thus deregulating important signaling pathways (Clarke et al., 2011).

Number	Eponym	Gene locus	Deficient enzyme	Storage product
I	Hurler/Scheie	4p16.3	α-L-iduronidare	Heparan sulfate / Dermatan sulfate
II	Hunter	Xq28	Iduronate 2-sulfatase	Heparan sulfate / Dermatan sulfate
III-A	Sanfilippo type A	17q25.3	Sulfamidase	Heparan sulfate
III-B	Sanfilippo type B	17q21	α-N-acetylglucosamidase	Heparan sulfate
III-C	Sanfilippo type C	8p11.1	Acetyl-CoA; α-glucosamidase N-acetyltransferase	Heparan sulfate
III-D	Sanfilippo type D	12q14	N-acetylglucosamidase 6-sulfatase	Heparan sulfate
IV-A	Morquio type A	16q24.3	Galactose 6-sulfatase	Keratan sulfate / Chondroitin sulfate
IV-B	Morquio type B	3p21.33	β-galactosidase	Keratan sulfate
VI	Maroteaux-Lamy	5q11-q13	Arylsulfatase B	Heparan sulfate / Dermatan sulfate
VII	Sly	7q21.11	β-glucuronidase	Heparan sulfate / Dermatan sulfate / Chondroitin sulfate
IX		3p21.3-p21.2	Hyaluronidase	Hyaluronan

Table 1: List of all MPS types with their eponym. For each Mucopolysaccaridosis is described the gene locus, the enzyme deficit and the storage product.

1.3 Mucopolysaccharidosis type II

Mucopolysaccharidosis type II, also called Hunter syndrome, is caused by the lack or deficiency of the lysosomal enzyme iduronate 2-sulfatase (IDS, EC 3.1.6.13). IDS is a glycosidase required for the hydrolysis of the 2-sulfate groups of L-iduronate 2-sulfate units, the first step of heparan sulfate and dermatan sulfate degradative pathway. The enzyme acts into the lysosomes and mutations altering its function lead to GAGs accumulation within the lysosomes in nearly all cell types.

The prevalence of this disease in Caucasian population ranges from 1:46.000 to 1:320.000 live births and it is twice higher in Ashkenazi and Sephardic Jews living in Israel (Chistiakov et al., 2014). Since MPSII follows an X-linked recessive inheritance, the vast majority of affected individuals are males. However, there are few cases of female patients. Most female cases of Hunter syndrome are due to an autosomal-X-chromosomal translocation or nonrandom X-chromosome inactivation (Morini et al., 2010).

Generally, it is possible to recognize 3 pathological phenotypes, according to the age of onset, disease severity and rate of progression:

Severe form: the disease has an early onset with a rapid symptom worsening and the diagnosis is usually completed at 3 years of age. Patients are affected by profound mental

retardation, early dysostosis multiplex, marked somatic changes and multi-organ involvement. They present a short life expectancy with death that occurs before 15 years of age, usually because of obstructive airway disease or cardiac failure.

Mild form: the disease has a late onset with delayed symptoms progression and diagnosis is usually completed around 10 years of age. Patients have mild or no mental retardation, stature is close to normal, while dysostosis and dysmorphism are only slowly progressive. Affected patients survive into adulthood with life expectancy of forty or fifty years and death may occur by cardiac failure.

Intermediate form: the disease has a late onset and slow progression. Patients present with a wide range of pathological manifestations, which lie between the mild and severe forms.

However, since MPSII is a very complex disease with high symptoms variability, there is no strict separation between the three forms and patients often show a continuum of pathological manifestations from the severe to the mild forms.

MPSII patients show impaired growth speed during their life, with an increased weight and height compared to unaffected controls at birth, from the first year onwards, the growth speed falls down and patients display a block in the development. There are no differences in the growth rate between patients with the severe and the mild forms and a short stature is the most typical feature in MPSII patients (Patel et al., 2015).

Patients appear normal at birth and the first clinical features emerge at 2 to 4 years of age and have a chronic progressive course. Lysosomal accumulation affects multiple organs and multiple systems with a wide range of pathological manifestations.

The clinical spectrum involves the following organs and tissues:

Central Nervous system (CNS): CNS involvement is a typical pathological feature of the severe forms and defines the neuronopathic type. Patients with CNS involvement present a progressive decline in intellectual functions with learning difficulties and a progressive neurological decline. Typical pathological manifestations are hydrocephalus, spinal cord compression, cerebral infarction and mental retardation (Al Sawaf et al., 2008).

Cardiovascular system: Heart dysfunction is a common feature in Hunter syndrome and is a contributing factor in the cause of death in both severe and mild forms. GAGs deposition in heart tissues leads to defects in cardiac structure that in turn causes the organ dysfunction.

Most patients show progressive valve thickening; other pathological manifestations include valvular regurgitation, valvular stenosis and cardiac hypertrophy (Lin et al., 2014).

Airway and respiratory: Airway obstruction and heart failure are the most common causes of death in MPSII, particularly in young patients (Giugliani et al., 2010).

GAGs accumulation in oropharyngeal and tracheo-bronchial tracts cause macroglossia, supraglottic narrowing and tracheomalacia. The respiratory system is also altered by pulmonary restriction due to the enlargement of internal organs and the rib cage rigidity, that generates riduced space for the lungs. Furthermore, respiratory alterations frequently induce some pathological complications, such as recurrent respiratory infections and sleep apnea (Wraith et al., 2008).

Sensory system: Patients present retinal dystrophy that causes defects in peripheral vision and poor dark adaptation. Other eye pathological features are papilledema and optic nerve atrophy. Hearing loss is also frequent and most patients exhibit recurrent otitis (Wraith et al., 2008).

Gastrointestinal: Storage of GAGs leads to increased organ size. In fact, hepatomegaly and splenomegaly are very common. Patients show protuberances of the abdomen due to umbilical and inguinal hernias.

Skeletal: Patients display several bone defects, including craniosynostosis, which will be deeply mentioned in the following paragraph.

1.4 Skeletal system alterations in Hunter syndrome

Skeletal abnormalities occur early in Hunter syndrome and are one of the main pathological features in all MPSs. Patients display defects in both endochondral and intramembranous ossification, that lead to a large spectrum of different pathological manifestations. Bones and cartilages in patients are characterized by altered growth and defects in shape and structure causing functional abnormalities (Clarke et al., 2015).

MPS patients show a characteristic pattern of bone alterations, called dysostosis multiplex, that can be detected with radiological analysis (Fig. 1).

The skull has an increased size and patients suffer from prematurely closed calvarial thickened sutures and a characteristic J-shape of the sella turcica. The ribs are thickened and assume a particular oar-like shape, which is characterized by an anterior enlargement and a posterior thinning. The clavicles have an altered shape, are short and broad. The spine shows dorsal kyphosis, hypoplasia of the lumbar vertebrae and some patients affected by the severe form also present with scoliosis. The pelvis has flaring of iliac wings, coxa-valga deformity and dysplastic femoral heads. The hands have a claw-like appearance, with bullet shaped phalanges and proximal pointing of metacarpals. Long

bones are short with enlarged diaphysis, altered epiphyseal centers and irregular metaphyseal appearance (Aldenhoven et al., 2009).

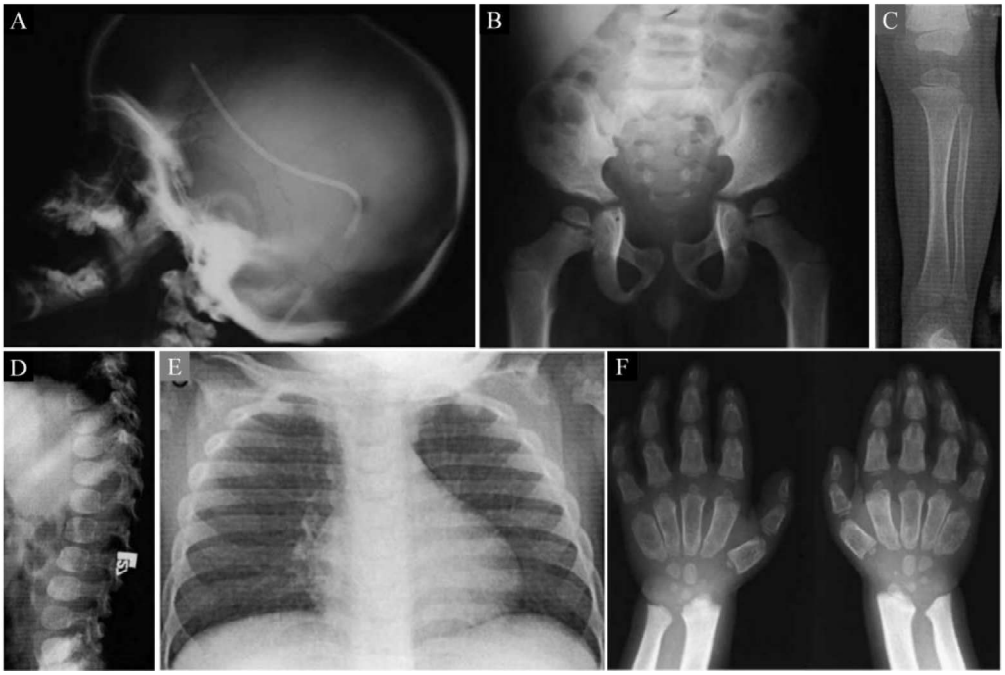

Figure 1: Dysostosis multiplex in Mucopolysaccharidosis type II. (A) Enlarged J-shaped sella turcica; (B) Pelvis is not well-formed and displays a small femoral head; (C) Diaphyseal thickening of lower extremity; (D) Lumbar spine with mild beacking of L1, L2 and L3; (E) Chest with calvarial thickening and oar-shaped ribs; (F) Irregular metaphyseal appearance. Images modified from (Muenzer et al., 2004) and (Morini et al., 2010).

Analysis in animal models for MPSs and in patients' samples show GAGs storage in all cells involved in ossification and bone remodeling: osteoblasts, osteoclasts and osteocytes (Polgreen et al., 2014). Glycosaminoglycans interact with several molecules involved in physiological and pathological processes, and their abnormally increased levels give rise to different cellular responses: metabolic, inflammatory and immunological. Inflammatory pathways are activated by the increased expression of IL-1 and TNFα cytokines, leading to altered processes in bone and cartilage development. These cytokines induce enzymes that degrade ECM components, stimulate osteoclastic bone resorption, inducing RANKL expression, and increase chondrocytes apoptosis (Fig. 2) (Opoka-Winiarska et al., 2013).

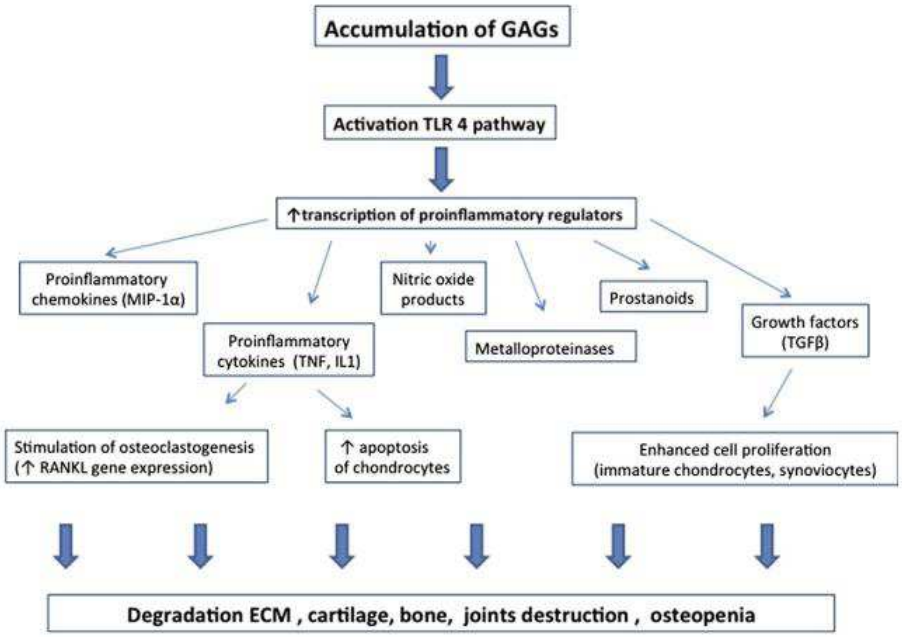

Figure 2: Metabolic inflammation in MPS diseases (Opoka-Winiarska et al., 2013).

1.5 Diagnosis and treatment

The first diagnosis is performed by clinicians that evaluate patient family history and symptoms. However, since Hunter syndrome is a rare disease and patients present a wide spectrum of different clinical presentations with variable severity, diagnosis is frequently misunderstood and delayed.

GAGs urinary assay is the first screening usually performed when an MPS disease is suspected. This assay is used to detect and quantify the stored glycosaminoglycans, but it does not give a definitive diagnosis. The final MPSII diagnosis is given by an enzymatic assay performed in leukocytes, fibroblasts or plasma, using an iduronate 2-sulfatase specific substrate. If there is a familial case of Hunter syndrome, it's possible to perform a prenatal diagnosis using the enzymatic assay in uncultured chorionic villi (Wraith et al., 2008).

The currently available therapies for MPSII are based upon Enzyme Replacement Therapy (ERT) and Hematopoietic Stem Cells Transplantation (HSCT).

ERT therapy consists in the weekly intravenous injection of an iduronate 2-sulfatase recombinant enzyme carrying high levels of Mannose 6-phosphate. Treated patients show a general reduction of GAGs amount in tissues and urine, a progressive normalization of the liver and spleen volumes and an improved respiratory function. However, the drug can't cross the blood-brain barrier, so it has no efficacy in the treatment of CNS-related

symptoms. There is also a limited drug delivery of the recombinant enzyme in the cardiac valves and hard tissues, such as bone.

HSCT is based upon the delivery of marrow-derived donor cells that provide a continuous source of secreted enzyme. Early administration of HSCT permits to block disease progression and improves some pathological features. HSCT is not able to recover Hunter syndrome-related bone abnormalities due to the limited enzymatic delivery in the skeletal-muscle tissue. Together with ERT or HSCT, patients have to be treated also with supportive symptomatic treatments to improve their life quality (Wraith et al., 2008).

The response to treatments depends on the disease severity and the age at which the treatment begins. It is now clear that the time in which therapies start is essential for the therapeutic outcome. If the treatment starts before or at the beginning of pathological manifestations, the therapy is extremely more successful. One of the main problems in therapies of MPS-related skeletal defects is that the treatment usually starts when an irreversible bone damage has already occurred, so the treatment can only slow the disease progression.

ERT and HSCT can reduce the burden of GAGs storage and slow down the progression of organ and tissue damage caused by the disease, but in some tissues, such as CNS and skeletal tissues, they are completely ineffective (Morini et al., 2010).

1.6 Genetics

Iduronate 2–sulfatase gene (*IDS)* maps to X chromosome, at Xq28.1. This gene spans approximatively 24kb and it contains nine exons and eight introns. It has been completely sequenced, leading to the characterization of the open reading frame composed of 1650bp and encoding for a 550 aminoacid protein.

A pseudogene (IDSP1), located at a distance of 20kb upstream of the 5' end of the active gene, has been identified. The pseudogene contains copies of exon 2, exon 3 and introns 2, 3 and 7 of the functional gene and it has 95% of similarity with the functional regions (Chistiakov et al., 2014).

More than 300 different disease-causing mutations have been identified, however genotype-phenotype correlation is still lacking. Most variants are point mutations in particular missense (44%), non-sense (10%) or splice-site alterations (9%). Small insertion/deletion represent 26% of all mutations, while the remaining 11% are large deletions, insertions, duplications or rearrangements between the *IDS* locus and the pseudogene (Lualdi et al., 2006).

Generally, full deletions and gross rearrangements have been associated with a severe clinical presentation, however, it has been described a case of a large deletion encompassing exons 2-4 that causes an intermediate form of the pathology (Bonuccelli et al., 1998). Patients displaying the mild form of MPSII, due to non-sense mutations very close to the N-terminal or frameshift mutations that produce a non active small polypeptide, have been identified (Kato et al., 2005). Patients, carrying other types of IDS gene mutations, have a variable spectrum of defects ranging from the severe to the mild forms.

However, in all patients the enzymatic activity assay, is unable to allow correlation between disease severity and enzymatic function .

1.7 Iduronate 2-sulfatase enzyme

IDS is a sulfatase that catalyzes the hydrolysis of sulfate ester bond in position 2 from the glycosaminoglycans heparan and dermatan sulfate. It is an housekeeping enzyme located into lysosomes, where it performs its optimal activity. IDS is synthesized as two precursor forms of 90kDa and 76kDa and successively modified with the adding of Mannose 6-Phosphate that targets the enzyme to the lysosomal compartment. IDS then undergoes to proteolytic cleavage and it's converted into a 45 to 42 kDa mature protein.

The enzyme hasn't been crystallized yet, but it shows approximatively 20% of homology with other enzymes of the sulfatase family. A structural model of the human IDS has been created using the homology with the crystal structure of human N-actylgalactosamine-4-sulfatase (4S) and Arylsulfatase A (ASA) (Fig. 3). This predicted tertiary structure has revealed that putative residues in the active site are Asp45, Asp46, Cys84, Lys135 and Asp334, which are also highly evolutionary conserved. One of the most important aminoacidic residue, located in the active site of the enzyme in humans, is the Cystein84, which is transformed into Formylglycine (FGly) residue by FGly generating enzymes (FGE) with a post translational oxidation (Sukegawa-Hayasaka et al., 2006).

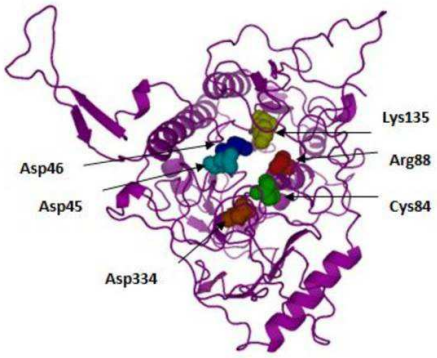

Figure 3: Tertiary structure model of Iduronate 2-sulfatase. The spheres indicates active site residues: Asp45, Asp46, Cys84, Arg88, Lys135 and Asp334 (Chkioua et al., 2011).

Human IDS has a high percent identity with the zebrafish (59,51%) and mouse (79,52%) orthologues. Zebrafish Ids is formed by 561 aminoacids and the active Cysteine residue is in the 78th aminoacidic position, while mouse IDS is composed of 552 aminoacids and the active Cysteine residue is in the 99th aminoacidic position.

Recently, it has been demonstrated that IDS, beyond its GAGs degradative role, may have other important molecular functions. It has been shown that zebrafish iduronate 2-sulfatase has an important role during early development (Moro et al., 2010). In particular, Ids deficiency causes in zebrafish an altered expression of important osteogenesis factors, such as Sox10, which is a marker of early differentiating neural crest precursors into chondroblasts. Moreover, in agreement with the same observations it has been shown that iduronate 2-sulfatase increases its expression during the transdifferentiation from mouse fibroblasts to osteoblasts (Mandal et al., 2013).

1.8 Lysosome

Lysosomes are the degradative organelles of the endosomal/lysosomal system that take part to endocytic, phagocytic and autophagic pathways. They mediate the internalization, recycling, transport and breakdown of cellular and extracellular components and facilitate the dissociation of receptors from their ligands.

Being one of the major homeostasis regulators, lysosomes are involved in many cellular processes: turnover of cellular components, recycling of cell membrane receptors, inactivation of pathogenic organisms, repair of plasma membrane and bone remodeling (Settembre et al., 2013).

Lysosomes are ubiquitously membrane-bound organelle with an acidic lumen of pH 4.5 and contain more than 60 different enzymes involved in the degradation of specific substrates. Lysosomes are delimited by a single-lipid bilayer membrane that is protected by a thick internal glycocalyx from the acidic environment of the lumen.

Extracellular materials reach the lysosomes through the endocytic pathway, whereas intracellular components enter the lysosomes through autophagy.

The endocytic pathway allows the internalization of extracellular molecules that need to be degraded into lysosomes through cell surface receptors or in the case of hydrophobic small molecules by passive diffusion. Digested materials and receptors can return to the cell membrane via the recycling endosomes (Appelqvist et al., 2013).

Lysosomes also participate in lysosomal exocytosis, that is a secretory pathway important for some processes such as immune responses, bone resorption, cell signaling and plasma membrane repair (Appelqvist et al., 2013).

1.9 Extracellular matrix

The extracellular matrix (ECM) is a highly dynamic structure surrounding cells and regulating many aspects of cell function. It's composed by a complex structure of collagens, proteoglycans, glycoproteins and elastin that bestow physical and biochemical ECM properties. It presents with a high level of organization with a well-defined quantity and distribution of structural components, which interact in a determinate manner to provide specific mechanical and physiological features (Tsang et al., 2010).

ECM is subjected to remodeling, to regulate different processes during development and maintain cell homeostasis. It has an intimate connection with cells and, through its constant remodeling, it modulates the transduction of signaling molecules that regulate differentiation, proliferation and cell death. The ECM regulation occurs by changes in its composition, and modification of its architecture (Lu et al., 2011). The following properties are characteristic of the extracellular matrix (Fig. 4) (Lu et al., 2011):

-Anchorage: through ECM, receptors can help to maintain cell polarity, tissue organization and cell function.

-Migration barrier: the ECM constitutes a barrier for migrating cells that could be more permissive by regulation of spatial and temporal ECM composition.

-Migrating track: ECM can promote cell movements, by influencing the direction of migration and providing force for the movement.

-Signal reservoir: ECM components can bind grow factors and ligands by assembling them in a limited space, creating a concentration gradient and simplifying their interaction with receptors.

-Low affinity coreceptor: ECM components can enhance the interaction between receptors and ligands. For example, heparan sulfate is necessary for the dimerization and activation of FGF receptor after the binding with FGF ligands.

-Signal presenter: ECM components can participate in signal transduction acting as endogenous grow factors and activating directly the signaling.

-Biochemical force: the matrix can change its biochemical properties by determining cell behavior and regulating the development. ECM rigidity or stiffness can influence cellular differentiation and stem cell lineage specification.

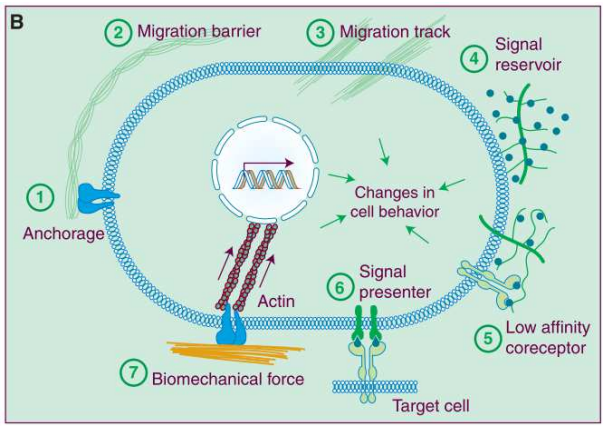

Figure 4: Representation of all the functional and structural properties of the extracellular matrix. The image is taken from (Lu et al., 2011).

1.10 Development of vertebrate skeleton

Bone development is a temporally and spatially regulated complex process based upon the expression of extracellular matrix components, transcription factors, growth factors and hormones.

The first event is the condensation and differentiation of mesenchymal progenitor cells from neural crest cells, that give rise to the craniofacial skeleton, and from the lateral plate of mesoderm, that gives rise to appendicular skeleton (Aszódi et al., 2000).

There are two bone developmental mechanisms: intramembranous ossification and endochondral ossification.

During intramembranous ossification, mesenchymal stem cells differentiate directly into osteoblasts and lead to the development of skull flat bones and most of the facial skeleton.

By endochondral ossification, mesenchymal progenitor cells generate a cartilaginous template that is progressively replaced by bone and gives rise to long bones, vertebrae and ribs. The initial cartilage is avascular and it is composed of chondrocytes, while at the periphery there are proliferating cells that form the perichondrium. Chondrocytes differentiate into hypertrophic chondrocytes that are surrounded by mineralized matrix produced by osteoblasts derived from perichondrium osteoprogenitor cells. In this phase

blood vessel invade the region and the growing capillaries transport mesenchymal cells that differentiate into osteoblasts and chondroclasts (Aszódi et al., 2000).

Long bones are characterized by a primary ossification center in the diaphysis, a secondary ossification center in the epiphysis and a growth plate between diaphysis and epiphysis that regulates the longitudinal growth. The growth plate is divided in a chondrocytes-rich reserve zone, a proliferative zone, pre-hypertrophic zone and hypertrophic zone (Fig. 5) (Aszódi et al., 2000).

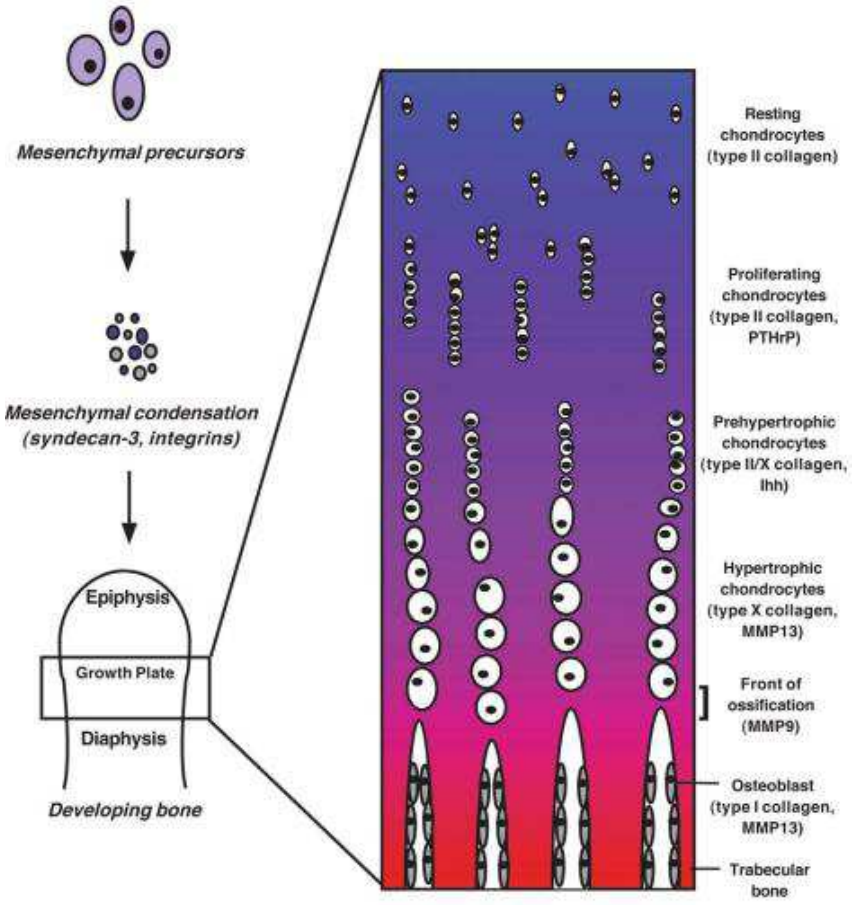

Figure 5: Endochondral ossification, growth plate composition and molecules synthesized in different bone developmental stages. (Behonick et al., 2003)

The different phases of intramembranous and endochondral ossification are characterized by typical changes in matrix composition. Cartilage cells, chondroblasts and chondrocytes, synthesize collagen fibrils of Collagen type II, type IX and type XI. The differentiation of chondrocyte cells is marked by different collagen elements and hypertrophic chondrocytes produce Collagen X that is involved in matrix mineralization. Early differentiated osteoblasts are characterized by the expression of Runt domain-containing transcription factor (Runx2), while at the end of differentiation these cells produce also Osterix (Osx or sp7), which is regulated by Runx2. Fully differentiate

osteoblasts express Osteocalcin (OCN or BGLAP) and Bone sialoprotein (BSP) (Harada & Rodan, 2003).

1.11 FGF signaling

Fibroblast growth factor (FGF) signaling is a crucial pathway required during development, but also to maintain cell homeostasis in adult organs. It is involved in multiple processes such as proliferation, differentiation, cell migration, angiogenesis, morphogenesis and regulation of metabolism.

The FGF family in humans is formed by 18 FGF ligands and 4 FGF receptors (FGFr).

FGF receptors are composed by a single peptide chain which carries a glycosylated extracellular ligand binding domain, a transmembrane domain and a cytoplasmic portion with tyrosine kinase activity. The extracellular chain has IgG-like domains that selectively bind heparan sulfate and FGFs, giving to each receptors the ability to link a unique subset of ligands.

FGF ligands have a conserved hydrophobic patch that interacts with FGF receptors (FGFr) and a unique heparan sulfate binding surface that differs among FGFs and gives their binding specificity (Mckeehan et al., 2009). Heparan sulfate specific interaction with FGF ligands permits to control the location and the trafficking of FGFs, provides the specificity of FGFs/receptors binding and regulates ligands lifetime and stability by protecting FGFs against proteinases. Extracellular matrix and tissue architecture have an important role in the regulation of FGF signaling activation (Mckeehan et al., 2009).

Crystallographic analysis has shown that the ternary complex, composed by FGFr-FGF-HS, recruits a second ternary complex forming a dimer with the stoichiometry of 2 FGFr-2 FGF- 2 HS. The dimerization is necessary for the transphosphorylation and activation of intracellular receptor kinases and the downstream pathways.

FGF signaling is associated with different downstream pathways, including RAS/mitogen-activating protein (MAP) kinase pathway, phosphoinositide 3 (PI3) kinase/AKT pathway and phospholipase C gamma (PLCγ) pathway (Fig. 6A). After the binding of FGF ligands to the receptor, there is a phosphorylation of tyrosine residues in the FGFr cytosplasmic domain and the consequent interaction of adaptor proteins associated with the signaling, that form a complex required for the activation of RAS/MAP kinase and PI3 kinase/AKT pathways. RAS/MAP kinase is implicated in cell differentiation and proliferation, while PI3 kinase/AKT pathway is associated with cellular survival, cell polarity and cell fate determination. The PLCγ pathway is activated

by the direct binding of PLCγ molecules to a phosphorylated tyrosine of the receptor and it controls cell morphology, adhesion and migration (Teven et al., 2014) (Fig. 6 A).
The negative regulation of the signaling occurs with the internalization and degradation of the FGF receptor or with the activation of MAPK phosphatases. The phosphatases Sprouty, Sef and Dusp6 are directly regulated by FGF signaling through a feedback autoinhibitory way and they block MAP kinase pathway activity. Sprouty and Sef proteins suppress RAS/MAP signaling at multiple levels within the pathway, while Dusp6 acts only by dephosphorylating ERK (Teven et al., 2014) (Fig. 6 B). All these regulators have an important control role in the spatio-temporal expression, intensity and duration of FGF signaling, that are essential factors in normal development and diseases.

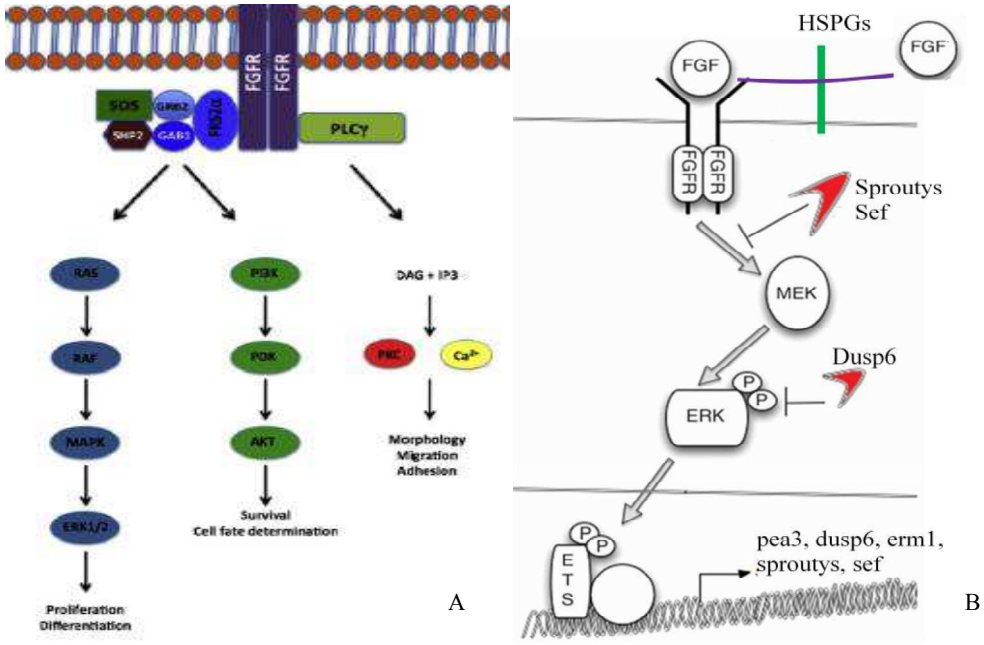

Figure 6: (A) FGF signaling downstream pathways, image modified from (Teven et al., 2014) (B) Schematic FGF/RAS/MAPK pathway showing Sproutys, Sef and Dusp6 blocking roles. Image modified from (Molina et al., 2009).

FGF signaling controls many embryonic and postnatal stages of skeletal development. It's involved in both intramembranous and endochondral ossification (Fig. 7) and mutations altering the FGF pathway activity cause different bone pathologies, such as chondrodysplasia and craniosynostosis (Ornitz et al., 2002). FGF ligands and receptors expression are strictly spatially and temporally regulated in bone and cartilage development. It has been shown that low FGF signaling activity is associated with proliferation, while enhanced pathway leads to cell differentiation and apoptosis (Ornitz et al., 2002). Then, by interacting with other cellular pathways, FGF signaling controls each step of the chondrogenic and osteogenic pathways. Moreover, it orchestrates the

balance among cell growth, differentiation and apoptosis, leading to the correct bone and cartilage morphogenesis (Ornitz et al., 2002).

FGF signaling has been found to activate the expression of important bone transcription factors, such as Runx2 and Osterix and bone matrix-related genes, such as Collagen1 (Felberet et al., 2015).

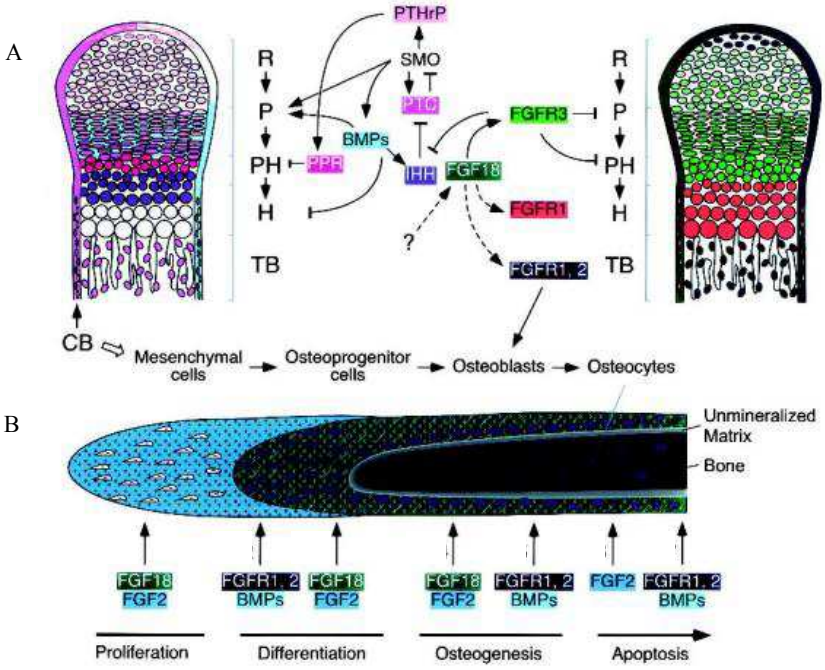

Figure 7: Regulatory pathways in endochondrial (A) and intramembranous (B) ossification. FGF signaling is involved in many stages: reserve (R), proliferating (P), prehypertrophic (PH) and hypertrophic (H) stages in chondrocytes progress; proliferation, differentiation, osteogenesis and apoptosis stages of osteoblasts maturation. Other signaling pathways are involved and interact with FGF signaling: Indian hedgehog (IHH), patched (PTC), smoothened (SMO), bone morphogenic proteins (BMPs), parathyroid hormone related peptide (PTHrP) and PTHrP receptor (PPR). Image modified from (Ornitz et al., 2002).

1.12 Zebrafish as animal model

Mouse models are the most frequently used biological tools for the study of human disorders, because they offer many advantages over other animal models, such as a high degree of protein sequence homology to human proteins and anatomical and physiological similarity with humans. However, given the complexity of generating mouse models for target diseases and for their performing molecular analysis, alternative animal models have been exploited by researchers in the past decades.

A recently largely used organism for the analysis of human diseases is the vertebrate *Danio rerio*, also called Zebrafish. It's a small teleost isolated from the Gange river,

which has been used from the 1930s as a vertebrate model for studies of developmental biology and embryogenesis.

In the last years, zebrafish has been also used for the analysis of pathogenic mechanisms of many human diseases and studies of drugs efficacy.

This organism has a small size: its length reaches 4cm in adults and 2mm in embryos, so it's possible to breed a high number of fish in tanks. A couple of zebrafish can produce up to 300 eggs in a week, enabling to perform large-scale studies in a short time.

Unlike mouse, zebrafish fertilization and embryonic development occurs externally, allowing their ease manipulation and direct observation. Furthermore it's possible to follow organ development using an optical microscope since zebrafish embryos are optically transparent. By adding phenylthiourea (PTU) to the fish water the pigmentation can be blocked and zebrafish are kept transparent also at late life stages.

Bioinformatics studies have detected a great similarity between the *Danio rerio* genome and the human one with a significant synteny among conserved genes. Zebrafish genome has been almost entirely sequenced and recent analysis have demonstrated that zebrafish has a diploid genome, with many genes that underwent duplication events during evolution (Lieschke et al., 2007).

The development of several techniques of forward and reverse genetics has amplified the possibility of using zebrafish as animal model. In the past decades forward genetic techniques, such as insertional retroviral mutagenesis and chemical mutagenesis with the use of N-ethyl-N-nitrosourea (ENU), have allowed to collect thousands of zebrafish mutants.

Among the different reverse genetic techniques a widely applied technology is the microinjection of antisense morpholinos, that induce a temporal block of gene transduction or interfere with transcript splicing, and the site-directed mutagenesis (Lieschke et al., 2007).

Transgenic zebrafish line expressing fluorescent proteins under the control of tissue-specific promoters or signaling-specific promoter elements, have permitted to follow *in vivo* the development of tissues and organs and to identify key signaling pathways involved in physiological processes (Hammond & Moro, 2012).

1.13 Zebrafish as model for bone diseases

Zebrafish has been also recently used as model to study bone development and ossification defects.

It shares similar developmental mechanisms in skeletal morphogenesis and bone cell types with higher vertebrates. However, fish bones are located in simple spatial patterns and they are composed of a small number of cells. Zebrafish bone mineralization starts already at 3dpf in the cephalic regions and when compared to higher vertebrates, craniofacial bones develop in a similar way (Fig. 8). Many of the molecular mechanisms controlling early stages of bone development are evolutionary conserved, including gene regulatory networks that regulate osteogenesis (Mackay et al., 2013). The zebrafish craniofacial skeleton contains bones that have both dermal and chondral origins, which arise from neural crest or mesodermal progenitor cells.

The external fertilization and the optical transparency, permit to completely follow the development of osteogenic and chondrogenic specific cells. Furthermore, by using fluorescent transgenic reporter lines marking different skeletal lineages, it's possible to image in real time bone formation. It is also possible to track *in vivo* bone matrix formation using particular dyes that bind to mineralized tissue, such as Alizarin red or calcein (Hammond & Moro, 2012).

Zebrafish can be used to study pathogenic mechanisms of bone-related disorders arising from very early stages of bone and cartilage development. To perform this task, more recently, different biosensor transgenic reporter fish for the main cell signaling pathways have been generated (Hammond & Moro, 2012).

A large-scale forward genetic screening has permitted to identify new gene functions important for bone formation and several mutant zebrafish lines have been characterized and correlated with human bone pathologies, such as osteogenesis imperfecta and craniosynostosis (Mackay et al., 2013).

Zebrafish have been studied also as model for lysosomal storage disorders with the generation of a mutant for Mucolipidosis II (Flanagan-Steet et al., 2009).

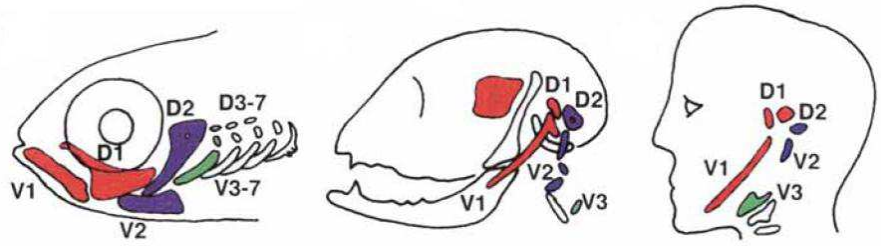

Figure 8: Schematic picture showing the structural of skeletal elements of zebrafish, mouse and human. D1: palatoquadrate (zebrafish) - incus (mouse and human); V1: Meckel's cartilage; D2: hyosymplectic (zebrafish) - stapes (mouse and human); V2: ceratohyal (zebrafish) - Reichert's cartilage (mouse and human); V3: ceratobranchial (zebrafish) - styloid bone (mouse and human). Modified from Schilling et al.,1997 (Schilling et al., 1997).

1.14 Animal models for Mucopolysaccharidosis type II

Spontaneous canine and feline animal models have been used to study new therapeutic strategies for mucopolysaccharidosis type II. However, the size and the lifespan of these models hamper the characterization of the disease. For this reason, a mouse model for Hunter syndrome has been generated few years ago (Garcia et al., 2007), harboring a large deletion of exon 4 and part of exon 5 in the iduronate 2-sulfatase gene, leading to the synthesis of a non-functional IDS enzyme.

IDS-KO mice have no pathological manifestations at birth, but develop typical MPSII manifestations over time, such as GAGs accumulation in tissues from 7 weeks (Fig. 9 A-B), increased organs size and elevated urine GAGs excretion from 4 weeks (Garcia et al., 2007).

The first macroscopically evident manifestations are visible by 8 months of age, when all mutant mice show broadened snout and abnormal skull development.

Radiological analysis in IDS-KO mice display sclerosis and enlargement of the skull bones from 4 weeks of age and appendicular bone enlargement from 10-13 weeks. The severity of skeletal defects is progressive and mutant mice show skull enlargement (Fig. 9 C), thickened long bones in the hind limbs, ribs and vertebrae, and an overall increased bone density (Fig. 9 D-E) compared with age-matched WT mice (Garcia et al., 2007).

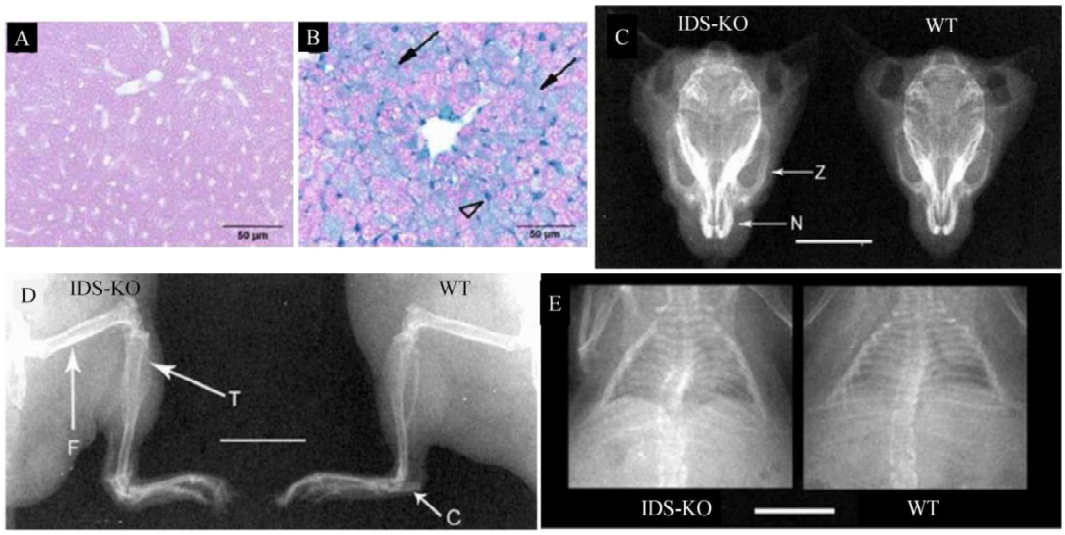

Figure 9: (A-B) Representative examples of Alcian blue staining and GAG accumulation in liver sample from 20 weeks old wild-type (A) and IDS-KO (B) mice. (C-E) Radiographs of an IdS-KO (age 57 weeks) and a wild-type mice (age 53 weeks) showing the head (C), hind limbs (B) and torso (C). IDS-KO mice display thickened bones of the skull, ribs and hind limb and the overall increased radio-opacity (bone density). Scale (white bar)=1 cm. Z, zygomatic bone; N, nasal bone; T, tibia; F, femur; C, calcaneus bone. Images modified from (Garcia et al., 2007).

An alternative vertebrate model for MPSII has been generated by using the morpholino technology in zebrafish. The reduced Ids activity detected in zebrafish morphants is associated with early development defects, such as altered migration and differentiation of neural crest cells into chondroblasts (Moro et al.,2010). Moreover zebrafish morphants display impaired development and altered facial cartilage morphogenesis (Fig. 10). These pathological manifestations have been shown to be related to increased TGFβ signaling that in turn upregulates mesodermal genes expression (Moro et al., 2010).

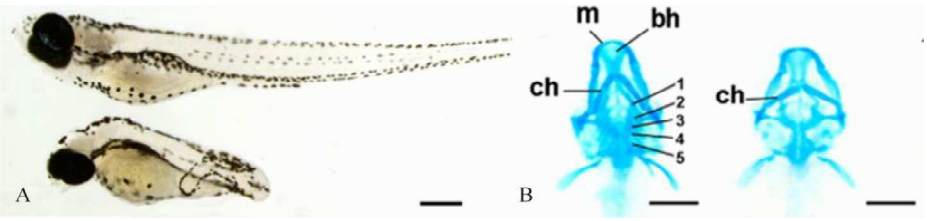

Figure 10: (A) Representative images of a WT embryo (top) and an Ids morphant (bottom) at 5dpf. (B) Abnormal head cartilage morphogenesis in Ids morphant (on the right) compared to WT (on the left) at 5dpf. ch:ceratohyal, m:Meckel's cartilage, bh:basihyal, 1-2-3-4-5:branchial arches. Images modified from (Moro et al., 2010)

2 METHODS

2.1 ZEBRAFISH

2.1.1 Zebrafish husbandry

All procedures involving fish husbandry and manipulation were evaluated and accepted by the Local Ethical Committee of the University of Padova.
All mating procedures were carried out at the Fish Facility in the Department of Biology of the University of Padova.
Larvae were kept for the first five days in Petri dishes, then maintained at 28°C for the following stages in 5 liters tanks filled with fish water at neutral pH.

2.1.2 Injection

For the microinjection experiments, the DNA constructs of interest were resuspended in Danieau buffer (8 mM NaCl, 0,7 mM KCl, 0,4 mM $MgSO_4$, 0,6 mM $Ca(NO_3)$, 2,5 mM HEPES, pH 7.6) and Red Phenol (Sigma, Milan, Italy) at the working concentration. All solutions were injected into one cell-stage embryos, using a light microscope and a microinjection apparatus.

2.1.3 Oligo Morpholino

Morpholino is a synthetic oligo of 25bp, designed to target a specific mRNA. This oligo recognizes and binds the target sequence, blocking mRNA translation or interfering with mRNA maturation by a direct binding to a specific splicing site.
Two different types of oligo morpholino were used:
-Translation blocking: The oligo is synthesized to bind a region near the ATG codon, sterically blocking the translation initiation complex and therefore knocking down protein expression. The ATG morpholino can block the translation of both maternal and zygotic transcripts.
-Splicing site blocking: The morpholino recognizes a splicing site on the pre-mRNA, modifying the normal splicing event. This oligo can target zygotic transcripts processing.
These synthetic oligos are modified when compared to normal nucleic acid sequences. They carry morpholino rings instead of deoxyribose sugar moieties and non-ionic phosphorodiamidate linkages replacing the anionic phosphates. Their modified structure

enables them to be nuclease-resistant and stable inside the cells. Moreover, they have been shown non-immunogenic and able to trigger enzymatic or signaling proteins response. Although the high resistance, each designed morpholino remains stable and active only for five to six days into cells before being degraded.

I have designed and used two different morpholinos: one against the ATG sequence (Ids start morpholino) and the other targeting a splicing donor site (Ids splicing morpholino) (Table 2 and 3). All experimental results obtained in morphants were compared with those from fish injected with control mismatch morpholinos, carrying a mismatched sequence and unable to recognize the target mRNAs (Ids splicing morpholino CONTROL and Ids start morpholino CONTROL) (Table 2).

Oligo name	Antisense sequence
Ids splicing morpholino	AATTATGCACGCGTCATACCAGGAT
Ids splicing morpholino CONTROL	AATAATCCACCCGTCATACGACGAT
Ids start morpholino	GTAAATACGAGCATTACATTCATTG
Ids start morpholino CONTROL	GTTAATACCAGGATTAGATTGATTG

Table 2: Sequences of the different morpholino used in the experimental procedures.

All morpholinos were purchased from Genetools (Philomath, OR, USA) and the stock solutions were resuspended in DNase/RNase free water in a final concentration of 300nM.

Several injection experiments have been performed in to choose the best morpholinos' concentration.

For Ids translation blocking morpholino, 3 different concentrations have been tested: 1ng/µl, 1,25ng/µl and 1,5ng/µl. Analyzing morphants' mortality and phenotypes, the 1,25ng/µl concentration was chosen, in agreement with a previous experimental set-up (Moro et al., 2010). To confirm the efficacy of the tested morpholino, Western blot analysis were performed using protein extracts from morphants and control larvae

The Ids splicing-blocking morpholino is designed to a target exon2 - intron2 donor splice site (Table 3). Five different concentrations were tested: 0,5ng/µl, 1ng/µl, 1,5ng/µl, 2ng/µl and 2,5ng/µl. By RT-PCR I amplified the region surrounding the splicing donor site (Table 4). Gel electrophoresis of the amplified region showed that in morphants there was a decrease in the intensity of the expected amplicon, and the appearance of lower weight bands, when compared to mismatch control sample (Fig. 11 and 12). Sequencing analysis of the fragment with highest molecular weight (Fig. 12 arrow) showed that the morpholino produced a deletion of 22bp between exon2 and exon3 (Fig. 13), creating a premature stop codon and the formation of a truncated 172 aminoacids protein (Fig. 14).

According to the sequencing profile of the low weight bands, I could conclude that the Ids splicing morpholino caused an alternative splicing, and triggered a nonsense-mediated

decay of the transcripts. Best results have been obtained with the 2,5ng/µl morpholino concentration and, therefore, all experimental procedures involving the splicing morpholino were done at the chosen optimal concentration.

	GGAATTCTCTAAACAGCATAAAACAAACATGTGAAAGAAGTATCTGAA ACGAAACCGCGCAACACA
Exon 1	ATGAATGTAATGTTCGTATTTACGTGTTGGTGGTTTGTTTTTATTTTTC ACCTTTTGGGGCGAGATGTTTTTGCAGCAAAAAGCAAAGATTTCAACGT TTTGTATTTAATTGCTGACGATCTGAGACCATCTTTAGGCTGTTATTCTG ATCCAGTGGTCAAATCACCGAACATCGATCAGCTTGCATCTTTGAGCGT AGTGTTTCATAACGCATATGCCCAG
Intron 1	GTATGTTGTATTAATGCTCATGGAA.....TATATTACAATGTGTTCTTTC AAAG
Exon2	CAAGCTGTTTGTGGACCTAGTAGAGTGTCTTTCCTAACAAGTCGAAGAC CAGACACCACAAAACTCTACGATTTCAACTCATACTGGAGAGTTCATGC TGGAAACTACACCACACTACCTCAATACTTCAAGTCTAATGGATACACC ACTTTATCAGTGGGCAAAGTCTTCCATCCTG
Intron2	GTATGACGCGTGCATAATTTTCACG.....TCTCTTTCACGTGCTTGTCC TCAAG
Exon3	GCATTGCCTCCAACCACTCGGATGATTACCCGTACAGCTGGTCTGTACC GCCGTATCATCCACCCTCTTTTGAATATGAAAAGAGGAAG

Table 3: Iduronate 2-sulfatase sequence of Exon 1-2-3 and Intron 1-2. In green the sequence targeted by the IDS start morpholino. In red the sequence targeted by the Ids splicing morpholino and in blue the splicing donor site. RefSeq NM_001080068

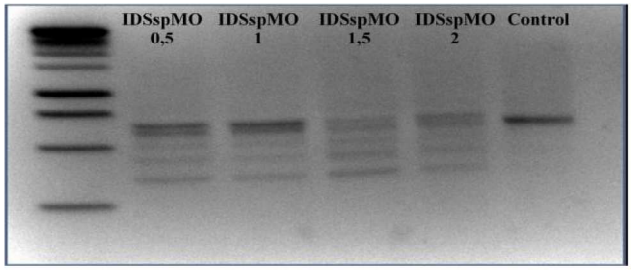

Figure 11: Gel electrophoresis showing the amplicons produced by Ids splicing morpholino at 0,5ng/µl, 1ng/µl, 1,5ng/µl and 2ng/µl concentration. Note the multiple bands in morphant extracts and the single band in the control sample.

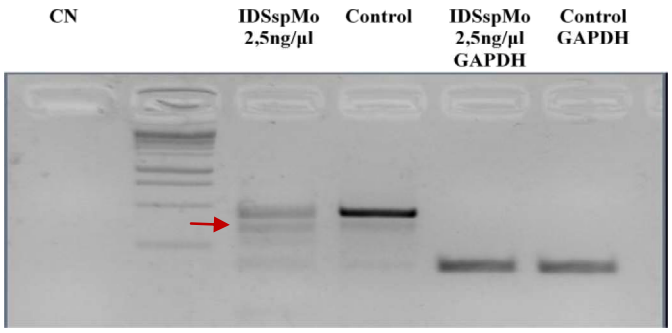

Figure 12: Gelelectrophoresis showing the amplicon produced by Ids splicing morpholino at 2,5ng/µl concentration As internal control the housekeeping GAPDH was amplified in the same sample. Note the lower amount of *ids* transcripts when compared with the control sample. The arrow shows the sequenced fragment.

Primer's name	Primer	RefSeq
External *ids* For	TCGTATTTACGTGTTGGTGGT	NM_001080068
External *ids* Rev	CCCTTCATAGAGCGCAAGAG	NM_001080068
Inner *ids* For	GCTTGCATCTTTGAGCGTAGT	NM_001080068
Inner *ids* Rev	CCCTTCATAGAGCGCAAGAG	NM_001080068
GAPDH For	GTGGAGTCTACTGGTGTCTTC	NM_001115114
GAPDH Rev	GTGCAGGAGGCATTGCTTACA	NM_001115114

Table 4: Primers' sequences used for PCR analyses

ATGAATGTAATGTTCGTATTTACGTGTTGGTGGTTTGTTTTTATTTTTCAC
CTTTTGGGGCGAGATGTTTTTGCAGCAAAAAGCAAAGATTTCAACGTTTT
GTATTTAATTGCTGACGATCTGAGACCATCTTTAGGCTGTTATTCTGATC
CAGTGGTCAAATCACCGAACATCGATCAGCTTGCATCTTTGAGCGTAGTG
TTTCATAACGCATATGCCCAGCAAGCTGTTTGTGGACCTAGTAGAGTGTC
TTTCCTAACAAGTCGAAGACCAGACACCACAAAACTCTACGATTTCAAC
TCATACTGGAGAGTTCATGCTGGAAACTACACCACACTACCTCAATACTT
CAAGTCTAATGGATACACCACTTTATCAGTGGGCAAAGTCTTCCATCCTG
GCATTGCCTCCAACCACTCGGATGATTACCCGTACAGCTGGTCTGTACCG
CCGTATCATCCACCCTCTTTTGAATATGAAAAGAGGAAGGTTTGCAAAG
ATAAAGACGGCACGTTGCACAGTAACCTGCTGTGTCCCGTGAACGTGTC
TGAAATGCCTCTAGGAACCCTTCCTGACATGGAGAACACAGAGGAGGCC
ATTCGACTCTTGCGCTCTATGAAGGGCTCACAAAAACCATTCTTCCTGGC
TGTCGGCTTCTATAAACCTCATATTCCTTTCAGAATCCCACAG

Exon 1
Exon 2
Exon 3
Exon 4

Figure 13: Iduronate 2-sulfatase cDNA sequence of exon 1-2-3-4. In yellow the 22bp deletion produced by Ids splicing morpholino.

```
  1   M  N  V  M  F  V  F  T  C  W  W  F  V  F  I  F  H  L  L  G
  1 aaATGAATGTAATGTTCGTATTTACGTGTTGGTGGTTTGTTTTTATTTTTCACCTTTTGG
 21   R  D  V  F  A  A  K  S  K  D  F  N  V  L  Y  L  I  A  D  D
 61 GGCGAGATGTTTTTGCAGCAAAAAGCAAAGATTTCAACGTTTTGTATTTAATTGCTGACG
 41   L  R  P  S  L  G  C  Y  S  D  P  V  V  K  S  P  N  I  D  Q
121 ATCTGAGACCATCTTTAGGCTGTTATTCTGATCCAGTGGTCAAATCACCGAACATCGATC
 61   L  A  S  L  S  V  V  F  H  N  A  Y  A  Q  Q  A  V  C  G  P
181 AGCTTGCATCTTTGAGCGTAGTGTTTCATAACGCATATGCCCAGCAAGCTGTTTGTGGAC
 81   S  R  V  S  F  L  T  S  R  R  P  D  T  T  K  L  Y  D  F  N
241 CTAGTAGAGTGTCTTTCCTAACAAGTCGAAGACCAGACACCACAAAACTCTACGATTTCA
101   S  Y  W  R  V  H  A  G  N  Y  T  T  L  P  Q  Y  F  K  S  N
301 ACTCATACTGGAGAGTTCATGCTGGAAACTACACCACACTACCTCAATACTTCAAGTCTA
121   G  Y  T  T  L  S  A  L  P  P  T  T  R  M  I  T  R  T  A  G
361 ATGGATACACCACTTTATCAGCATTGCCTCCAACCACTCGGATGATTACCCGTACAGCTG
141   L  Y  R  R  I  I  H  P  L  L  N  M  K  R  G  R  F  A  K  I
421 GTCTGTACCGCCGTATCATCCACCCTCTTTTGAATATGAAAAGAGGAAGGTTTGCAAAGA
161   K  T  A  R  C  T  V  T  C  C  V  P  *  T  C  L  K  C  L  *
481 TAAAGACGGCACGTTGCACAGTAACCTGCTGTGTCCCGTGAACGTGTCTGAAATGCCTCT
181   E  P  F  L  T  W  R  T  Q  R  R  P  F  D  S  C  A  L  *  R
```

Figure 14: Prediction of Ids aminoacid sequence with the 22bp deletion in the transcripts. In yellow the first aminoacid alteration and in red the premature stop codon.

2.1.4 Protein extraction

Proteins were extracted from 50 morphant and control larvae at 2dpf. Before the lysis, fish yolk was removed using a Deyolking buffer (55mM NaCl, 1,8mM KCl, 1,25mM $NaHCO_3$) and the samples were washed with Washing buffer (110mM NaCl, 3,5mM

KCl, 2,7mM$CaCl_2$, 10mM Tris-HCl pH 8.5). Tissue lysis was performed by using a Tissue extraction lysis buffer II (Invitrogen) added with protease and phosphatase inhibitors. Samples were homogenized with a sonicator and proteins were isolated from other cellular components by centrifugation.
Protein extracts were quantified under spectrophotometric analysis using Pierce BCA Protein Assay kit (Thermo Fisher Scientific).

2.1.5 Western blot

This technique permits to evaluate amount of a protein of interest in a protein lysate using a specific antibody. In this work western blot analysis have been performed to evaluate the degree of Ids knockdown in protein extracts of morphant fish and control samples.
30µg of zebrafish protein extracts have been separated on Nu-PAGE® Novex® 4–12% Bis-Tris Gels (Invitrogen) after a denaturation and transferred to PVDF membranes. The membranes were subsequently incubated with antibodies against iduronate 2-sulfatase (1:1000; Novus biologicals) and β-actin (1:5000; Santa Cruz) at 4°C overnight after blocking with Western blocker solution (Sigma) for 2h. β-actin was used as an endogenous control for protein quantification, while a HeLa cells sample was used to verify the specificity of the used antibody.
After the incubation with horseradish peroxidase conjugated secondary antibody (1:2000; Sigma) for 1 h at room temperature, visualization was performed with SuperSignal West Pico Chemiluminescent Substrate detection kit (Thermo Scientific) followed by exposure to X-ray film (Thermo Scientific).
Ids quantification was performed by band specific densitometric analysis (ImageJ) and normalizing the value obtained with that of β-actin specific bands.

2.1.6 Synthesis of RNA antisense probe

RNA labeled probes have been used for *in situ* hybridization analysis to recognize transcripts of interest. Plasmids containing the partial coding sequence of a target gene, flanked by phagic RNA polymerase transcription initiation sequences were used to synthesize antisense riboprobes. To generate the antisense riboprobes plasmids have been linearized upstream of the target cDNA coding sequences, while the probes have been transcribed using a downstream promoter (Table 5). The transcription process was carried out in the presence of digoxigenin-labeled nucleotides allowing the generation of a labeled antisense riboprobe, using mMessage mMachine SP6, T7 or T3 Kit (Ambion).

Probe	Plasmid	Enzyme for linearization	Promoter
mcherry	pME	ApaI	T7
GFP	pME	ApaI	T7
fgfr3	pBSII SK	KpnI	SP6
fgf3	pBSII SK	SalI	T3
fgf8	pBSII SK	XhoI	T7
pea3	pSPORT6.1	KpnI	T7
ntl	pBSII SK	KpnI	T7
spry4	BluScript	SalI	SP6

Table 5: RNA antisense probe synthesized with information about plasmid, enzyme used for linearization and promoter used for their synthesis.

2.1.7 In situ hybridization (ISH)

This technique allows to detect transcripts of a gene of interest using a labeled antisense riboprobe complementary to the target sequence. In whole mounted larvae after ISH, it's possible to identify the spatial distribution of target transcripts in different anatomical regions.

I performed in situ hybridization in larvae of different developmental stages using the probes for:

- *Runx2b,* a marker expressed in the early stages of ossification.
- *ColX(col10a1)*, a marker of hypertrophic chondrocytes.
- *mCherry* and *GFP* for the detection of the reporter protein in transgenic.
- *fgfr3,* one of FGF signaling receptors.
- *fgf3* e *fgf8,* two FGF signaling ligands.
- *pea3, ntl* e *spry4,* FGF signaling target genes.

The hybridization temperature was different according to the probe length and the percentage of G-C content (Table 6).

The probes were digoxigenin-labeled, therefore recognized by an alkaline phosphatase-conjugated antibody against-digoxigenin. The alkaline phosphatase substrate NBT/BCIP was used to perform the colorimetric detection of the *in situ* hybridization.

After ISH, larvae are mounted in 85% glycerol and photos have been acquired using a Leica S8AP0 microscope.

Probe	Temperature of hybridization
Runx2b	62°C
ColX	62°C
mcherry	62°C
GFP	62°C
fgfr3	64°C
fgf3	62°C
fgf8	62°C
pea3	64°C
ntl	64°C
spry4	64°C

Table 6: RNA antisense probes used and their temperature of hybridization

2.1.8 Crispr/Cas9

CRISPR (Clustered Regularly Interspaced Short Palindromic Repeats)/Cas9 is a new gene editing tool used to efficiently achieve target gene modifications in different animal models, including zebrafish. This system is naturally present in Eubacteria and Archea as an adaptive immune response against exogenous genetic elements such as plasmids and phages.

It's possible to reproduce this system *in vitro* through the synthesis of a guide RNA (gRNA) and the mRNA encoding Cas9 endonuclease. The gRNA is an RNA sequence, formed by the fusion of a CRISPR-RNA(crRNA) and a transactivating RNA (tracRN), that guides the Cas9 enzyme to the target sequence. The crRNA is complementary to the sequence of interest in the genome, while the tracRNA is an RNA element recognized by the Cas9 enzyme. The genome target is generally 20bp long and upstream of a PAM (Protospacer Adjacent Motif) sequence 5'NGG/NCC. The endonuclease cleaves the target sequence at the PAM motif producing a double strand break and by NHEJ (Non-homologous end joining) repairing, unpredictable gene mutations such as insertions and deletions can be produced at the target locus.

To create a zebrafish mutant, a predesigned gRNA and the mRNA encoding for Cas9 have been injected in one-cell stage embryos. The synthesis of the gRNA was performed with T7 Megashortscript kit (Ambion), the mRNA of Cas9 was synthesized with mMessage mMachine SP6 kit (Ambion). Injected fish (F0) are generally mosaics carrying several mutations in different cell lineages. Only germline mutations can be transmitted to the offspring. The F0 fish are then crossed with wild type fish, to produce the F1 carrying a single inheritable mutation. Homozygous mutant fish can be obtained only in the second generation progeny (F2) by incross of two heterozygous carriers. To produce an *iduronate 2-sulfatase* fish mutant, I followed the protocol illustrated by Jao and colleagues (Jao et al., 2013).

PCS2-cas9 and pT7cas9sgRNA2 plasmids were purchased from Addgene.

The plasmid PCS2-cas9 contains a Cas9 cDNA, flanked by SV40 large T-antigen nuclear localization signals (nls) at the N-terminus and C-terminus.

The pT7cas9sgRNA2 plasmid carries the crRNA:trascRNA backbone downstream to a region in which it is possible to clone the sequence complementary to the target gene region.

The target sequence needs to be 23bp long with GG/NG/GN residues at the 5' end, for the efficient T7-mediated transcription from the promoter, and a PAM motif, for efficient Cas9 binding (Jao et al., 2013).

A target sequence in the first and second exon of the *ids* was chosen and cloned in the pT7cas9sgRNA2 plasmid.

Two different software have been used to define the sequence of interest:

E-CRISP (http://www.e-crisp.org/E-CRISP/)

CHOPCHOP (https://chopchop.rc.fas.harvard.edu/) (Fig. 15)

A target sequence in the first part of the *ids* exon 2 (GTTAGGAAAGACACTCTACTAGG) was identified by in silico analysis. To create a double-stranded oligo to be cloned in the gRNA plasmid, I produced two single-stranded oligos according to previous published guidelines (Jao et al.,2013). The sequences of the two oligos are: 5'-TAGGTAGGAAAGACACTCTACT-3' and 5'-ATCCTTTCTGTGAGATGACAAA-3'.

A Cas9 mRNA and the gRNA have been transcribed and co-injected in one cell-stage embryos at different concentrations to evaluate both the toxicity and the efficacy. Injected fish have been analyzed for mortality and phenotypic abnormalities, allowing to define the optimal concentrations as 30ng/µl for gRNA and 100ng/µl for Cas9. Injected fish at 2dpf were sacrificed and genotypized to identify the indels.

Ranking	Target sequence	Genomic location	Exon	Strand	GC content (%)	Off-targets		
						0	1	2
1	CTTGAAGTATTGAGGTAGTGTGG	chr14:21892486	2	+	43	0	0	0
2	TGGATACACCACTTTATCAGTGG	chr14:21892458	2	-	43	0	0	0
3	GACTTTGCCCACTGATAAAGTGG	chr14:21892450	2	+	48	0	0	0
4	GTTAGGAAAGACACTCTACTAGG	chr14:21892580	2	+	43	0	0	0
5	TGTCTGGTCTTCGACTTGTTAGG	chr14:21892563	2	+	48	0	0	0
6	TCGTAGAGTTTTGTGGTGTCTGG	chr14:21892547	2	+	48	0	0	0
7	TCATACTGGAGAGTTCATGCTGG	chr14:21892517	2	-	48	0	0	0
8	GGATACACCACTTTATCAGTGGG	chr14:21892457	2	-	48	0	0	0
9	GTGGGCAAAGTCTTCCATCCTGG	chr14:21892439	2	-	57	0	0	0

Figure 15: CHOPCHOP results for target sequences in iduronate 2-sulfatase exon 2. The red arrow show the chosen target sequence.

2.1.9 DNA extraction

DNA was extracted from whole larvae or adult tail samples. Tissues were digested with SDS-containing lysis buffer (Tris/HCl 1M, NaCl 1M, EDTA 0,5M, SDS 20%) and a 10mg/ml proteinase K solution (10µg/ml) at 55°C overnight. Total genomic DNA was purified by phenol chloroform extraction and ethanol precipitation. Purified DNA was dissolved in DNase-free water and quantified with NanoDrop instrument (Agilent).

2.1.10 High resolution melting (HRM)

High resolution melting (HRM) is a rapid method for the detection of mutations or polymorphisms in double stranded DNA samples. This technique relies on the different melting temperatures of the WT or mutated DNA amplicons. This method was used to screen for candidate fish mutants in the F0 generation.

In the presence of a fluorescent dye (LCGreen Plus™) linking the double strand DNA amplicons are denaturated and then renaturated to produce heteroduplex.

To screen for F0 fish, a large sequence around the target region encompassing all possible mutant alleles was scrutinized (Table 7).

Once identified the type of induced mutation a second pairs of oligos was used to perform genotyping and detect homozygous mutant fish.

	Primer	RefSeq
Primer to screen F0 fish For	GATCAGCTTGCATCTTTGAGC	NM_001080068
Primer to screen F0 fish Rev	TTGTGGTGTCTGGTCTTCGA	NM_001080068
Primer to screen Ids-KO fish For	TGTGTTCTTTCAAAGCAAGCTG	NM_001080068
Primer to screen Ids-KO fish Rev	TTGTGGTGTCTGGTCTTCGA	NM_001080068

Table 7: Primer used to amplify the target *ids* region for HRM analysis.

2.1.11 Characterization of the mutant allele by cloning

To better define the mutant allele, the amplicon containing the targeted sequence was purified, and ligated to a TOPO vector (Invitrogen™). Transformed competent cells were plated on agar containing the selective antibiotic. Single grown colonies were picked and cultured in Luria-Bertani medium. The extraction and purification of plasmid DNA was performed using commercial kits provided by Qiagen (QIAprep®).

Plasmids from different colonies were sequenced and analyzed (Fig. 16).

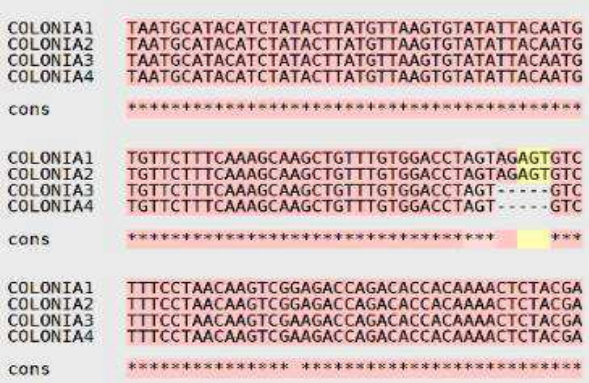

Figure 16: Comparison between four different colonies after sequencing. Colonies 3 and 4 display a deletion of 5bp compared to colonies 1 and 2.

2.1.12 Homozygous mutant fish screening using PCR analysis

To identify homozygous mutant fish, a complementary PCR-technique was used. This approach was based upon the design of a reverse oligo containing a stretch of nucleotides at the 3' end complementary to the 5bp deletion. In the presence of the mutant allele the reverse oligo fails to anneal, thus preventing the generation of an amplicon as shown in Fig. 17 (Table 8).

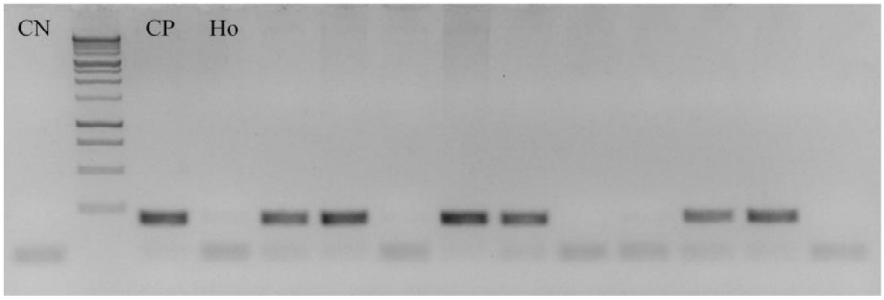

Figure 17: Gel electrophoresis of the amplicons obtained from homozygous mutant and WT sibling DNA. CN: negative control, CP: positive control (WT sequence), Ho: homozygous Ids mutant.

	Primer	RefSeq
Primer that amplify on the deletion For	GCTTGCATCTTTGAGCGTAGT	NM_001080068
Primer that amplify on the deletion Rev	GACTTGTTAGGAAAGACACTCTA	NM_001080068
Primer that amplify around the deletion For	GCTTGCATCTTTGAGCGTAGT	NM_001080068
Primer that amplify around the deletion Rev	ACGTCTATTTAGTCAGTGGGTTT	NM_001080068

Table 8: List of primer used to screen homozygous fish

2.1.13 Enzymatic assay

This assay was used to quantify Ids enzymatic activity in 2dpf larva and isolated organs (brain, liver and muscle) of 2 months old Ids-KO and WT fish. Samples were obtained by

homogenizing larvae or tissues in ice with a lysis buffer (Invitrogen). Debris was pelleted twice by centrifugation at 4°C and supernatants were collected and assayed for total protein concentration (mg/ml) by the Bio-rad protein assay (Biorad).
Iduronate 2-sulfatase activity was determined by a 2-step fluorimetric assay using the substrate 4-methylumbelliferyl-α -iduronate 2-sulfate (MU- αldu-2S). Results were obtained using 4-methylumbelliferone as a standard and were normalized to total protein levels. Ids activity was expressed as 1 nmol of MU- αldu-2S substrate hydrolysed in 4 h per mg total proteins (nmol/4h/mg).

2.1.14 Paraffin-embedding and sectioning

Zebrafish were fixed in 4% PFA in PBS, washed in PBS and dehydrated in ethanol solutions of increasing concentrations. Zebrafish samples were dehydrated with butanol. All solutions were removed and substituted with paraffin. Sectioning was performed using a microtome and tissue sections were collected on Superfrost slides.

2.1.15 Immunohystochemistry

Immunohystochemical analysis was carried out on whole mount zebrafish. For whole mount immunohystochemistry a previously published protocol was considered (Inoue & Wittbrodt, 2011). Zebrafish were fixed in 4% PFA in PBS and stored in 30% sucrose. Primary antibody (Iduronate 2 sulfatase 1:100, Novus) (GFP 1:100, Thermo Fisher) was incubated 3 days at 4°C, while the secondary antibody (Goat anti-Mouse IgG Fc TRITC conjugate 1:200, Thermo Fisher) (Goat anti-Rabbit IgG (H+L) FITC conjugate 1:200, Thermo Fisher) was incubated 2 days at 4°C in the dark.

2.1.16 Transgenic reporter lines

I have used different transgenic zebrafish reporter lines:
-Lipan *Tg(lfabf:dsRed; elaA:EGFP)* expressing the fluorescent protein dsRed under the control of a liver-specific promoter and the fluorescent protein GFP under the control of a pancreas-specific promoter. This line was used to analyze liver size in fish morphants and mutants (Korzh et al., 2008).
-*Tg*(*sox10:mRFP)*^{vu234} express the fluorescent protein RFP under the control of a Sox10 promoter. Sox10 is a marker of neural crest precursors that may differentiate into chondroblasts (Kirby et al., 2006).

-*Tg(Col2a1aBAC:mCherry)*^{hu5900} express the fluorescent protein mCherry under the control of a Collagen 2-specific promoter (Hammond & Schulte-merker, 2009).
-*Tg(Ola.Sp7:NLS-GFP)*^{zf132} express the fluorescent protein GFP under the control of a Osterix specific- promoter (Spoorendonk et al., 2008).
-*TgBAC(col10a1:Citrine)*^{hu7050} express the fluorescent protein Citrine under the control of a Collagen X-specific promoter (Mitchell et al., 2013).
To evaluate which signaling pathways may be involved in MPSII pathogenesis newly generated transgenic lines have been used:
-*Tg(BMPRE:EGFP)*^{ia18} and *Tg(BMPRE:nlsmCherry)*^{ia17} transgenic reporter lines for the BMP signaling pathway (Moro et al., 2013).
-*Tg(12xSBE:EGFP)*^{ia16} and *Tg(12xSBE:nlsmCherry)*^{ia15} transgenic reporter lines for the TGFβ signaling pathway (Casari et al., 2014).
-*Tg(12xGli-Hsv.TK:GFP)*^{ia11}and *Tg(12xGli-Hsv.Ul23:nlsmCherry)*^{ia10} transgenic reporter lines for the Shh signaling pathway (Corallo et al., 2013).
-*Tg(7xTCF-Xla.Siam:GFP)*^{ia4} and *Tg(7xTCF-Xla.Siam:nlsmCherry)*^{ia5} transgenic reporter lines for the canonical Wnt signaling pathway (Moro et al., 2012).
-*Tg(EPV.Tp1-Mmu.Hbb:nlsmCherry)*^{ia7} transgenic reporter line for the Notch signaling pathway (Moro et al., 2013).
-*Tg(Dusp6:d2EGFP)*^{pt6} transgenic reporter line for the FGF signaling pathway. This line express the fluorescent d2GFP destabilized protein under the control of a Dusp6 promoter, whose expression is regulated by the FGF signaling (Molina et al., 2007).

2.1.17 Image acquisition

Fluorescence was visualized and acquired using the conventional fluorescence dissecting microscope Leica M165FC and the confocal microscope Nikon C2 H600L. For brightfield and fluorescence imaging with the dissecting microscope, embryos and larvae were anesthetized with tricaine and mounted in 2% methylcellulose. For confocal imaging, anesthetized embryos and larvae were embedded in 1% low melting agarose. The fluorescence was visualized using 488 nm (for GFP, d2GFP and Citrine) and 561 nm (for mCherry and dsRED) lasers and 20x or 40x immersion objectives (Nikon).

2.1.18 Image analysis

Images were analyzed using ImageJ program or Imaris software, on confocal Z-stack projections or conventional fluorescence microscope acquisitions.

Statistical analyses were carried out with Prism software (GraphPad).

2.1.19 Alcian blue in whole mount fish

This technique was used to analyze the cartilage in 5dpf fish. Larvae were fixed overnight in 4% PFA in PBS at 4 °C, washed in PBS and stained overnight at room temperature in Alcian blue solution (70% EtOH, 1% HCl, 0.1% Alcian blue). Larvae were then cleared in 3% hydrogen peroxide and 1% KOH, rinsed in 70% EtOH and whole mounted in 85% glycerol.

2.1.20 Alizarin red in whole mount fish

This technique was used to analyze bone in 6dpf fish. Larvae were fixed for 1 h at room temperature in 4% PFA in PBS, washed in 50% ethanol and dehydrated overnight in 95% ethanol. Staining was carried out in Alizarin solution (0.25%, w/v, in 2% KOH) for 3 h and larvae were then briefly cleared in 2% KOH (w/v) and stored in KOH/glycerol (20 : 80).

2.1.21 Alizarin red staining *in vivo*

This technique was used to analyze the mineralization of zebrafish bones *in vivo*. Fish were put in fish water added with Alizarin-3-methyliminodiacetic acid for 3 hours at 28°C without light.

2.1.22 *In vivo* lysosomal analysis

Control and Ids ATG morpholinos, were coinjected in one-cell stage embryos with hsp70-Lamp1-RFP, a plasmid carrying the cDNA for the lysosomal membrane protein Lamp1 and the cDNA encoding the fluorescent protein RFP. The transcriptional regulation of the expression cassette was under the control of a heat-shock inducible promoter. The plasmid was used to *in vivo* label lysosomes allowing to verify their number, and morphological alterations at different conditions.

2.1.23 RNA extraction

Total RNA was extracted from pools of fifty zebrafish mutants, WT or morphants. The phenol/guanidine isothiocyanate extraction method (Trizol®, Lifetechnologies) was

performed. In order to eliminate any genomic contamination, a DNase treatment was carried out in all RNA samples.

2μg of total RNA were reverse transcribed into cDNA using the SuperScript® III Reverse Transcriptase (Invitrogen) kit .

2.1.24 Real time PCR analysis

This technique is used to precisely quantify transcripts levels of a target gene, using a fluorescent dye (Syber-Green) which is incorporated during the process of PCR amplification

Transcripts levels of a target gene are generally normalized by comparison with those of endogenous housekeeping genes.

Data were analyzed using a manually set threshold and the baseline was set automatically to obtain the threshold cycle (C_t) value for each target. Relative gene expression among samples was determined using the comparative C_t method ($2 - \Delta\Delta C_t$).

Primer used for the PCR reaction were designed using Primer3 program (http://primer3.ut.ee).

The housekeeping gene chosen during this research study was: glyceraldehyde-3-phosphate dehydrogenase (GAPDH)

For zebrafish were used primer that amplify transcripts of *GFP, pea3*, *erk1*, *erm1* and *gapdh* genes (Table 9).

Zebrafish Gene	Primer	RefSeq
GFP For	TAAACGGCCACAAGTTCAGC	Published (Berkovits & Mayr, 2015)
GFP Rev	AAGTCGTGCTGCTTCATGTG	Published (Berkovits & Mayr, 2015)
pea3For	CGATGAGCAGTTTGTTCCTG	NM_131425
pea3 Rev	CTTGTGGCTGCAGGACTG	NM_131425
erk1For	TGACCCTGAACATGACCACA	NM_201507
erk1 Rev	GGTCCAGATAGTGCTTCCCA	NM_201507
erm1For	TGTTCCAGATTTCCAGTCGG	NM_001309209
erm1 Rev	AGTCTCTGCTCTTGTCCACA	NM_001309209
gapdh For	GTGCAGGAGGCATTGCTTACA	NM_001115114
gapdh Rev	GTGGAGTCTACTGGTGTCTTC	NM_001115114

Table 9: Primers used for Real time PCR analysis of Zebrafish samples.

2.2 MOUSE

2.2.1 Alcian blue Alizarin red staining in whole mount mice

This staining was used to analyze cartilage and bone tissues in Ids-KO and WT mice.
Mice were sacrificed and skin and organs were removed. Fixation was carried out in 95% ethanol for 5 days. Samples were washed with water and stained with 1% Alcian blue at pH 1.0 for 3 days. Mice samples were refixed with 95% ethanol overnight and put in 1% KOH solution for 5 days. After several washes with water, a solution of Alizarin red 1% pH 4.2 was added for 5 days. Samples were washed with 1% KOH and stored in glycerol.

2.2.2 Alcian blue-Nuclear fast red staining

This technique was used to analyze glicosaminoglycans accumulation in liver .
Tissue sections were deparaffinized with xilene and rehydrated with ethanol solutions of decreasing concentration . After several washes with distilled water and 0,1M Citric acid was added to the samples for 3 minutes. Sections were stained with 1% pH 1.0 Alcian blue for 20 minutes. After several washes with distilled water, a Nuclear fast red solution was added to the samples for 10 minutes. Sections were washed and dehydrated with ethanol solutions of increasing concentration.

2.2.3 Paraffin-embedding and sectioning

Mouse samples were fixed in 4% PFA in PBS, washed in PBS and dehydrated in ethanol solutions of increasing concentrations. Before dehydratation, mice bones were decalcified using a solution of 10% EDTA in PBS and samples were dehydrated in xylene. All solutions were removed and substituted with paraffin. Sectioning was performed using a microtome and tissue sections were collected on Superfrost slides.

2.2.4 Immunohystochemistry

Immunohystochemistry analysis was carried out on paraffinized sections. Paraffin-embedded sections were deparaffinized with xilene and progressively rehydratated with ethanol solutions. Antigen retrieval was achieved with 1mM pH6.0 Sodium Citrate using a steam chamber. The primary antibody (PEA3, GeneTex) (COL2A1, Santa Cruz) (Osteocalcin, Santa Cruz) was incubated overnight at 4°C, while the secondary antibody

(Goat anti rabbit-Alkaline Phosphatase, Sigma) was incubated 1 hour at room temperature and NBT-BCIP staining was performed.

2.2.5 RNA extraction

Total RNA was extracted from 1 week and 2 weeks old mouse samples, including the cranial vault, femur diaphysis and femur epiphysis. The phenol/guanidine isothiocyanate extraction method (Trizol®, Lifetechnologies) was performed. In order to eliminate any genomic contamination, a DNase treatment was carried out in all RNA samples.
2μg of total RNA were reverse transcribed into cDNA using the SuperScript® III Reverse Transcriptase (Invitrogen) kit .

2.2.6 Real time PCR analysis

This technique has been described in 2.1.24 paragraph.
Mice cDNA was reverse transcripted from RNA extracted from cranial vault, femur diaphysis and femur epiphysis samples of 1 week and 2 weeks knockout and WT mice.
The housekeeping gene chosen during this research study was: beta-2-microglobulin (B2M).
For mice were used primer that amplify transcripts of *collagene 2 (Col2a1)*, *osteocalcin*, *collagene X (Col10a1)*, *interluchine1 β (IL1β)*, *TNFα*, *pea3*, *erk1*, *dusp6* and *b2m* genes (Table 10).

Mouse Gene	Primer	RefSeq
collagene 2 For	AAGGGTCACAGAGGTTACCC	NM_031163
collagene 2 Rev	GTCCTCTCTCACCAGGCAG	NM_031163
osteocalcin For	GAGGGCAATAAGGTAGTGAACAGA	NM_007541
osteocalcin Rev	AAGCCATACTGGTTTGATAGCTCG	NM_007541
collagene X For	ATGCTGAACGGTACCAAACG	NM_009925
collagene X Rev	GGAATGCCTTGTTCTCCTCT	NM_009925
IL1β For	ACCTGTGTCTTTCCCGTGGAC	Published (Chen et al., 2015)
IL1β Rev	GGGAACGTCACACACCAGCA	Published (Chen et al., 2015)
TNFα For	AGCCCACGTCGTAGCAAACC	Published (Chen et al., 2015)
TNFα Rev	CATCGGCTGGCACCACTAGT	Published (Chen et al., 2015)
pea3For	CCTTCTGCAGCAAATCTCCC	NM_001316365
pea3 Rev	CTGCTCATCACTGTCCGGTA	NM_001316365
erk1For	TACGGCATGGTCAGCTCAG	NM_011952
erk1Rev	AGGATGTCTCGGATGCCTATAA	NM_011952
dusp6For	ATGCGGGCGAGTTCAAATAC	NM_026268
dusp6Rev	CAAGCAATGCACCAGGACAC	NM_026268
b2m For	CGGCCTGTATGCTATCCAGA	NM_009735
b2m Rev	ATTTCAATGTGAGGCGGGTG	NM_009735

Table 10: Primers used for Real time PCR analysis of mouse samples.

2.3 HUMAN

2.3.1 Real time PCR analysis

This technique has been described in 2.1.24 paragraph.

Human cDNA was obtained from RNA extracted from Hunter syndrome patients or healthy controls. Anonymized samples were obtained from Biobank of Genova Institute G. Gaslini.

The housekeeping gene chosen during this research study was: glyceraldehydes-3-phosphate dehydrogenase (GAPDH).

For human samples were used primer that amplify transcripts of *dusp6, erk1, pea3* and *gapdh* genes (Table 11).

Human Gene	Primer	RefSeq
dusp6For	CGTTCTACCTGGAAGGTGGC	NM_001946
dusp6 Rev	CCGAGGAAGAGTCAGAGCTG	NM_001946
erk1For	CAACCACATTCTGGGCATCC	NM_002746
erk1 Rev	CTTGGTCTTGGAGGGCAGAG	NM_002746
pea3For	CTACACCTTCAGCAGCAAATCG	NM_001079675
pea3 Rev	TCACTGTCTGGTACCTGAGCTTC	NM_001079675
gapdh For	CGAGCCACATCGCTCAGAC	NM_002046
gapdh Rev	ACAATATCCACTTTACCAGAGTTAAAAGC	NM_002046

Table 11: Primer used for Real time PCR analysis of human samples.

3 AIM OF THE PROJECT

Mucopolysaccharidosis type II (MPSII or Hunter syndrome) is a rare disease caused by mutations in the *IDS* gene, encoding for the lysosomal enzyme iduronate 2-sulfatase (IDS). IDS is involved in the catabolism of the glycosaminoglycans(GAGs) heparan and dermatan sulfate, and mutations altering its activity lead to substrates accumulation into the organelle. Pathological manifestations, caused by GAGs storage, include metabolic and functional alterations ultimately leading to cell death.

Traditionally, glicosaminoglycans accumulation has been considered the primary cause of pathological defects. However, recent experimental evidences suggest that the molecular pathogenesis could be more complex and that other cellular mechanisms may contribute to the disease onset.

The aim of my PhD project was to expand the current knowledge on the pathogenesis of MPSII-related bone defects, by evaluating whether the loss of iduronate 2-sulfatase activity may lead to early developmental cell signaling alterations before the onset of lysosomal GAGs accumulation.

To this purpose, a zebrafish model for MPSII was generated and characterized at a molecular level, thus allowing to screen for candidate target signaling pathways affected by IDS loss of function.

The second part of the PhD project was then focused on the molecular characterization of a candidate pathway in a murine model of Hunter syndrome, to assess whether the cascade of pathogenetic events detected in the fish model was conserved in a mammalian system.

Finally, in the last part of the research project my investigation aimed at establishing in fibroblasts obtained from a selected cohort of Hunter syndrome patients whether the candidate signaling pathway defects may be related to the degree of disease severity.

4 RESULTS

4.1 Iduronate 2-sulfatase expression in zebrafish bones

I have used zebrafish as animal model to analyze how IDS functional alterations lead to the pathological skeletal phenotype in Hunter syndrome.

It has been previously shown that iduronate 2-sulfatase has an important role in development and ossification (Moro et al., 2010) (Mandal et al., 2013). However, the precise mechanisms involved in the IDS-dependent control of bone development are currently unknown. I began to analyze Ids expression in the bone compartment during development. To this purpose, I used the transgenic reporter line (*Tg(Ola.Sp7:NLS-GFP)*^{zf132}), in which the expression of the GFP reporter gene is driven by the osterix promoter, which is activated during osteoblast differentiation. In 5dpf transgenic fish, I performed a double immunohistochemistry using a primary antibody against GFP protein and a primary antibody against Ids protein. As expected Iduronate 2-sulfatase was largely expressed in the head, but with high level of expression in the cephalic bones. At 5dpf zebrafish the first cephalic bones, i.e. opercle, brachiostegal ray and cleithrum have formed (Fig. 18), and the double immunohystochemistry enabled me to detect colocalization between the GFP and Ids protein (Fig. 19 A-B-C).

A highly magnified evaluation at confocal microscopy revealed a peculiar expression of the enzyme in the opercle. I found a consistent Ids expression in the proximal opercle region that is the most osteogenic zone (Fig. 19 D-E-F). In the brachiostegal ray, Ids was present in all the Osterix-positive regions (Fig. 19 G-J-K). In the cleithrum there was less colocalization between GFP and Ids, compared with the other bones. While Osterix was clearly expressed in the edges of the cleithrum, the enzyme was barely detectable in these regions while it was more expressed in the core region of the cleithrum (Fig. 19 H-I-L).

These results show that Iduronate 2-sulfatase enzyme is expressed in osteogenic regions supporting its active role in bone development.

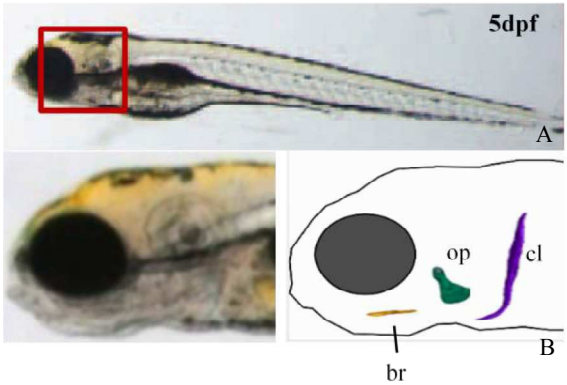

Figure 18: (A) 5dpf zebrafish, the red square show the head region analyzed with the double immunohistochemistry. (B) Zebrafish head and a picture that show the localization of first ossificated bones.
br: brachiostegal ray; cl: cleithrum; op: opercle.

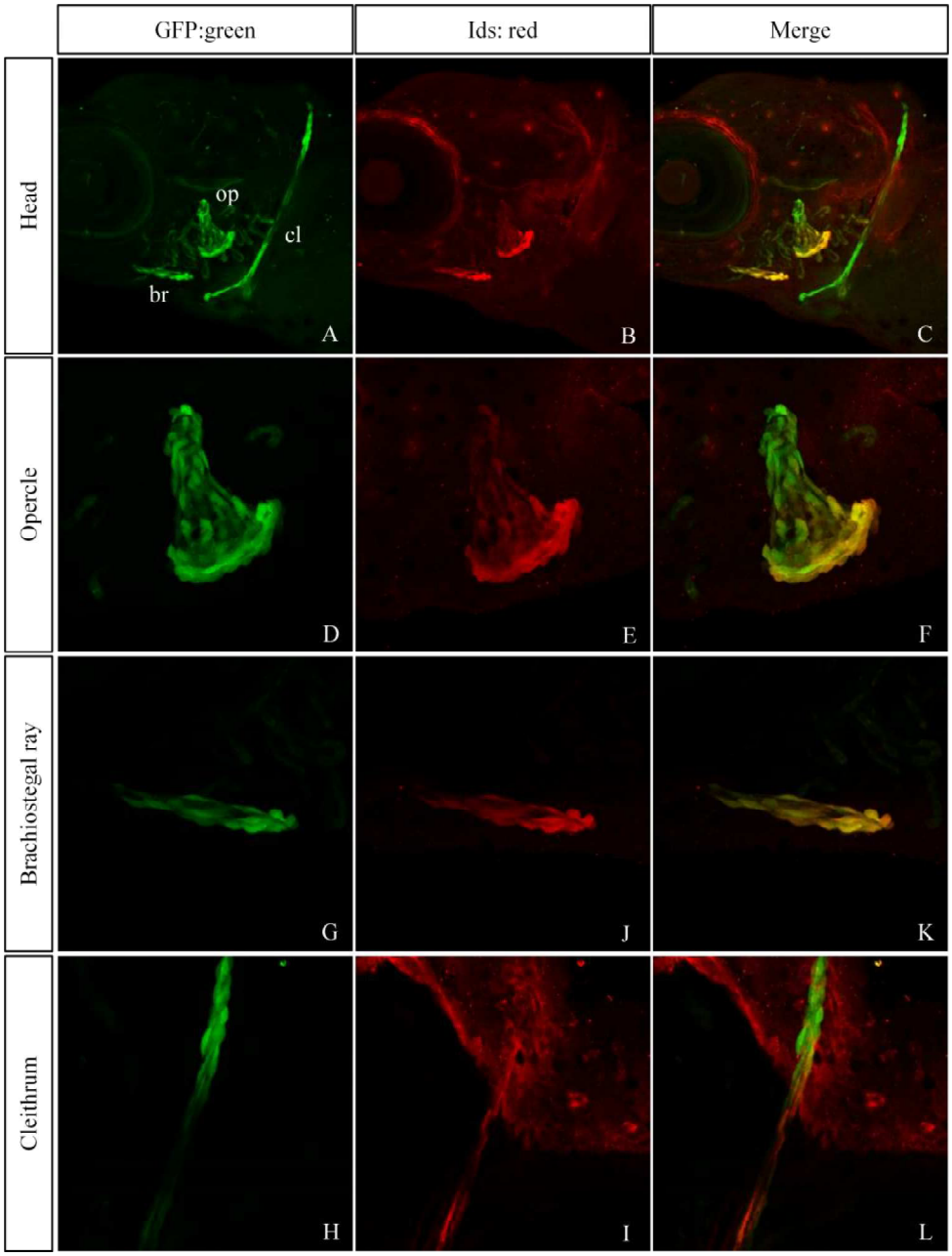

Figure 19: Double immunohystochemistry in 5dpf Osterix transgenic reporter line. In green GFP protein and in red Iduronate 2-sulfatase enzyme are shown. (A-B-C) Ids enzyme is largely expressed in zebrafish head and it colocalizes with GFP protein. (D-E-F) High magnification of the opercle. Iduronate 2-sulfatase is present especially in the distal regions of the opercle that are the most osteogenic parts of the bone. (G-J-K) High magnification of the brachiostegal ray. There is full colocalization of Ids protein and GFP expression. (H-I-L) High magnification of the cleithrum. Osterix is expressed only in the dorsal tip of the cleithrum while Ids show only a weak colocalization with the bone marker. The enzyme is present also in central part of the cleithurm. Images taken with confocal microscope with 20x and 40x (high magnification) lens. br: brachiostegal ray; cl: cleithrum; op: opercle.

4.2 Morpholino-based Ids knock down (KD) in zebrafish

I have used a zebrafish model for Mucopolysaccharidosis type II obtained with the microinjection of a translation initiation-blocking morpholino oligo designed for the *ids* transcript. This model has been already described and partially characterized (Moro et al., 2010). Morphant fish have been previously shown to display a decreased Iduronate 2-sulfatase activity (Fig. 20 A) and a high embryonic mortality which is partially rescued by coinjecting the morpholino with the human recombinant IDS protein, Elaprase (Fig. 20 B).

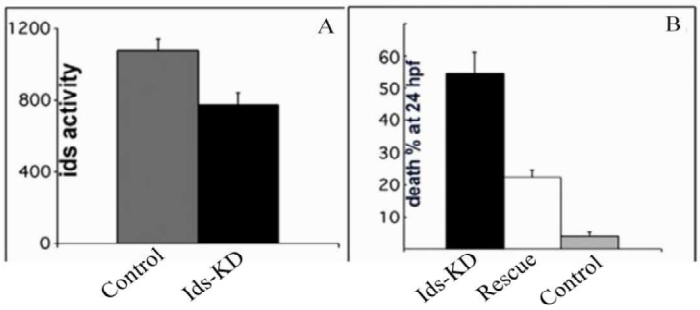

Figure 20: (A) Ids-KD morphants exhibit lower enzyme activity when compared with control fish. (B) Embryonic mortality rate is higher in morphant when compared with control fish and it is partially rescued by coinjecting the morpholino with the recombinant enzyme Elaprase. Image modified from (Moro et al., 2010).

4.2.1 Characterization of the Ids-KD morphant

I performed Western blot analysis in order to detect Ids protein levels in morphant fish and compared them with that of control fish. Ids-KD fish demonstrated a significant decrease in IDS protein levels when compared with mismatched morpholino-injected controls (Fig. 21). As I expected, the morpholino was not able to completely block *ids* translation, but the residual amount of enzyme was very low when compared with control.

Since hepatomegaly is one of the main pathological alterations in Hunter patients, I analyzed liver morphology in morphant fish. Ids-KD fish from 6dpf displayed increased liver size when compared with controls. I used a transgenic reporter line *Tg(lfabf:dsRed;elaA:EGFP)*, also called Lipan, that express the fluorescent protein dsRed under the control of a liver specific promoter and the fluorescent protein EGFP under the control of a pancreas specific promoter. This transgenic line permits to in vivo observe zebrafish liver using a fluorescent microscope. Using an in silico analysis, based upon the use of ImageJ-processed confocal acquisitions, I found that at 6dpf the Ids-KD liver is statistically significant bigger when compared to the control one (Fig. 22). Moreover, the

difference between morphant and control liver size increased at 10dpf (Fig. 22) (Fig. 23). Alcian blue staining of paraffinized liver tissue sections from 10dpf larva showed accumulation of GAGs in morphant liver, that was not detectable in control samples (Fig. 24).

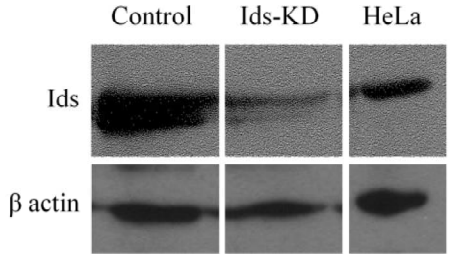

Figure 21: Representative Western blot analysis of three independent experiments. Ids-KD morphants show a significant knock down of Iduronate 2-sulfatase protein compared with controls.

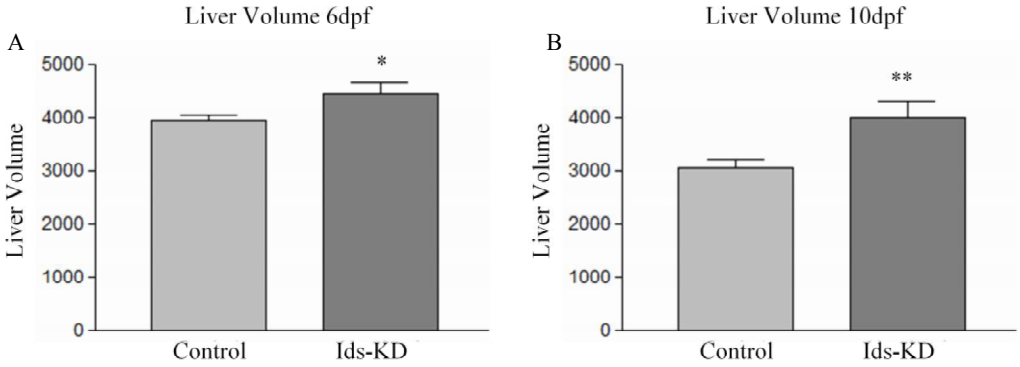

C

	6dpf			10dpf		
	Mean	Standard deviation	p-value	Mean	Standard deviation	p-value
Control	3945,9	409,3	0,031	3041,1	557,0	0,005
Ids-KD	4443,9	767,4		4001,6	1112,1	

Figure 22: Increased liver volume size in 6dpf (A) and 10dpf (B) Ids-KD fish when compared with control fish. (C) Mean liver volume of 6dpf and 10dpf Ids-KD and control fish, analysis assessed in 15 fish for each group. Numbers in Y-axis are defined as arbitrary units. T-test analysis shows that the differences between morphant and control organ size are statistically significant (* $p<0,05$; ** $p<0,02$).

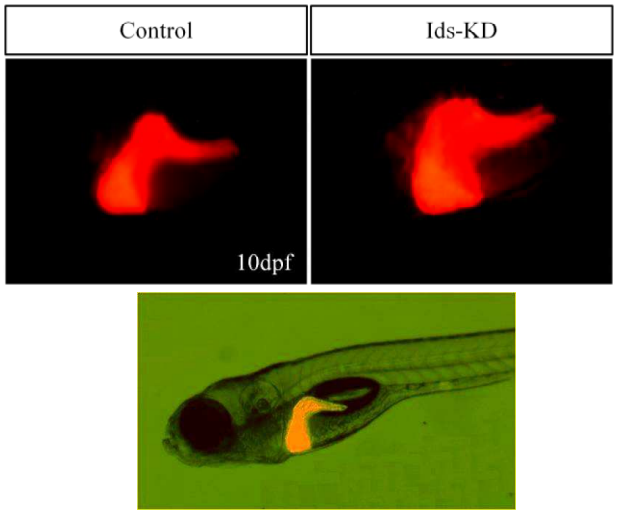

Figure 23: Rappresentative Ids-KD and control livers in Lipan transgenic line. It's possible to notice the increased area of the morphant organ when compared with the control liver.

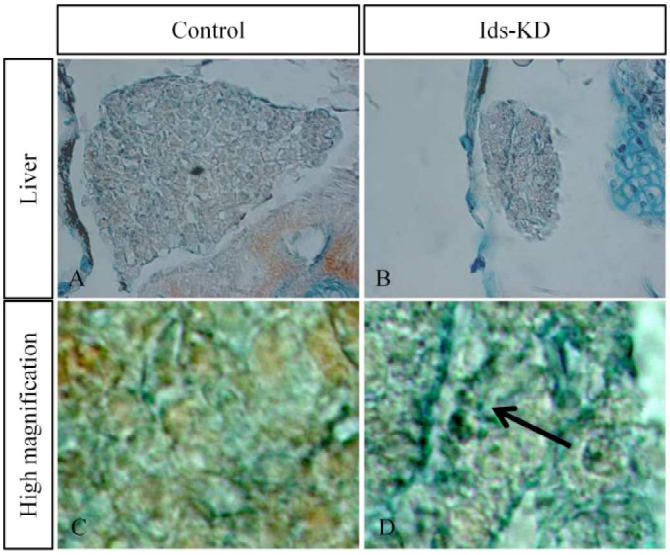

Figure 24: Alcian blue staining of paraffinized sections, a representative 10dpf larva liver (A)(B). Morphants display GAGs accumulation in the liver (D) that is not present in controls (C). Images: A and C: sagittal (A->P) sections; B and D: transversal (V->D) sections.

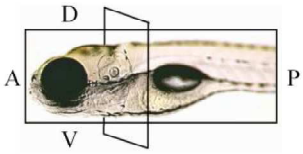

I was then interested to know whether morphants are characterized by alterations in lysosomal morphology and whether any GAGs accumulation is detectable also in fish. So I coinjected the translation initiation-blocking morpholino and the control morpholino with a heat shock-inducible Lamp1-RFP plasmid. Lamp1 is a lysosomal membrane protein and the expression of this chimeric fusion protein enables to detect lysosomal morphology in living fish. I, therefore, analyzed several injected embryos at different developmental stages and I observed that the first lysosomal alterations are visible from 3dpf in Ids-KD fish. In particular, 3dpf morphant fish exhibit a reduced number of lysosomes, with impaired morphology and cellular localization (Fig. 25 A) when compared with control fish (Fig. 25 B). Moreover some trunk epithelial cells in Ids-KD fish show abnormal shape when compared with controls (Fig. 25 C-D).

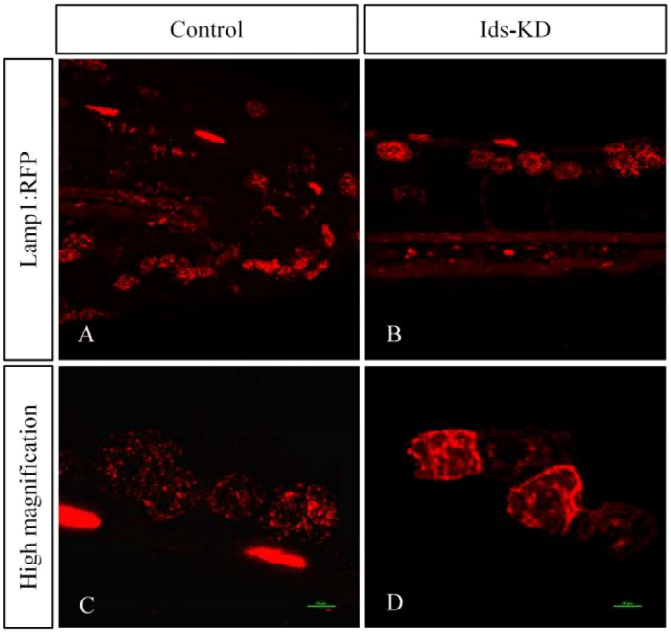

Figure 25: Representative confocal acquisition of Ids-KD fish and controls injected with a plasmid encoding for a Lamp1 protein fused in frame with RFP fluorescent protein. Morphant fish exhibit some altered cells with abnormal lysosomes (B-D) that are not detected in controls (A-C).

4.2.2 Ids-KD fish display early ossification defects

I used a zebrafish reporter line for Sox10 (*Sox10:mRFP*), that is a marker of migrating cranial neural crest cells that differentiate in osteoblasts and chondroblasts. I injected one cell-stage embryos for this reporter line with the translation initiation-blocking morpholino for *ids* or mismatch control morpholino. Fluorescence analysis showed a down regulation of the *Sox10:mRFP* transgene, in 1 dpf Ids-KD fish when compared with age-matched controls (Fig. 26 A-B). These data were also confirmed with *in situ* hybridizations using a probe against the fluorescent protein (Fig. 26 C-D).

I also performed *in situ* hybridizations in 2dpf and 3dpf zebrafish morphant and control larvae for *runx2b* and *collagenX* bone markers. *Runx2b* is expressed at early stages of ossification in both cartilage and bone primordia. *CollagenX* is expressed during both intermediate and mature stages of osteoblast differentiation. At 2dpf *runx2b* was expressed in the opercle, brachiostegal ray and ceratobranchial arch 5. I found an increased expression of this marker in all examined bone elements of Ids-KD fish when compared with control fish (Fig. 27 A-B). *CollagenX* probe labels the opercle and cleithrum bones in 3dpf larvae. When comparing Ids-KD fish with controls I found that *collagenX* was similarly expressed in the cleithrum, while in the opercle its expression was reduced in morphants (Fig. 27 C-D).

These results show that Ids has a key role in the very early stages of ossification and Ids-KD fish display alterations in bone markers expression at 2dpf and 3dpf before any detectable lysosomal impairment.

Moreover, morphants exhibit abnormal head cartilage morphogenesis, as shown by evident morphological alterations detected by Alcian blue staining (Fig. 28 A-B). Using Alizarin staining I was able to observe also ossification defects in Ids-KD (Fig. 28 C-D).

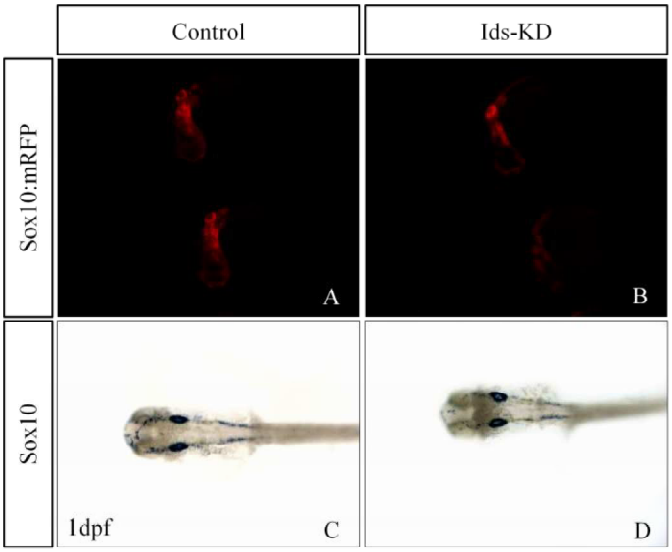

Figure 26: *Sox10:mRFP* transgenic line injected with *ids* morpholino and mismatched morpholino. Fluorescent analysis show a downregulation of Sox10 in Ids-KD (B) fish compared to controls (A). This result is confirmed by in situ hybidrization using a probe against RFP fluorescent protein (C-D).

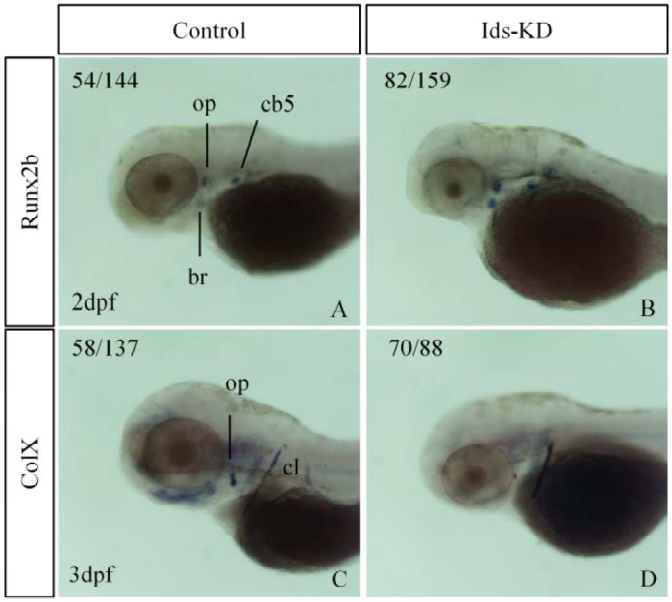

Figure 27: *In situ* hybridization analysis show an up regulation of *runx2b* marker in 2dpf Ids-KD fish (B) compared to controls (A). Three independent experiments have been performed. It's possible to observe also a down regulation of *collagenX* expression in 3dpf Ids-KD fish opercle (D) when compared with controls (C). br: brachiostegal ray; cb5:ceratobranchial arch 5; cl:cleithrum; op: opercle.

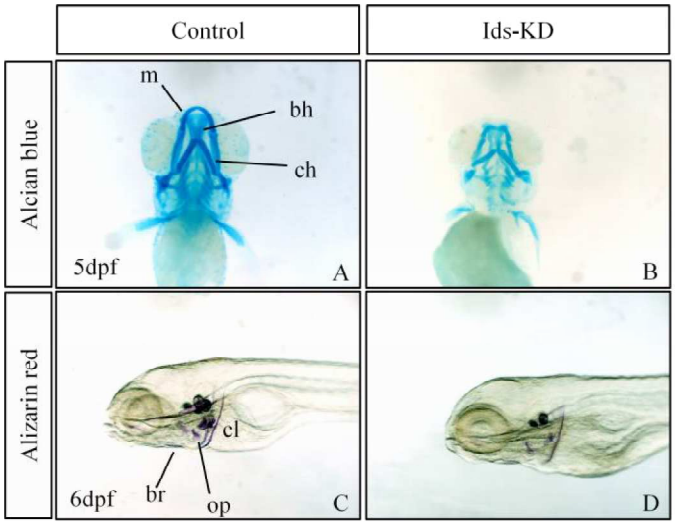

Figure 28: Alcian blue staining analysis display altered cartilage morphogenesis in the head of 5dpf morphants (A-B). Alizarin red staining show an impaired bone development in 6dpf Ids-KD fish (C-D). 15 fish have been analyzed for each group. bh: basihyal; br:brachiostegal ray; ch: ceratohyal; cl: cleithrum; m: Meckel's cartilagine; op: opercle.

4.2.3 FGF signaling is impaired in Ids-KD fish

To assess downstream pathways affected by Ids loss of function I injected the translation initiation-blocking morpholino for *ids* in a set of transgenic reporter fish for Wnt, TGFβ, BMP, SHH, Notch and FGF signaling. In repeated independent experiments I found an upregulation of the FGF signaling reporter line (*Tg(dusp6:d2GFP)*^{pt6}) in 2 dpf morphant fish when compared with controls, both using fluorescence analysis approach (Fig. 29 A-B) and in *situ hybridization* by means of a antisense riboprobe against the GFP fluorescent protein (Fig. 29 C-D).

To validate my observations, I also performed several quantitative real-time PCR analysis for GFP in pooled 2dpf FGF transgenic reporter line injected with the morpholino and mismatch control morpholino. As shown in Fig. 30, I found an up regulation of the fluorescent protein expression in Ids-KD compared with controls, that correspond to FGF signaling up regulation. Using the same quantitative RQ-PCR, I also analyzed the expression of some FGF signaling markers: *pea3*, *erk1* and *erm1*, in morphant and control samples. In independent experiments I was able to find a statistically significant up-regulation of these markers in Ids-KD compared with controls (Fig. 31 A-C).

Using pools of 6dpf zebrafish larvae injected with both the morpholino and control morpholino samples, I was able to find that the FGF reporter activity was consistently upregulated at 6dpf (Fig. 30), In agreement with these observations, *pea3* and *erm1* expression were still significantly higher in morphants, when compared with pooled

control samples, while *erk1* transcripts were reduced at the same stage (Fig. 31 B-D). These results showed a dysregulation of FGF signaling in morphants in the early stages of development that is maintained during time.

To further validate these results I performed *in situ* hybridization analysis with antisense riboprobes against the FGF targets, *pea3*, *ntl* and *spry4*, FGF ligands *fgf3* and *fgf8* and FGF receptor *fgfr3*.

As shown in Fig. 32 and 33, I found an up regulation of *fgfr3*, *fgf3*, *ntl* and *spry4* transcripts in 1dpf Ids-KD fish compared to controls, and an up regulation of *fgf8* and *pea3* transcripts in 2dpf morphants compared to age-matched fish injected with mismatched morpholino.

These results confirmed the data obtained by quantitative real time PCR analysis and showed that FGF signaling targets are more expressed in morphants fish in respect with control (Fig. 32 and 33).

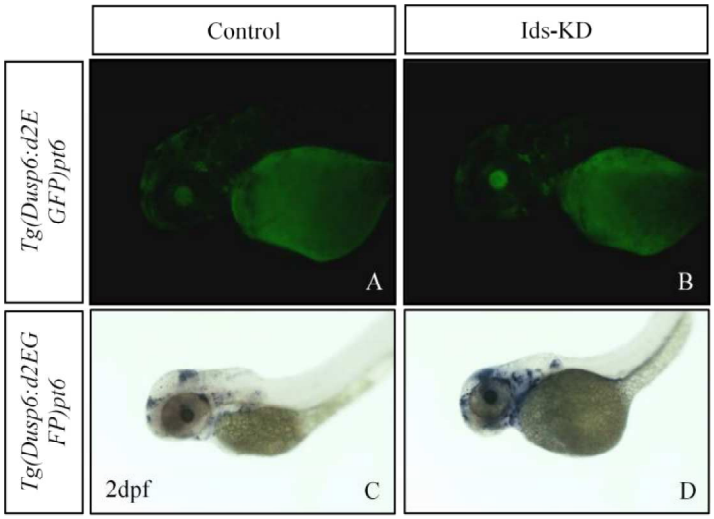

Figure 29: The transgenic line *Tg(Dusp6:d2EGFP)*^{pt6} injected with morpholino against *ids* ATG or with a mismatched morpholino, show an upregulation of FGF signaling in morphants (A) when compared with controls (B). This result was confirmed by in situ hybridization using a probe against *GFP* transcript (C,D). Three independent experiments have been performed.

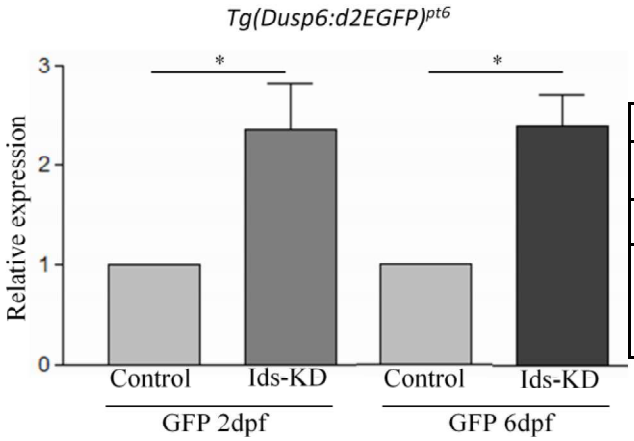

	GFP		
	Mean	**Standard deviation**	**p-value**
Control	1	/	/
Ids-KD 2dpf	2,73	1,02	0,041
Ids-KD 6dpf	2,39	0,63	0,022

Figure 30: Real time PCR analysis performed on pool samples of 50 fish, from 2dpf and 6dpf *Tg(Dusp6:d2GFP)pt6* fish injected with the morpholino or mismatch control morpholino. Data are expressed as a mean of four independent experiments. In Ids-KD there is a significant reporter gene upregulation, in morphants at both 2dpf and 6dpf, when compared with age-matched controls. (t-test; * p<0,05).

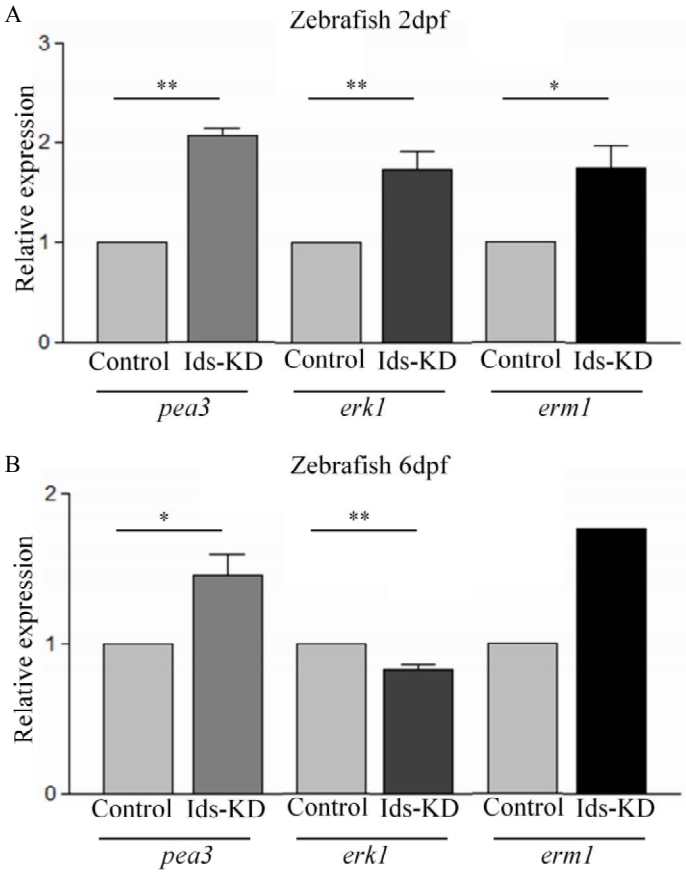

C	Zebrafish 2dpf		
	Mean	**Standard deviation**	**p-value**
Control	1	/	/
Ids-KD *pea3*	2,07	0,13	0,005
Ids-KD *erk1*	1,73	0,41	0,016
Ids-KD *erm1*	1,72	0,50	0,028

D	Zebrafish 6dpf		
	Mean	**Standard deviation**	**p-value**
Control	1	/	/
Ids-KD *pea3*	1,46	0,30	0,026
Ids.KD *erk1*	0,83	0,06	0,012
Ids-KD *erm1*	1,77	/	/

Figure 31: Real time PCR analysis performed on pool samples of 50 Ids-KD fish or control fish at 2dpf and 6dpf. (A) (C) At 2dpf it was possible to see increased expression of *pea3, erk1* and *erm1* in Ids-KD compared with controls. (B) (D) At 6dpf morphant fish show up-regulation of *pea3 and erm1* transcripts and a down regulation of *erk1* transcripts, when compared with age-matched controls. Data are expressed as a mean of four independent experiments. T-test analysis was performed for each marker (* $p<0,05$; **$p<0,02$).

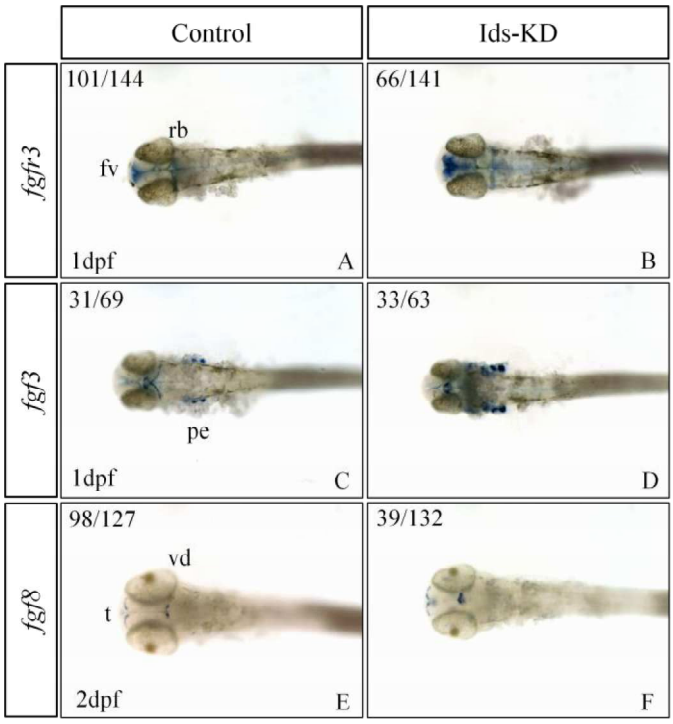

Figure 32: In situ hybridization for FGF receptor and FGF ligands transcripts. It's possible to detect increased expression of *fgfr3* (A,B), *fgf3* (C,D) and *fgf8* (E,F) transcripts in morphants when compared with age-matched controls. Three independent experiments have been performed. fv: forebrain ventricular zone; pe: pharyngeal endoderm; rb: rhombomere boundaries; t: telencephalon; vd: ventral diencephalon

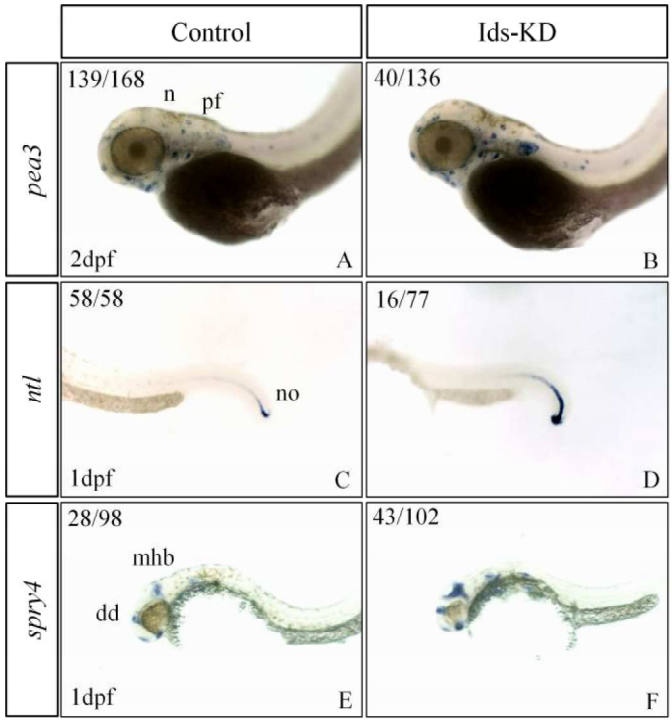

Figure 33: In situ hybridization enabled the analysis of FGF signaling markers affected by IDS loss of function. It's possible to detect increased expression of *pea3* (A,B), *ntl* (C,D) and *spry4* (E,F) transcripts in morphants when compared with age-matched controls. Three independent experiments have been performed. dd: dorsal diencephalon; mhb: midbrain hindbrain boundary; n: neuromast; no: notochord; pf: pectoral fin; t: telencephalon

4.3 Zebrafish morphant with alternative *ids* splicing

Using a custom pre-designed splicing sit-blocking morpholino I have generated an alternative fish model with a transient loss of Ids function. The morpholino targets the splice acceptor site between exon2 and intron2 of the *ids* gene.

4.3.1 Zebrafish splicing morphant characterization

Using gel electrophoresis analysis, I first verified the specificity of the splicing site-blocking morpholino. To this purpose, I amplified the region containing the splicing site in cDNA obtained from RNA extracted from morphants or controls and I compared the results. Fish injected with a mismatched morpholino display an intense high molecular weight band other two bands of weak intensity. As shown in Fig.34, morphant extracts display the high molecular band with a weaker intensity. Morphant fish injected with splicing site-blocking morpholino exhibit a better phenotype and a minor mortality rate when compared with morphant injected with translation initiation-blocking morpholino (data not shown).

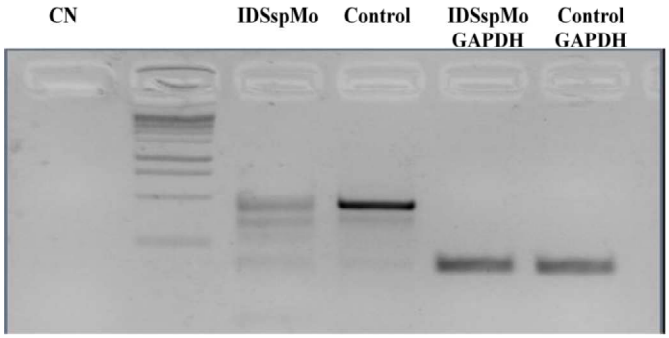

Figure 34: Electrophoresis gel analysis of splicing variants in fish injected with splicing site-blocking morpholino or mismatched morpholino. Morphants show a high number of alternatively spliced transcript variants when compared with controls.

4.3.2 FGF signaling analysis in Ids splicing morphants

Given the previous observations that translation-initiation blocking morpholino for Ids produced a dysregulation of the FGF pathway, I decided to verify whether FGF reporter activity could be similarly affected by the splicing-blocking morpholino using the reporter line (*Tg(Dusp6:d2EGFP)*^{pt6}). Morphant fish displayed a reduction of reporter fluorescence when compared with mismatch control (Fig. 35 A-B). This result was also confirmed by *in situ* hybridization using a riboprobe against *GFP* transcript (Fig. 35 C-D).

Quantitative Real time PCR analysis in whole morphant lysates did not show any obvious difference in the amount of *GFP* transcripts between morphants and controls (Fig. 36). Moreover there was no altered expression of FGF signaling markers *pea3*, *erk1* and *erm1*, in fish injected with the splicing-blocking morpholino, when compared with fish injected with the mismatch morpholino (Fig. 36).

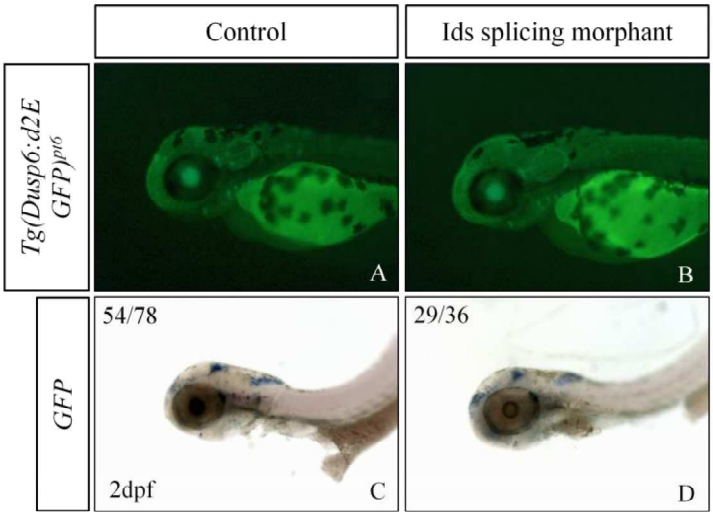

Figure 35: The transgenic line *Tg(Dusp6:d2EGFP)*^{pt6} injected with splicing morpholino or with a mismatched morpholino, show a down regulation of FGF signaling in morphants (B) when compared with mismatch controls (A). Representative *Tg(Dusp6:d2EGFP)*^{pt6} larva after *in situ* hybridization using a riboprobe against GFP transcript (C-D). Three independent experiments have been performed. A modest decrease in reporter expression is visible in morphants

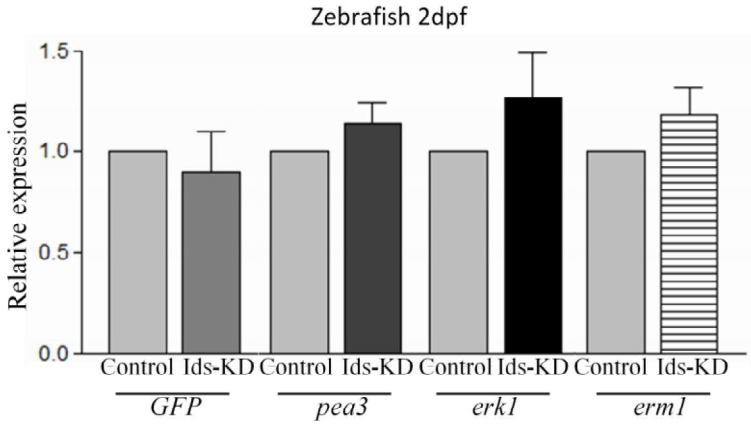

Zebrafish 2dpf			
	Mean	**Standard deviation**	**p-value**
Control	1	/	/
Ids-KD *GFP*	0,90	0,35	0,630
Ids-KD *pea3*	1,14	0,18	0,262
Ids-KD *erk1*	1,27	0,38	0,294
Ids-KD *erm1*	1,18	0,24	0,270

Figure 36: Quantitative Real time PCR analysis performed on pool of 50 *Tg(Dusp6:d2GFP)pt6* fish at 2dpf, injected with the splicing morpholino or mismatched morpholino. Data are expressed as a mean of four independent experiments. There are no statistically differences between morphants and control in terms of GFP and FGF signaling markers expression. (t-test analysis).

4.4 Zebrafish Ids$^{-/-}$ mutant

The transient morpholino-based knockdown model suffers from limited applicability to translational studies, due to the generation of an incomplete enzymatic deficiency and the restricted temporal activity of the morpholino itself, thus, hampering any investigation at late life stages. In order to evaluate the downstream effects of a complete loss of Ids function and to study the pathological alterations in adult fish, I created a stable mutant zebrafish line for the *ids* gene using the Crispr/Cas9 technology.

This new tool for genome editing can target and modify specific gene loci with high efficiency, leading to the rapid creation of zebrafish mutants.

4.4.1 Generation of a mutant zebrafish model for Mucopolysaccharidosis type II

To generate a full loss of Ids function fish model, I selected a target sequence in one of the first two exons of the Ids coding sequence. Mutations lying in the most proximal coding regions have an higher chance of destroying the active site, changing the frameshift and creating a premature stop codon.

To this purpose, I chose a target sequence in the first part of exon 2, generating a mutant fish with a 5 bp deletion (sequence CTACT) from nucleotide 241 to nucleotide 245 (Fig. 37). This deletion causes a frameshift, altering the protein sequence from aminoacid 82 and leading to the generation of a premature stop codon at the aminoacid in position 118 (Fig. 38).

The mutated protein has some characteristics that make this zebrafish mutant a good candidate model for MPSII:

- Deleted aminoacids are highly evolutionary conserved and have an important role for Ids enzymatic activity.

-Since the deletion is located near the active aminoacid Cystein 78, it has a high chance of influencing the active site conformation or change the ligand affinity.

-Early stop codon causes a truncated protein that may alter protein modification and enzymatic function.

Figure 37: Alignment between the mutated sequence (MS) and the reference sequence of a wild type gene (RS). The mutated sequence has been amplified in the region of the deletion and sequenced using a reverse primer. Underlined in red is labeled the target sequence, with the deletion of 5 bp.

Figure 38: A Truncated Ids protein is produced by the Crispr/Cas9 application. Highlighted in red is the target sequence without the five nucleotides. From aminoacid 82 the sequence is altered and the red arrow shows the premature stop codon at aminoacid position 118.

4.4.2 Enzymatic assay of mutated Iduronate 2-sulfatase

To evaluate the enzymatic activity in homozygous mutant ($Ids^{-/-}$) fish, an enzymatic assay in 2dpf $Ids^{-/-}$ larvae was performed and results were compared with that of age-matched heterozygous $Ids^{+/-}$ and WT fish.

As shown in Fig. 39, homozygous mutants, obtained from an incross breeding among $Ids^{-/-}$ fish, exhibited reduced enzymatic activity that was decreased to 2% of that of wild type fish. Since the measured activity is close to the lowest sensitivity threshold of the assay it is plausible that the produced deletion has completely abolished enzymatic activity. It is interesting to notice that heterozygous fish generated from a cross between homozygous female mutants and WT males, have the same enzymatic activity of homozygous fish. On the contrary, heterozygous fish obtained from a cross between WT females and homozygous male mutants have a 60% reduction of enzymatic activity when compared to age-matched WT (Fig. 39). These data may support the idea that at 2dpf the maternal *ids*

transcripts are still present in zebrafish larvae and contribute for almost half of the detected Ids activity.

The same activity assay was also performed in 3 months-old homozygous, heterozygous and WT fish organs (brain, liver and muscle). In all examined organs of $Ids^{-/-}$ fish there was no detectable enzyme activity. On the contrary, $Ids^{+/-}$ fish exhibited the same Iduronate 2-sulfatase activity of WT fish at the brain and muscle level, but half liver enzymatic activity when compared with age-matched control tissues (Fig. 40).

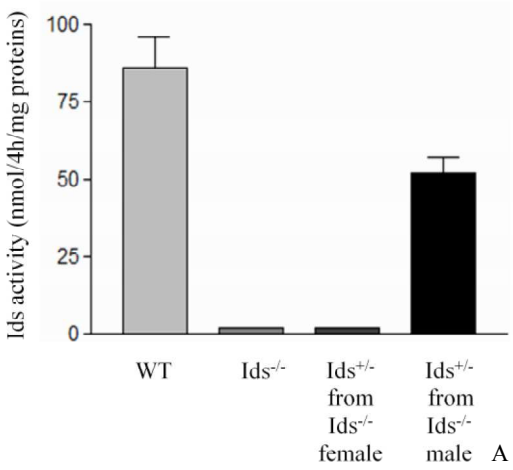

A

	Activity mean	Standard Deviation
WT	86,02	13,66
$Ids^{-/-}$	1,79	0,22
$Ids^{+/-}$ from homozygous female	1,81	0,13
$Ids^{+/-}$ from homozygous male	51,89	6,87

B

Figure 39: (A) Graphic representation of Iduronate 2-sulfatase activity in 2dpf WT, homozygous mutants and heterozygous fish. $Ids^{-/-}$ homozygous mutant and heterozygous fish obtained from incross between homozygous mutant females and WT males almost do not have enzymatic activity. $Ids^{+/-}$ fish obtained from a cross between homozygous males and WT females display almost half enzymatic activity, when compared with age-matched WT fish. (B) Mean enzymatic activity of 2dpf WT, homozygous fish $Ids^{-/-}$, heterozygous fish $Ids^{+/-}$ obtained from cross between homozygous females and wt males or between wt females and homozygous males.

	WT (3 months)			Ids$^{-/-}$ (3 months)			Ids$^{+/-}$ (3 months)		
	Liver	**Brain**	**Muscle**	**Liver**	**Brain**	**Muscle**	**Liver**	**Brain**	**Muscle**
Activity mean	4,24	2,90	1,93	0,62	0,72	0,45	2,35	2,87	1,97
Standard deviation	0,09	0,06	0,64	0,26	0,52	0,14	0,03	1,10	0,66

A

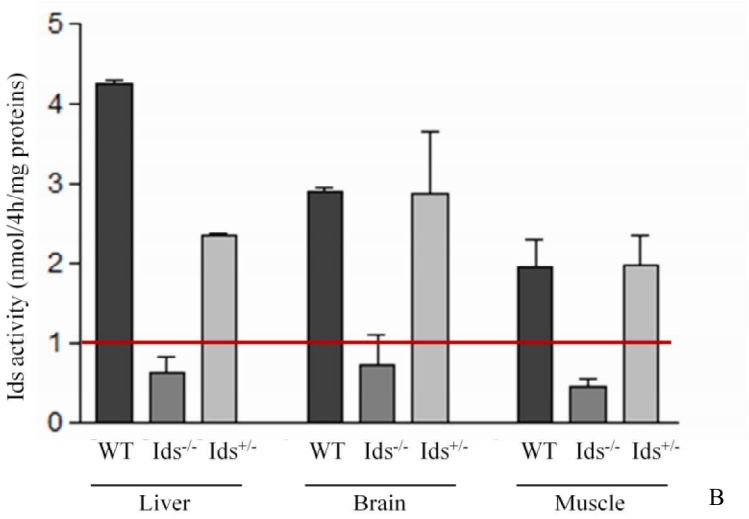

B

Figure 40: (A) Mean enzymatic activity of Iduronate 2-sulfatase in liver, brain and muscle of 3 months-old WT, homozygous Ids$^{-/-}$ and heterozygous Ids $^{+/-}$ fish. (B) Graphic representation of Iduronate 2-sulfatase activity in organs of 3 months WT, homozygous Ids$^{-/-}$ and heterozygous Ids$^{+/-}$ fish. The red line represent the assay sensitivity; values under the line may be considered as "no activity".

4.4.3 Ids$^{-/-}$ mutant fish characterization

Mutant fish have the same growth rate of wild type fish in the first week, but they show an increased size (almost 12%) at 15dpf (Fig. 41 A-B). Mutants also display altered head formation with the presence of a bending on the midbrain (Fig. 41 C-D).

Adult Ids$^{-/-}$ fish don't show significant external pathological manifestations that can allow their easy identification. In adult mutant fish only a dorsal and ventral swelling can be detected (Fig. 41). Homozygous fish can reach sexual maturity and produce offspring; however they exhibit a shorter lifespan when compared with wild type siblings.

At 3 months of age Ids$^{-/-}$ mutant fish show increased liver size and volume when compared with age-matched wild type fish (Fig. 42).

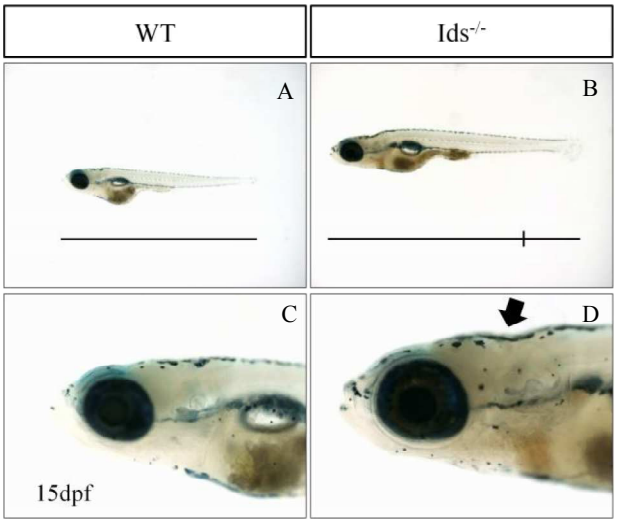

Figure 41: (A-B) Whole-mount 15dpf WT (A) and Ids$^{-/-}$ fish (B). Ids$^{-/-}$ fish display a bigger length and size when compared with age-matched control fish. The bottom line shows the different length. (C-D) High magnification of the WT (C) and Ids$^{-/-}$ (D) head. The arrow indicates the bending on midbrain in mutant fish.

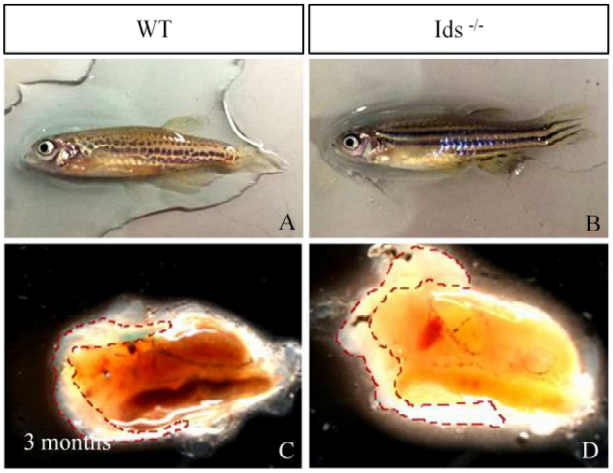

Figure 42: (A-B) Whole mount 3 months'old WT fish (A) and Ids$^{-/-}$ fish (B) . (C-D) Representative liver from 3-month-old control fish (C) and Ids-/- fish (D), showing the enlarged liver size in the homozygous mutant.

4.4.4 Homozygous mutant fish display altered ossification at 6dpf and 15dpf

To evaluate the downstream effects of Ids loss of function on bone formation, I performed Alizarin red staining in 6dpf and 15dpf Ids$^{-/-}$ mutant and age-matched wild type fish. Ids$^{-/-}$ mutant fish at 6dpf showed increased Alizarin staining of bone elements, when compared with age-matched wild type fish. A different shape and size of some bone elements was noticeable in Ids$^{-/-}$ mutant fish. For instance, the opercle in the proximal region appeared bigger when compared with the one of age-matched wild type fish (Fig. 43). A further increased Alizarin staining of bone elements was detected on 15dpf Ids$^{-/-}$ mutant fish (Fig. 44), supporting the hypothesis that at early stages of development in mutant fish bone mineralization occurs more rapidly when compared with age-matched wild type fish.

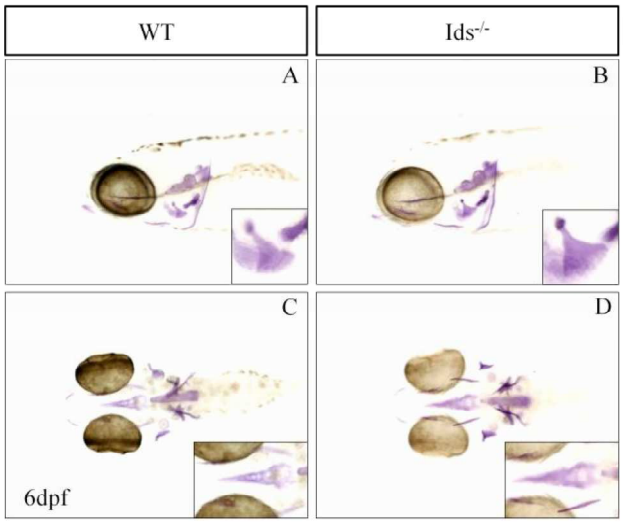

Figure 43: Alizarin red staining in 6dpf WT fish and Ids-/- fish. (A-B) Lateral head view with opercle high magnification. (C-D) High magnification of the parasphenoid. Homozygous fish (B) (D) display increased mineralization when compared with age-matched control fish (A) (C). Top images are lateral view, with anterior to the left, while bottom images are dorsal view with anterior to the left.

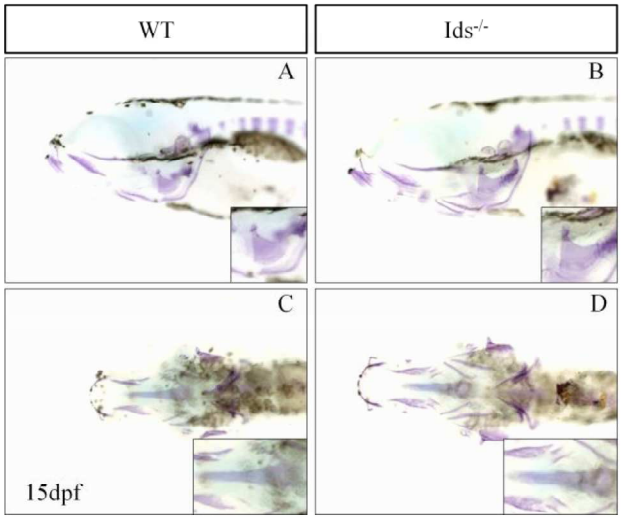

Figure 44: Alizarin red staining in 15dpf WT fish and Ids-/- fish. (A-B) Lateral head view with opercle high magnification. (C-D) Dorsal head view with parasphenoid high magnification. Homozygous fish (B) (D) display a major ossification compared to age-matched control fish (A) (C). Top images are lateral view, with anterior to the left, while bottom images are dorsal view with anterior to the left.

4.4.5 Reporter zebrafish lines for bone markers

To evaluate the effects of Ids functional impairment on the bone differentiation program, I took advantage of specific transgenic fish lines *Tg(Col2a1aBAC:mCherry)*^{hu5900}, *TgBAC(col10a1:Citrine)*^{hu7050} and *Tg(Ola.Sp7:NLS-GFP)*^{zf132}. These transgenic fish express a fluorescent protein under the control of cartilage/bone cell lineage-specific promoters. In particular, I put homozygous mutants in transgene background and I analyzed the offspring from incrossed transgenic mutant carriers.

4.4.5.1 Collagen II expression in Ids$^{-/-}$ mutant fish

Transgene expression was evaluated in *Tg(Col2a1aBAC:mCherry)*^{hu5900} at four time points: 4dpf, 7dpf (Fig. 45), 11dpf and 15dpf (Fig. 46).

In particular, confocal analysis of fluorescent reporter protein expression in the craniofacial cartilages ceratohyal, palatoquadrate, Meckel's cartilage and basihyal of homozygous and age-matched wild type siblings, was carried out. Since Collagen II is expressed by chondrocytes, the amount of reporter protein in *Tg(Col2a1aBAC:mCherry)*^{hu5900} reflected the amount of cartilage.

Ceratohyal cartilage: This cartilage is a component of the branchial arch. At 4dpf there was difference between WT and mutant fish. However, at 7dpf it was possible to notice a rapid increase of cartilage volume in Ids$^{-/-}$ fish and the difference was statistically significant when compared to wild type control fish. Mutant fish displayed a rapid decrease of ceratohyal cartilage volume between 7dpf and 11dpf and the final cartilage volume in mutants was smaller when compared with age-matched WT controls (Fig. 47).

Palatoquadrate cartilage: This is a dorsal component of the mandibular arch. Mutant fish showed increased cartilage volume at 7dpf when compared with age-matched controls, and the difference was statistically significant. At 4dpf, 11dpf and 15dpf, Ids$^{-/-}$ exhibited a similar cartilage volume when compared with age-matched WT fish (Fig. 48).

Meckel's cartilage: It's a ventral component of the mandibular arch. Mutant fish demonstrated the same cartilage volume of control fish at 4dpf and 11dpf. However, Ids$^{-/-}$ showed a statistically significant increased volume at 7dpf and decreased volume value at 15dpf, respectively, when compared with age-matched control fish (Fig. 49).

Basihyal cartilage: It's a component of the pharyngeal arch. WT fish and Ids$^{-/-}$ fish showed the same cartilage volume at 4dpf. Control fish showed an almost linear increase in cartilage volume up to 15dpf, while mutant fish demonstrated a rapid increase of the volume between 4dpf and 7dpf and a decrease from 7dpf and 15dpf (Fig. 50).

Summarizing, these results showed that while WT fish displayed a linear growth of the cartilages volume from 4dpf to 15dpf, mutant Ids$^{-/-}$ fish cartilage elements developed with a different trend that was the same for all the analyzed cartilages. There were no differences in the cartilage volume between mutant fish and controls at 4dpf, but at 7dpf Ids$^{-/-}$ fish showed a statistically significant rapid increase of cartilage volume. From 7dpf to 11dpf there was indeed a rapid decrease of cartilage volume in mutant fish which was consistently kept reduced at later life stages, i.e. from 11dpf to 15dpf .

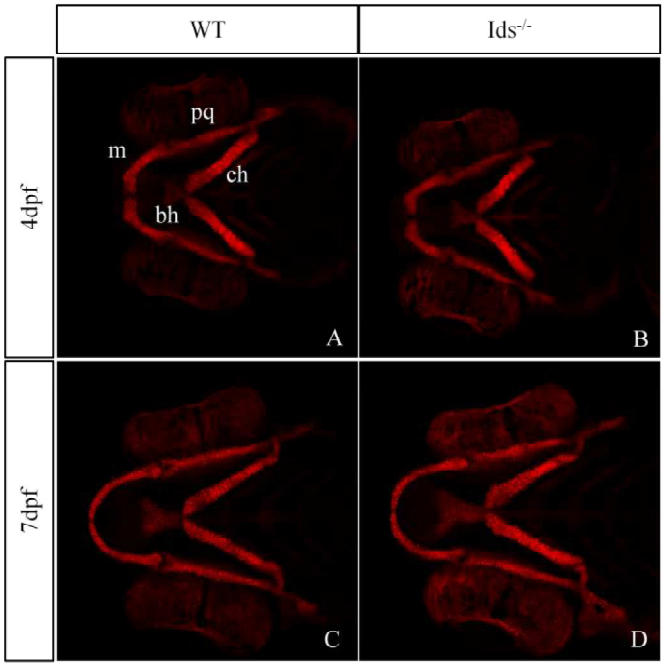

Figure 45: Representative image of a 4 dpf (top) and 7 dpf (bottom) wild type and Ids mutant *Tg(Col2a1aBAC:mCherry)*^{hu5900} fish. Ids$^{-/-}$ fish display increased fluorescence when compared with age-matched controls. bh: basihyal; ch: ceratohyal; m: Meckel's cartilage; pq: palatoquadrate. All images are ventral views, with anterior to the left.

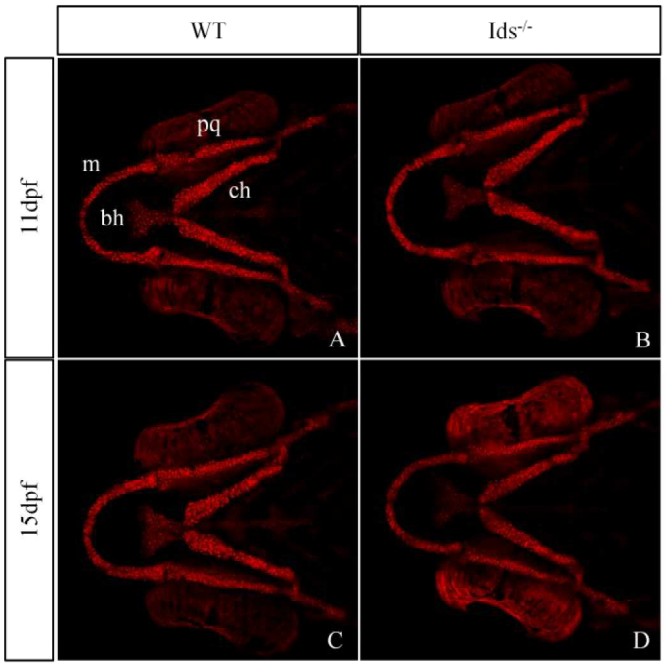

Figure 46: Representative image of a 11 dpf (top) and 15 dpf (bottom) wild type and Ids mutant *Tg(Col2a1aBAC:mCherry)*^{hu5900} fish. bh: basihyal; ch: ceratohyal; m: Meckel's cartilage; pq: palatoquadrate. All images are ventral views, with anterior to the left.

Ceratohyal (ch)								
	4dpf		7dpf		11dpf		15dpf	
	WT	Ids$^{-/-}$	WT	Ids$^{-/-}$	WT	Ids$^{-/-}$	WT	Ids$^{-/-}$
Mean (µm^3)	219183	210809	259782	317325	278898	261526	288963	262965
Standard deviation	30665	28641	40798	28240	71514	37857	42748	32256
p value	0,578		0,019		0,502		0,148	

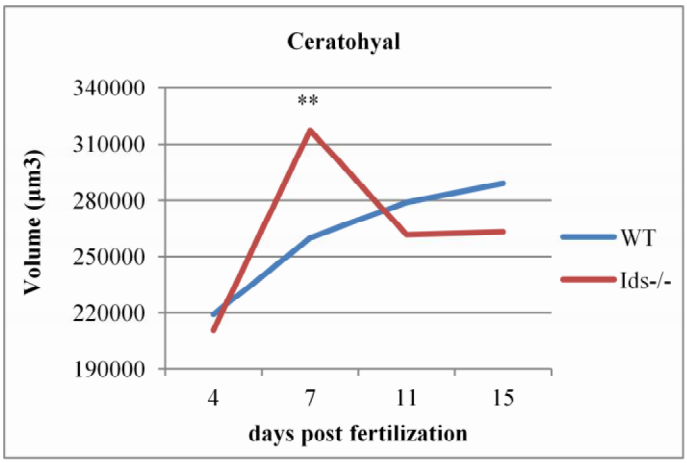

Figure 47: Mean Imaris-calculated volume of Collagen II transgene expression in the ceratohyal cartilage of 4dpf, 7dpf, 11dpf and 15dpf zebrafish Ids$^{-/-}$ mutant and WT. (t-test **p<0,02).

Palatoquadrate (pq)								
	4dpf		7dpf		11dpf		15dpf	
	WT	Ids$^{-/-}$	WT	Ids$^{-/-}$	WT	Ids$^{-/-}$	WT	Ids$^{-/-}$
Mean (µm^3)	143579	121579	209599	263114	224325	235145	247079	247977
Standard deviation	38269	35923	11813	36950	75389	25006	34642	64178
p value	0,3108		0,0053		0,7217		0,9776	

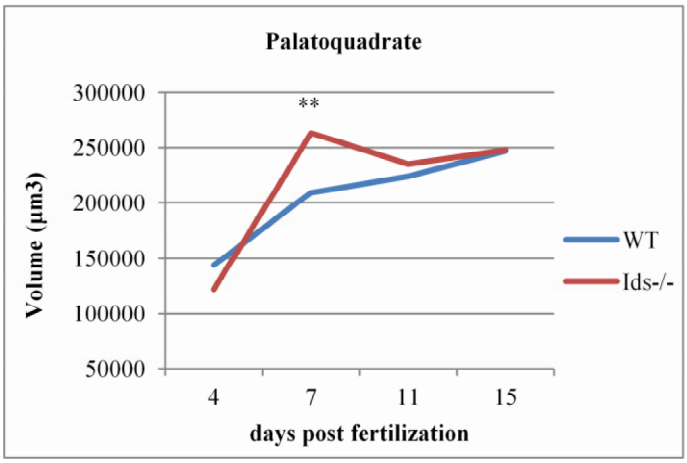

Figure 48: Mean Imaris-calculated volume of Collagen II transgene expression in the palatoquadrate cartilage of 4dpf, 7dpf, 11dpf and 15dpf zebrafish Ids$^{-/-}$ mutant and age-matched WT. (t-test **p<0,02).

Meckel's cartilage (m)								
	4dpf		7dpf		11dpf		15dpf	
	WT	Ids$^{-/-}$	WT	Ids$^{-/-}$	WT	Ids$^{-/-}$	WT	Ids$^{-/-}$
Mean (µm^3)	108507	104244	155718	176688	146756	140800	164330	143951
Standard deviation	14947	22918	12769	8813	52355	25868	25922	23064
p value	0,6477		0,006		0,7293		0,1004	

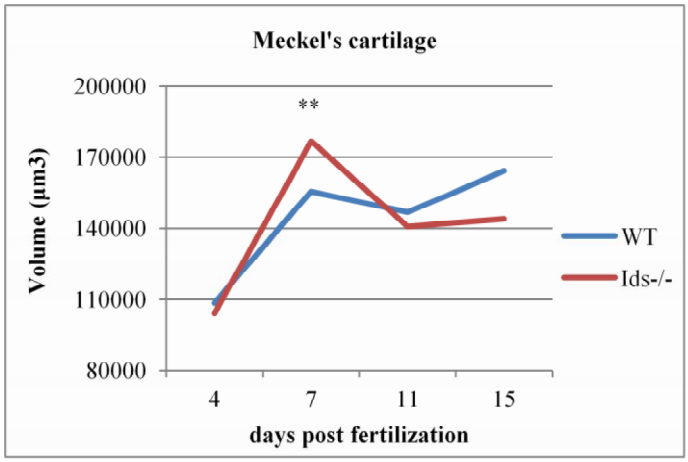

Figure 49: Mean Imaris-calculated volume of Collagen II transgene expression in the Meckel's cartilage of 4dpf, 7dpf, 11dpf and 15dpf zebrafish Ids$^{-/-}$ mutant and age-matched WT. (t-test **p<0,02).

Basihyal (bh)								
	4dpf		7dpf		11dpf		15dpf	
	WT	Ids$^{-/-}$	WT	Ids$^{-/-}$	WT	Ids$^{-/-}$	WT	Ids$^{-/-}$
Mean (µm^3)	39948	45956	54531	117506	52040	68934	77938	61356
Standard deviation	19731	23933	20764	31125	34128	12174	30706	24873
p value	0,6981		0,0434		0,2841		0,3727	

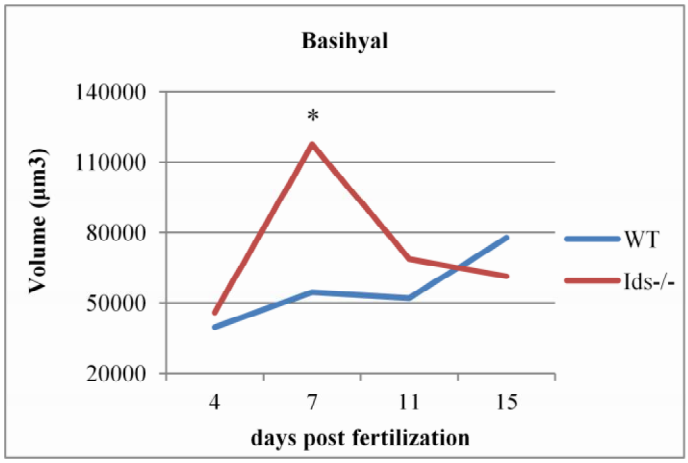

Figure 50: Mean Imaris-calculated volume of Collagen II transgene expression in the basihyal cartilage of 4dpf, 7dpf, 11dpf and 15dpf zebrafish Ids$^{-/-}$ mutant and WT. (t-test *p<0,05).

To evaluate potential head developmental abnormalities occurring in Ids$^{-/-}$ mutants, I performed in silico analysis of the distance between the palatoquadrate cartilages, the one between the Meckel's cartilage and the ceratohyal cartilages, the ratio of these two values, and the angle between the left and the right ceratohyal cartilages in agreement with a previous investigation (Fig. 51) (Petrey et al., 2012).

As regards the distance between palatoquadrate cartilages (PQ-PQ) I obtained the following results: at 4 dpf mutant fish display a smaller PQ-PQ distance when compared with age-matched WT. This parameter similarly increased up to 7dpf, while from 7dpf to 11dpf the distance between palatoquadrate cartilages increased in Ids$^{-/-}$ fish and decreased in WT fish. From 11dpf to 15dpf the distance indeed decreased in Ids$^{-/-}$ fish and increased in WT fish, reaching the same value at 15dpf (Fig. 52). This data represent the head width thus suggesting a different rate of head development between WT fish and Ids$^{-/-}$ fish.

Concerning the distance from the Meckel's cartilage to the ceratohyal cartilages (M-CH): I detected a similar increased distance in Ids$^{-/-}$ and WT fish from 4 dpf to 11 dpf. From 11dpf to 15dpf, WT fish demonstrated an increased M-CH distance while Ids$^{-/-}$ did not display any changes (Fig. 53). Therefore, while the head length was linearly growing in WT fish, mutant fish showed a growth arrest from 11dpf.

When considering the ratio between the PQ-PQ distance and the M-CH distance WT fish and mutant fish displayed a different behavior from 4dpf to 15dpf. The ratio value decreased in a linear way in WT fish, while Ids$^{-/-}$ fish showed a more rapid decrease from 4dpf to 7dpf and a slower decrease from 7dpf to 15dpf when compared with age-matched WT controls (Fig. 54).

Concerning the angle between the left and the right ceratohyals (CH to CH angle): WT fish and Ids$^{-/-}$ fish displayed a different trend. WT fish showed a linear decrease in the angle value from 4dpf to 15dpf. On the contrary, mutant fish exhibited a decreased angle size from 4dpf to 7dpf, an increased size from 7dpf to 11dpf and then a decreased angle size from 11dpf to 15dpf (Fig. 55).

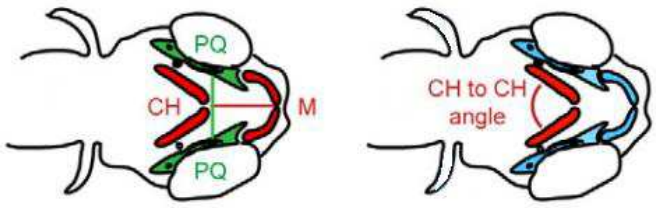

Figure 51: Representation of parameters analyzed. PQ: palatoquadrate cartilage, CH: ceratohyal cartilage, M: Meckel's cartilage. Image modified from Petrey et al., 2012.

PQ-PQ

	4dpf			7dpf		
	Mean	Standard deviation	p-value	Mean	Standard deviation	p-value
WT	327156	17220,80	0,120	343389	10237,89	0,565
Ids$^{-/-}$	311671	3465,63		347151	2295,27	

	11dpf			15dpf		
	Mean	Standard deviation	p-value	Mean	Standard deviation	p-value
WT	327161	33975,33	0,107	334340	16336,71	0,989
Ids$^{-/-}$	353826	20189,43		334578	30572,41	

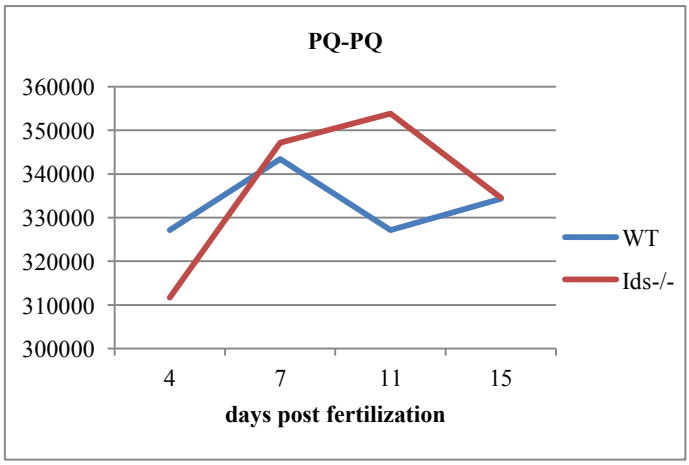

Figure 52: Distance between palatoquadrate cartilages in Ids$^{-/-}$ and WT fish at 4dpf, 7dpf, 11dpf and 15dpf. Values in the Y-axis are expressed as arbitrary units.

M-CH

	4dpf			7dpf		
	Mean	Standard deviation	p-value	Mean	Standard deviation	p-value
WT	158759	23265,86	0,783	191214	12944	0,087
Ids$^{-/-}$	154359	25115,41		207180	2687,68	

	11dpf			15dpf		
	Mean	Standard deviation	p-value	Mean	Standard deviation	p-value
WT	210688	23101,37	0,230	245334	15948,98	0,068
Ids$^{-/-}$	225799	19776,10		225640	13454,78	

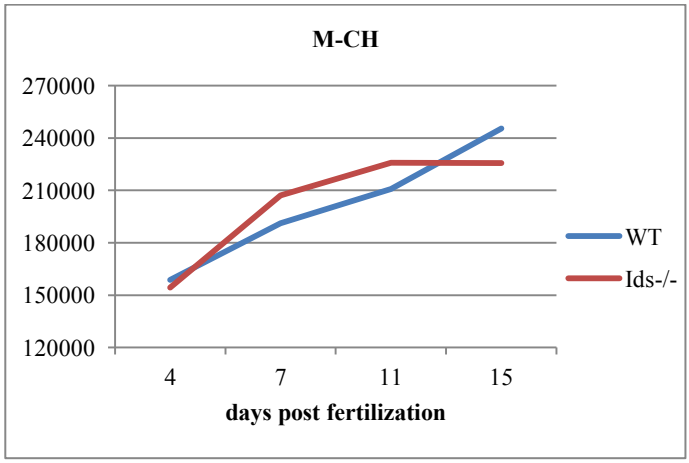

Figure 53: Distance between the Meckel's cartilage and ceratohyal cartilage in $Ids^{-/-}$ and WT fish at 4dpf, 7dpf, 11dpf and 15dpf. Values in the Y-axis are expressed as arbitrary units.

PQ-PQ / M-CH

	4dpf			7dpf		
	Mean	Standard deviation	p-value	Mean	Standard deviation	p-value
WT	2,08	0,20	0,783	1,80	0,11	0,358
$Ids^{-/-}$	2,07	0,42		1,68	0,03	

	11dpf			15dpf		
	Mean	Standard deviation	p-value	Mean	Standard deviation	p-value
WT	1,56	0,12	0,777	1,37	0,07	0,381
$Ids^{-/-}$	1,57	0,10		1,48	0,13	

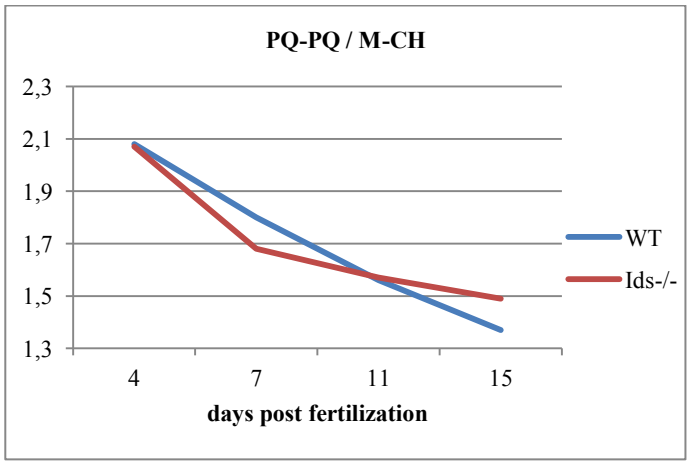

Figure 54: Ratio between the PQ-PQ/ distance and the M-CH distance in $Ids^{-/-}$ and WT fish at 4dpf, 7dpf, 11dpf and 15dpf. Values in the Y-axis are expressed as arbitrary units.

CH to CH angle

	4dpf			7dpf		
	Mean	Standard deviation	p-value	Mean	Standard deviation	p-value
WT	78,48	5,73	0,377	64,00	11,01	0,461
Ids$^{-/-}$	89,94	16,27		60,21	2,05	

	11dpf			15dpf		
	Mean	Standard deviation	p-value	Mean	Standard deviation	p-value
WT	57,95	12,81	0,412	53,67	2,89	0,672
Ids$^{-/-}$	63,53	6,99		53,42	7,08	

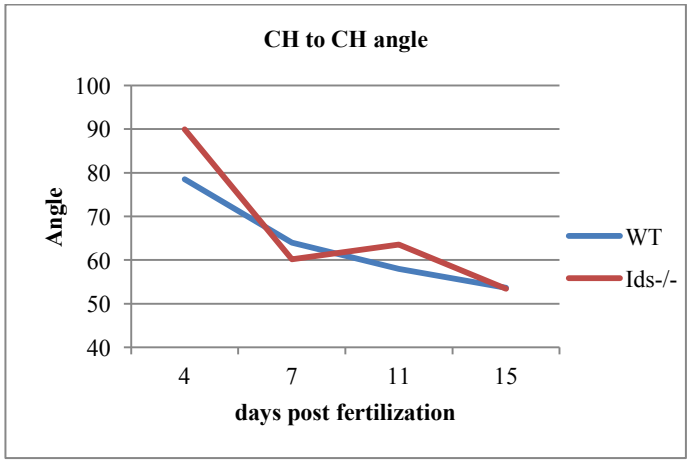

Figure 55: Angle between the left and the right ceratohyals in Ids$^{-/-}$ and WT fish at 4dpf, 7dpf, 11dpf and 15dpf. Values in the Y-axis are expressed as arbitrary units.

4.4.5.2 Collagen X expression in Ids$^{-/-}$ mutant fish

To analyze collagen X expression in WT fish and Ids$^{-/-}$ fish I took advantage of the transgenic reporter line *TgBAC(col10a1:Citrine)*^{hu7050}. Homozygous mutant and age-matched wild type transgenic fish were stained *in vivo* with Alizarin red, to evaluate the extent of bone mineralization together with Collagen X expression during bone development. CollagenX is expressed in hypertrophic chondrocytes and it is involved in matrix mineralization (Shen et al., 2005).

To this purpose I examined three bones: opercle, cleithrum and brachiostegal ray at two time points of development: 7dpf and 15dpf.

At 7dpf and 15dpf WT fish display a reduced number of cells expressing the collagen X transgene compared to age-matched Ids$^{-/-}$ fish. However, the signal intensity appeared stronger in WT when compared with mutant fish in all analyzed bones. The opercle was the bone that showed more differences in signal intensity between mutant and WT fish. In Ids$^{-/-}$ fish collagen X was expressed in all bone surfaces and particulary in the opercle

proximal region, which is the most osteogenic region of the opercle. On the contrary, WT fish showed a lower collagen X expression.

In WT fish, cleithrum displayed more collagen X-expressing cells, especially in the upper and lower ends of the bone, while in $Ids^{-/-}$ cleithrum the signal was evenly expressed (Fig. 56 and 57 A, D).

Alizarin red staining was more intense in WT fish opercle when compared with the mutant fish one. However, the staining in the mutant fish opercle was spread in a larger surface when compared with the WT fish one (Fig. 56 and 57 B, E).

Further in silico-based analysis of CollagenX expression demonstrated that at 7dpf collagen X is generally more expressed in mutant fish bones, when compared with those of age-matched controls. In the brachiostegal ray the degree of increased expression, expressed as "volume value" is almost three time (Fig. 58) higher, while in the opercle (Fig. 59) and in the cleithrum is two time and half time higher (Fig. 60) in $Ids^{-/-}$ fish respectively, when compared with age-matched WT fish. At 15dpf there were no differences in Collagen X expression in mutant fish and WT fish bones (Fig. 58, 59 and 60).

To further evaluate other potential differences in bone development between mutant fish and WT fish, I examined the in-silico reconstruction of collagen X expression profile in the opercle. At 7dpf $Ids^{-/-}$ fish opercle display on average a different opercle shape and an increased area of collagen X expression when compared with WT opercle. In mutant fish the opercle proximal region size is increased and has a shape that is expected at later stages. At 15dpf the $Ids^{-/-}$ opercle maintain a different shape when compared with the WT opercle, with a swelling of its proximal part (Fig. 61). Since collagen X is expressed by osteoblasts that in turn release mineralized matrix and induce bone growth, an increased amount of this marker expression induces a more rapid increased rate of ossification. Therefore, 7dpf mutant fish exhibit a rapid increase in bone development which is reduced at later stages, while WT fish display a linear increase in the opercle growth.

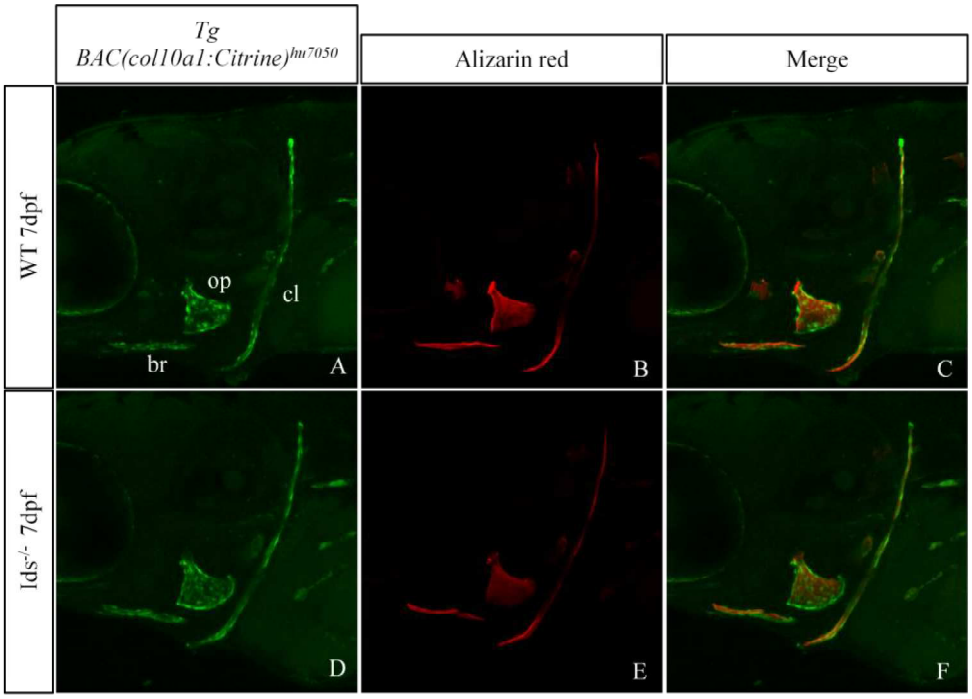

Figure 56: *TgBAC(col10a1:Citrine)* ^{hu7050} Ids$^{-/-}$ fish and WT control stained *in vivo* with Alizarin red. (A, D) At 7dpf WT fish display a reduced number of cells that express CollagenX when compared with Ids$^{-/-}$ fish, but in WT the signal is stronger than in mutants. (B, E) Alizarin red staining is stronger in WT fish when compared with mutants. br: brachiostegal ray; cl: cleithrum; op: opercle.

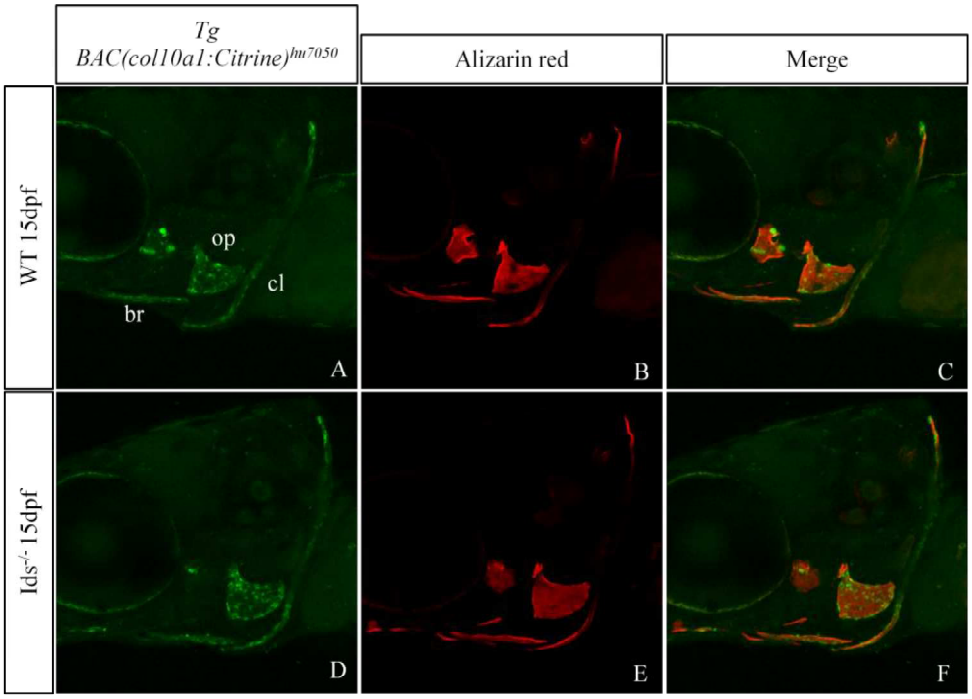

Figure 57: *TgBAC(col10a1:Citrine)*^{hu7050} Ids$^{-/-}$ fish and WT controls stained *in vivo* with Alizarin red. (A, D) At 15dpf WT fish display a reduced number of cells collagenX-expressing cells compared to Ids$^{-/-}$ fish, but in WT the signal is stronger than in mutants.

(B, E) Alizarin red staining is stronger in WT fish compared to mutants. br: brachiostegal ray; cl: cleithrum; op: opercle.

Brachiostegal ray (Collagen X)				
	7dpf		15dpf	
	WT	Ids$^{-/-}$	WT	Ids$^{-/-}$
Volume Mean (µm^3)	10590	30347	9673	9298
Standard deviation	7321	13641	5618	0
p-value	0,0434			

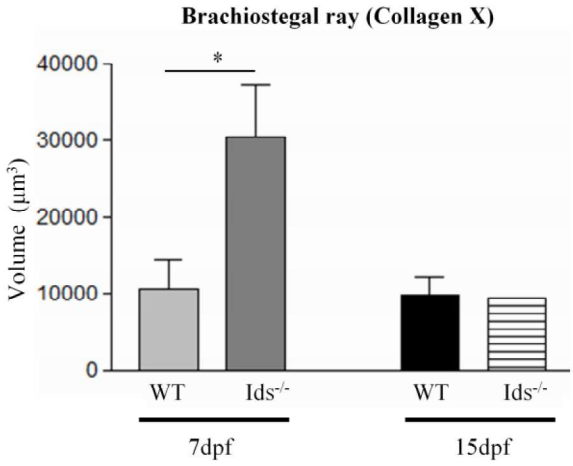

Figure 58: Volume of collagenX expression in the brachiostegal ray of 7dpf and 15dpf Ids$^{-/-}$ and WT transgenics. At 7dpf there is a statistically significant increase of collagen X volume expression in mutants when compared with age-matched WT fish. (t-test *p<0,05).

Opercle (Collagen X)				
	7dpf		15dpf	
	WT	Ids$^{-/-}$	WT	Ids$^{-/-}$
Volume Mean (µm^3)	47181	87187	39106	28163
Standard deviation	26274	32075	14863	29118
p-value	0,1019		0,4856	

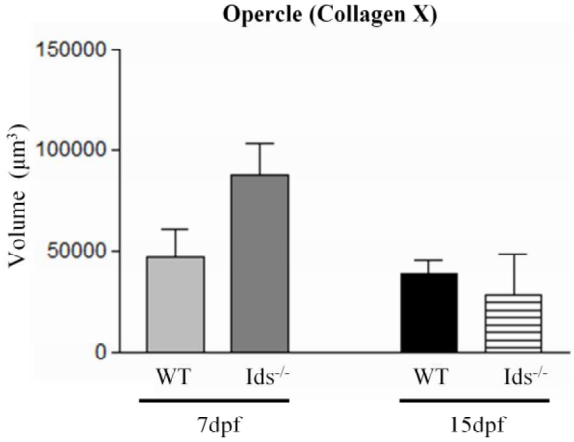

Figure 59: CollagenX expression in the opercle of 7dpf and 15dpf Ids$^{-/-}$ and age-macthed WT fish . At 7dpf a light but not significantly increased volume of collagen X expression is detected in mutants when compared with age-matched WT.

Cleithrum				
	7dpf		15dpf	
	WT	Ids$^{-/-}$	WT	Ids$^{-/-}$
Volume Mean (μm^3)	50325	78141	15689	16515
Standard deviation	7877	13384	5540	8080
p-value	0,0116		0,8724	

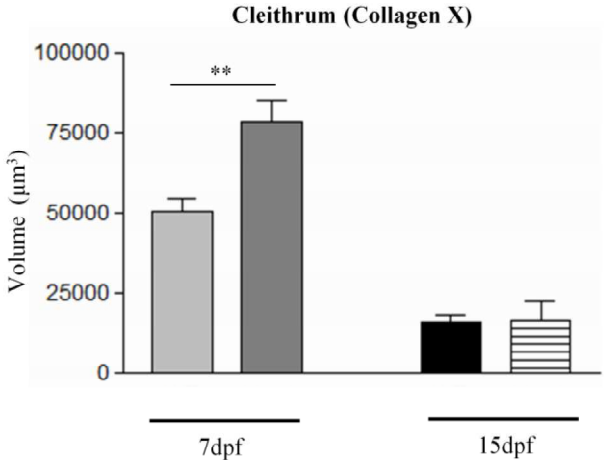

Figure 60: CollagenX expression in the cleithrum of 7dpf 15dpf Ids$^{-/-}$ and WT transgenics . At 7dpf a statistically significant increase in collagen X expression volume is detected in mutants when compared with age-matched WT. (t-test **p<0,02).

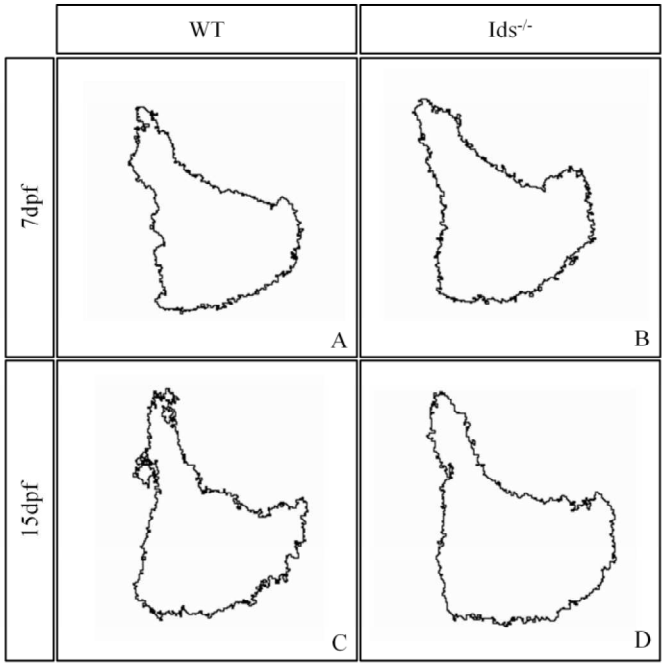

Figure 61: Opercle's profile of Collagen X expression. Ids mutants show a different opercle shape when compared with age-matched WT at 7dpf (A, B) and 15dpf (C, D).

4.4.5.3 Osterix expression in Ids$^{-/-}$ mutant fish

I used the transgenic reporter line *Tg(sp7:EGFP)^{b1212}* to analyze the expression of Osterix in WT fish and Ids$^{-/-}$ fish. Osterix is an osteoblast marker and it is required for osteoblast differentiation and bone formation (Baek et al., 2009).

I studied Osterix expression in three bones: brachiostegal ray, opercle and cleithrum at 7dpf and 15 dpf WT and Ids$^{-/-}$ fish.

At 7dpf and 15dpf mutant fish display the same Osterix expression intensity of WT fish. However, the region of transgene expression in the brachiostegal ray and opercle of mutant fish appears wider when compared with control fish. Conversely, in the cleithrum a decreased fluorescence is observed in Ids$^{-/-}$ fish, when compared with age-matched WT fish (Fig. 62 and 63 A, D).

By using an *in silico* approach to analyze transgene expression, I found that Ids mutant fish showed a statistically significant increased expression of Osterix in the brachiostegal ray and opercle at 7dpf when compared with age-matched controls, while similar transgene expression levels were detected in the same regions at 15dpf (Fig. 64 and 65). In the cleithrum there were no differences of osterix expression between WT and Ids-/- fish at 7dpf , while at 15dpf mutants displayed a statistically significant decrease of osterix expression when compared with control fish (Fig. 66).

To summarize, while in both the opercle and brachiostegal ray of Ids mutants increased osterix transgene expression levels were detectable at 7dpf, the cleithrum was characterized by a significant decreased osterix expression at 15 dpf. To further evaluate changes in bone development caused by Ids loss of function, I analyzed, by in silico analysis, the opercle shape of *Tg(sp7:EGFP)*^{b1212} mutants and age-matched WT. At 7dpf mutants opercle displayed an increased size when compared with that of age-matched WT, especially in the proximal regions. At 15 dpf Ids-/- opercle appeared very similar to the bone of mutant fish at 7dpf (Fig. 67).

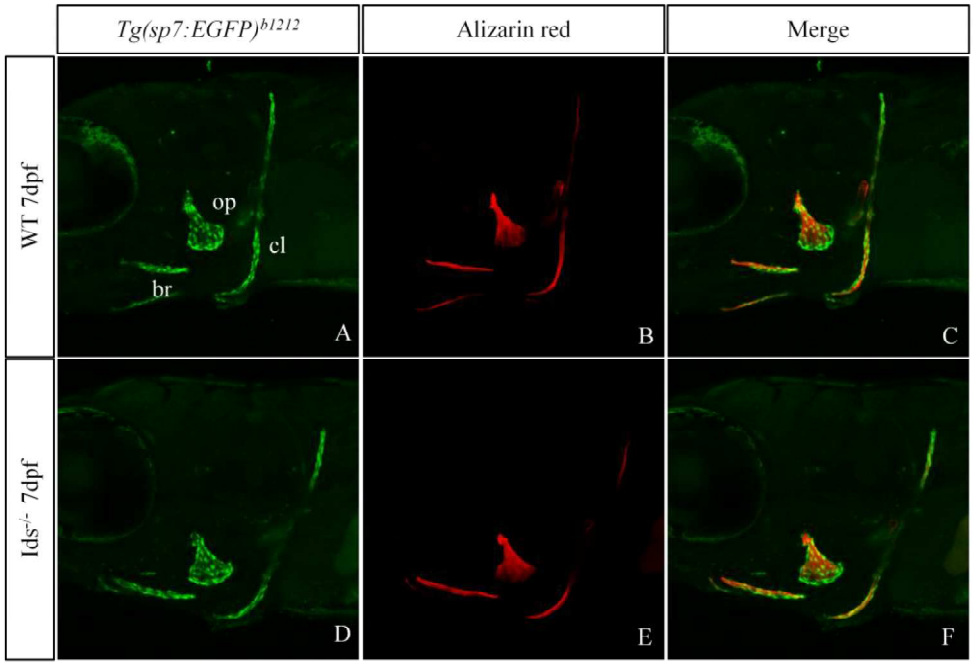

Figure 62: *Tg(sp7:EGFP)*^{b1212} Ids$^{-/-}$ fish and controls stained *in vivo* with Alizarin red. (A, D) At 7dpf WT fish display a reduced number of Osterix-expressing cells when compared with age-matched Ids$^{-/-}$ fish, but in WT the signal is stronger than in mutants. (B, E) Alizarin red staining is stronger in WT fish compared to mutants. br: brachiostegal ray; cl: cleithrum; op: opercle.

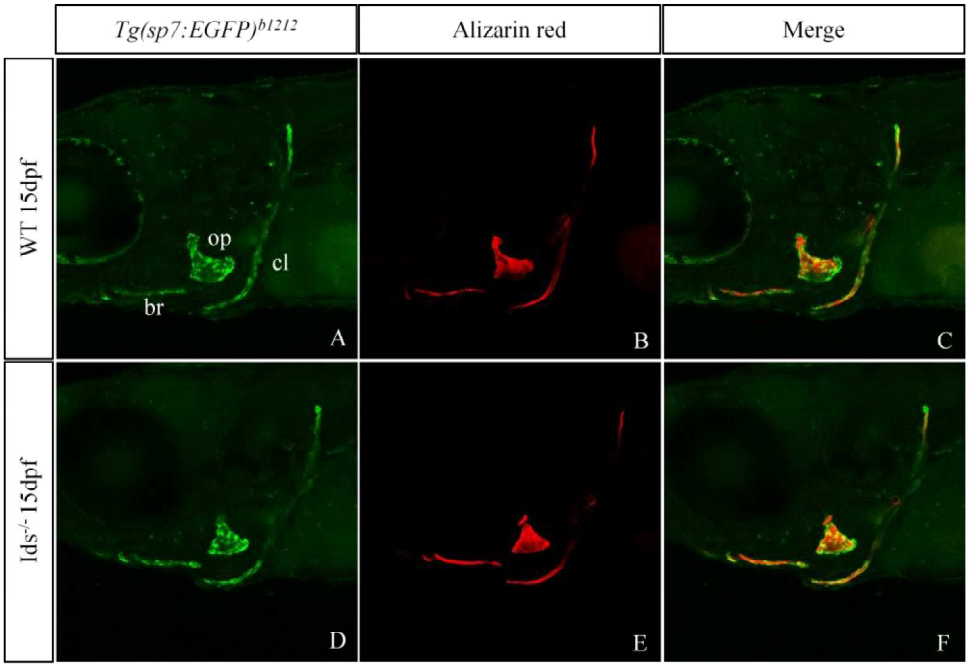

Figure 63: *Tg(sp7:EGFP)*^{b1212} Ids$^{-/-}$ fish and controls stained *in vivo* with Alizarin red. (A, D) At 7dpf WT fish display a reduced number of Osterix-express in cells when compared with age-matched Ids$^{-/-}$ fish. (B, E) Alizarin red staining is stronger in WT fish compared to mutants. br: brachiostegal ray; cl: cleithrum; op: opercle.

Brachiostegal ray (Osterix)				
	7dpf		15dpf	
	WT	Ids $^{-/-}$	WT	Ids $^{-/-}$
Volume Mean (μm^3)	17836	34757	19347	17516
Standard deviation	7217	6379	9503	4938
p-value	0,0216		0,7818	

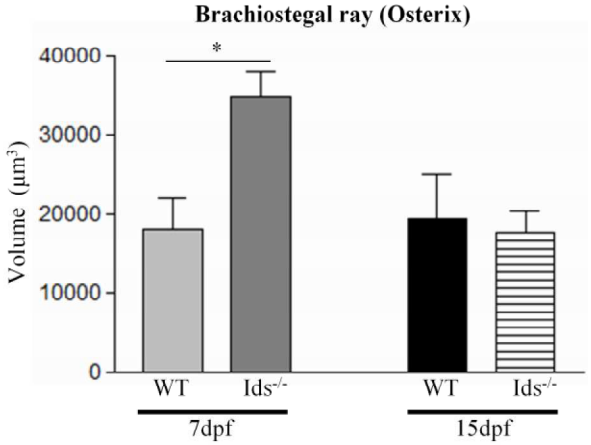

Figure 64: Osterix expression volume in brachiostegal ray of Ids-/- and WT fish. At 7dpf there is a statistical significant increase of osterix expression in mutants when compared with age-matched controls. At 15 dpf there are no differences between Ids$^{-/-}$ and WT. (t-test *p<0,05).

Opercle (Osterix)				
	7dpf		15dpf	
	WT	Ids $^{-/-}$	WT	Ids $^{-/-}$
Volume Mean (μm^3)	41731	92159	100713	70102
Standard deviation	29135	21332	28790	6701
p-value	0,0315		0,1473	

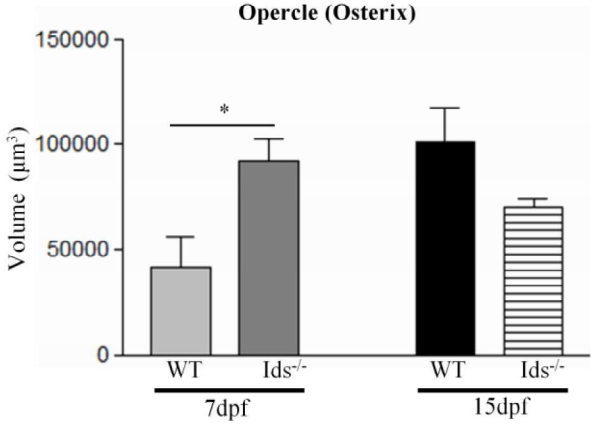

Figure 65: Volume of Osterix expression in the opercle of Ids$^{-/-}$ and WT fish. At 7dpf there is a statistically significant increase of osterix expression in mutants when compared with controls. At 15 dpf there are no differences between Ids$^{-/-}$ and WT. (t-test *p<0,05).

Cleithrum (Osterix)					
	7dpf			15dpf	
	WT	Ids $^{-/-}$		WT	Ids $^{-/-}$
Volume Mean (μm^3)	70160	55469		51240	24601
Standard deviation	38145	19049		4917	5059
p-value	0,5165			0,0028	

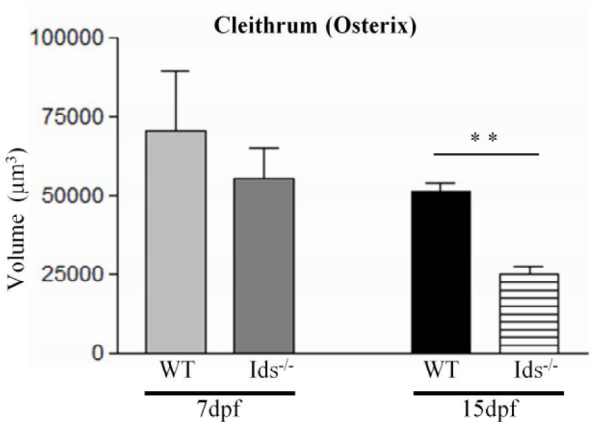

Figure 66: Volume of Osterix expression in cleithrum of Ids$^{-/-}$ and WT fish. At 7dpf there are no differences between Ids$^{-/-}$ and WT. At 15 dpf there is a statistically significant decrease of osterix expression in mutants when compared with age-matched controls. (t-test **p<0,02).

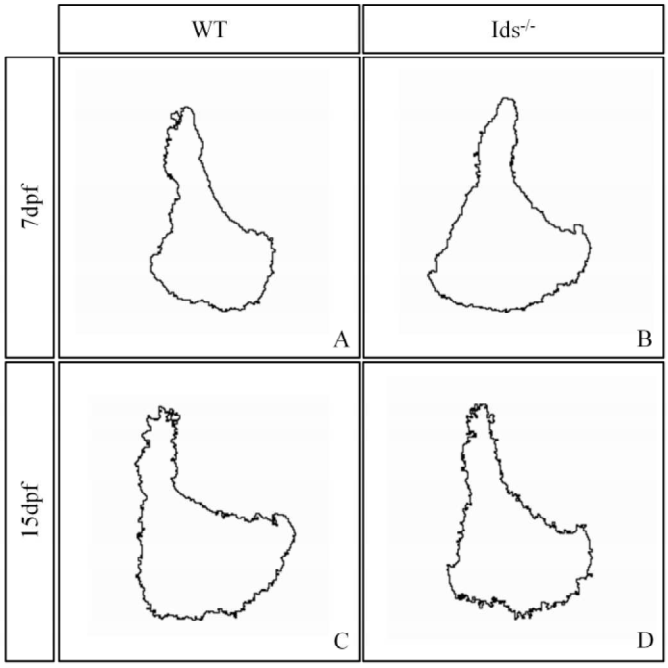

Figure 67: Osterix expression profile in the opercle of Ids$^{-/-}$ and WT fish. (A) (B) At 7dpf there is a larger transgene expression domain in the opercle of mutants when compared with that of age-matched controls. (C) (D) At 15dpf osterix expression appears increased in the opercle of WT fish, while in the mutants opercle the transgene expression domain appears slightly reduced.

4.4.6 Ids$^{-/-}$ mutant fish display altered mineralization

To analyze bone mineralization Alizarin staining have been performed in7dpf and 15dpf mutant fish and age-matched WT controls. Analysis of confocal images showed increased amount and extent of bone mineralization in Ids$^{-/-}$ fish (Fig. 56 B-E) (Fig. 57 B-E) (Fig. 62 B-E) (Fig. 63 B-E).

In particular, in silico analysis of Alizarin red staining volume in the brachiostegal ray, opercle and cleithrum was performed. Brachiostegal ray and opercle displayed increased mineralization at 7dpf in mutant fish when compared with age-matched controls, while at 15dpf no differences were observed (Fig. 68 and 69). In the cleithrum there was no difference at 7dpf, while bone mineralization decreased in $Ids^{-/-}$ fish at 15dpf when compared with age-matched WT (Fig. 70).

The in silico reconstruction of Alizarin staining profile demonstrated a similar mineralized opercle area in mutants when compared to that of control at 7dpf, while it increased in mutants at 15dpf. Ids-/- fish displayed also an altered opercle shape at both 7dpf and 15dpf when compared to that of controls. In particular mutant fish showed an increased proximal region of the opercle that appeared expanded when compared with that of WT fish (Fig. 71).

Brachiostegal ray (Alizarin)				
	7dpf		15dpf	
	WT	$Ids^{-/-}$	WT	$Ids^{-/-}$
Volume Mean (μm^3)	22671	36042	41214	36563
Standard deviation	10339	3646	11339	5809
p-value	0,0122		0,4611	

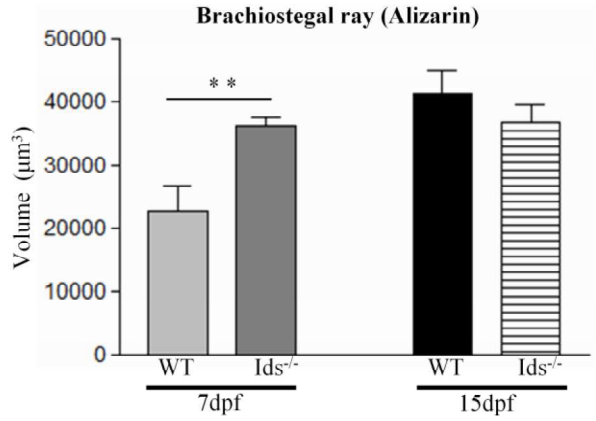

Figure 68: Alizarin red staining volume in the brachiostegal ray of $Ids^{-/-}$ and WT fish. At 7dpf there is a statistically significant increase in alizarin red stained regions of the brachiostegal ray of mutants when compared with those of controls. At 15 dpf there are no differences between $Ids^{-/-}$ and WT fish. (t-test **p<0,02).

Opercle (Alizarin)					
	7dpf			15dpf	
	WT	Ids $^{-/-}$		WT	Ids $^{-/-}$
Volume Mean (μm^3)	61488	102332		123385	100512
Standard deviation	27996	12579		28993	32212
p-value	0,0073			0,2293	

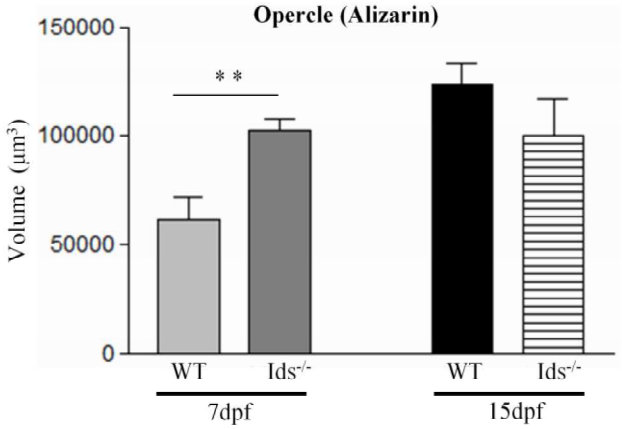

Figure 69: Alizarin red staining volume in the opercle of Ids-/- and WT fish. At 7dpf there is increased alizarin red stained region of the opercle of mutants when compared to that of controls. At 15 dpf there are no differences between Ids$^{-/-}$ and WT fish. (t-test **p<0,02).

Cleithrum (Alizarin)					
	7dpf			15dpf	
	WT	Ids $^{-/-}$		WT	Ids $^{-/-}$
Volume Mean (μm^3)	50050	54895		50991	32779
Standard deviation	23578	23434		19176	12414
p-value	0,7181			0,1129	

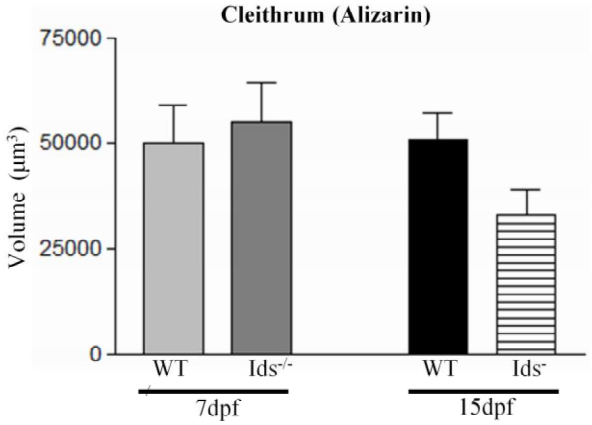

Figure 70: Alizarin red staining volume in the cleithrum of Ids$^{-/-}$ and WT fish. At 7dpf there are no differences between Ids$^{-/-}$ and WT. At 15 dpf there is an increased stained region of mutants cleithrum when compared to that of controls.

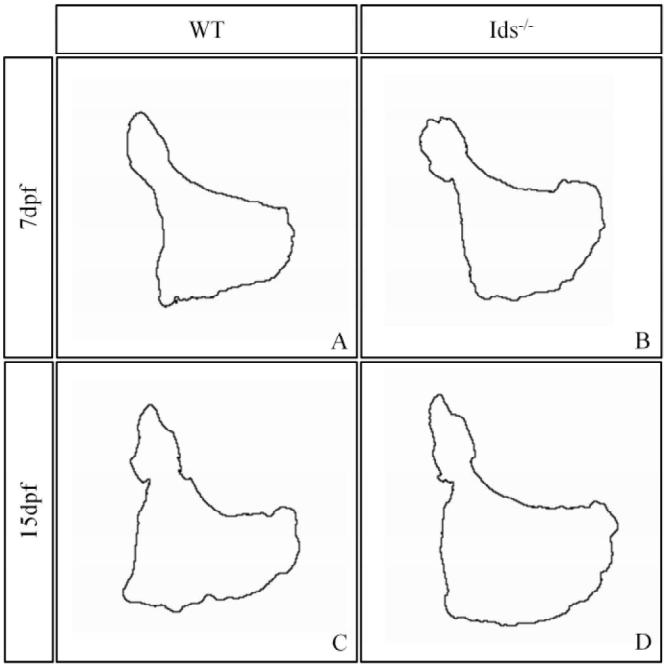

Figure 71: Alizarin red staining profile in the opercle in 7dpf and 15dpf Ids$^{-/-}$ and WT fish. (A,B) At 7dpf mutant fish display an altered shaped, opercle when compared to the control one. (C,D) In 15dpf Ids$^{-/-}$ fish the mineralized opercle regions is bigger when compared to that of age-matched controls

4.4.7 FGF signaling dysregulation in Ids$^{-/-}$ mutant fish

To verify whether changes in FGF signaling regulation could be responsible for bone differentiation and mineralization defects, I analyzed Ids$^{-/-}$ mutant fish in the transgenic *Tg(Dusp6:d2EGFP)^{pt6}* background.

Fluorescent microscopy analysis showed that homozygous mutant reporter fish exhibit an FGF signaling down regulation when compared to that of WT reporter fish (Fig. 72).

Heterozygous reporter fish display a variable degree of FGF signaling activity, according to parental genetic background. In particular, heterozygous Ids$^{+/-}$ fish generated from the cross of homozygous female fish with WT males, showed a variable degree of fluorescence intensity when compared to age-matched control siblings (Fig. 73 A,B,C). Indeed, heterozygous Ids$^{+/-}$ fish obtained from the cross between WT female fish and homozygous males displayed instead a comparable FGF reporter transgene intensity when compared to WT (Fig. 73 D,E,F). To better quantify the extent of FGF reporter transgene differences between Ids$^{-/-}$ homozygous, heterozygous Ids$^{+/-}$ and control siblings, I performed real time PCR analysis on pooled samples of *Tg(Dusp6:d2EGFP)^{pt6}* fish in the different Ids background. Quantitative real time PCR analysis showed a significant reduction of *GFP, pea3*, *erk1* and *erm1* transcripts in homozygous fish when compared to age-matched controls (Fig. 74 and 75).

Heterozygous fish obtained from the cross between homozygous Ids$^{-/-}$ female and WT males, showed a weak up regulation of *GFP* transcripts when compared with controls,

while the expression of FGF signaling markers *pea3*, *erk1* and *erm1* were similar with that of WT. Heterozygous fish coming from the cross between WT female fish and homozygous males did not show any significant differences in the expression of *GFP* and FGF signaling markers transcripts when compared to age-matched WT (Fig 74 and 75).

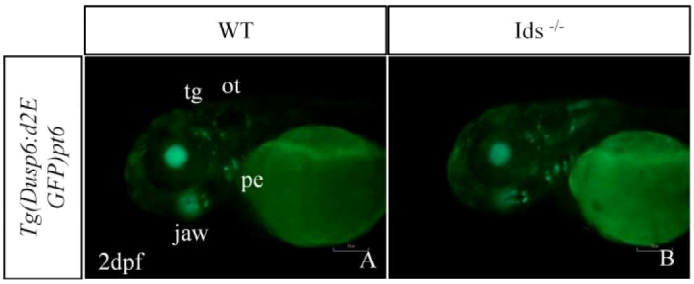

Figure 72: *Tg(Dusp6:d2EGFP)*^{pt6} WT and Ids-/- fish at 2dpf. Mutant fish (A) display a decreased GFP expression when compared to that of WT (B). ot: otic vesicle, pe: pharyngeal endoderm, tg: trigeminal ganglia.

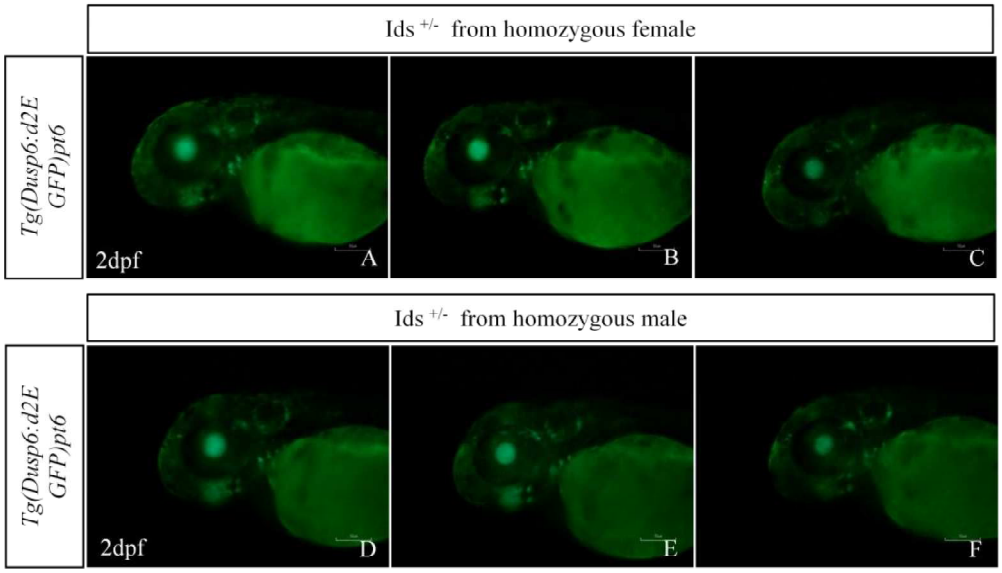

Figure 73: Heterozygous fish show a vary variable GFP expression at 2dpf. (A,B,C) Ids$^{+/-}$ that coming from a cross between an homozygous female and a WT male show heterogeneous GFP expression. (D,E,F) Heterozygous fish coming from a cross between a WT female and an homozygous male do not display any significant difference of GFP expression when compared to WT fish (Fig. 71A).

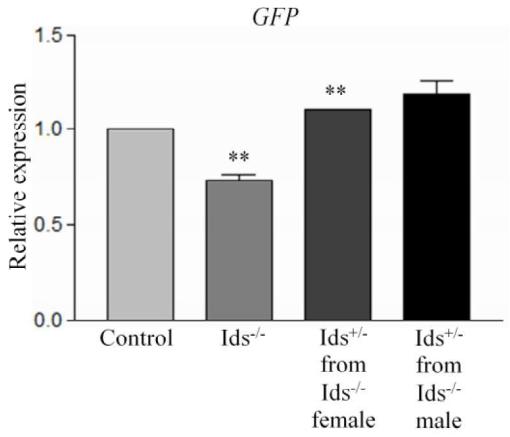

	GFP		
	$Ids^{-/-}$	$Ids^{+/-}$ from $Ids^{-/-}$ female	$Ids^{+/-}$ from $Ids^{-/-}$ male
Mean	0,73	1,11	1,19
Standard deviation	0,06	0,01	0,1
p-value	0,018	0,002	0,084

Figure 74: Quantitative real time PCR analysis of FGF signaling reporter transgene in WT and $Ids^{-/-}$ fish at 2 dpf. Homozygous Ids mutant fish show a down regulation of reporter transgene expression when compared with controls. Heterozygous coming from the cross between homozygous females and WT males show a weak up regulation of GFP transcripts when compared with controls. There are no differences in GFP expression between WT and heterozygous $Ids^{+/-}$ fish coming from the cross between WT females and homozygous males. Data are expressed as a mean of four independent experiments. (t-test **p<0,02).

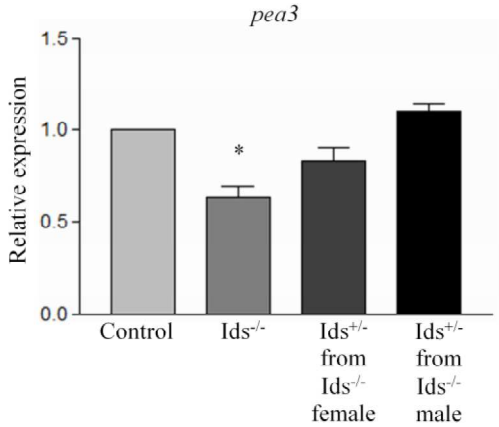

	pea3		
	$Ids^{-/-}$	$Ids^{+/-}$ from $Ids^{-/-}$ female	$Ids^{+/-}$ from $Ids^{-/-}$ male
Mean	0,64	0,83	1,1
Standard deviation	0,1	0,13	0,09
p-value	0,025	0,151	0,198

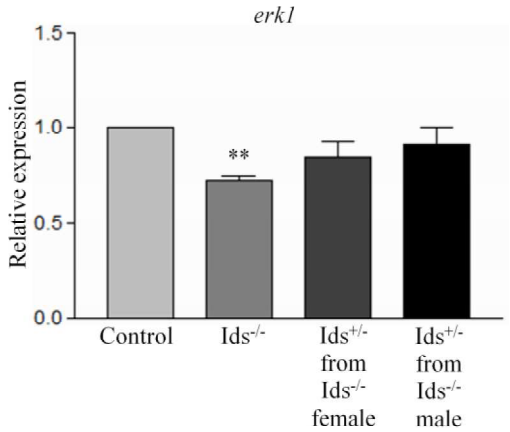

	erk1		
	$Ids^{-/-}$	$Ids^{+/-}$ from $Ids^{-/-}$ female	$Ids^{+/-}$ from $Ids^{-/-}$ male
Mean	0,72	0,85	0,91
Standard deviation	0,03	0,15	0,16
p-value	0,004	0,225	0,422

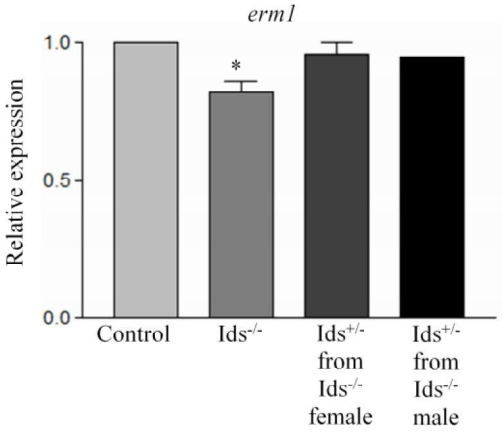

	erm1		
	$Ids^{-/-}$	$Ids^{+/-}$ from $Ids^{-/-}$ female	$Ids^{+/-}$ from $Ids^{-/-}$ male
Mean	0,82	0,95	0,95
Standard deviation	0,07	0,07	/
p-value	0,049	0,389	/

Figure 75: Quantitative real time PCR analysis for *pea3, erk1* and *erm1* in WT and $Ids^{-/-}$ fish at 2 dpf. Homozygous fish show a down regulation of all markers expression when compared to controls, while no differences are seen betweenWT and heterozygous fish. Data are expressed as a mean of four independent experiments. (t-test *p<0,05; **p<0,02).

4.5 Mouse model for Mucopolysaccharidosis type II

All the experiments were performed in an already previously described mouse model for Hunter syndrome (Garcia et al., 2007). This mouse model has a deletion of exon 4 and part of exon 5 of the *Ids* gene leading to the transduction of a non-functional enzyme.
All examined IDS-KO mice derived from an inbreeding between an homozygous female and an hemizygous male, and therefore the offspring was deprived of *Ids* maternal transcripts. Mice have been analyzed at different ages, from postnatal day 0 to 6 months.

4.5.1 Characterization of IDS-KO mice

Although widely previously characterized, IDS-KO mice were briefly examined in the present study to specifically ascertain parameters influencing our analysis, including body weight and GAG deposits, at several progressive time-points. I measured IDS-KO and WT mice body weight, from 1 week to 6 months. IDS-KO mice showed a statistically significant reduced weight at 5 weeks when compared with age-matched WT. In all other examined time points there were no statistically significant differences between the two groups (Fig. 76 and 77).
To qualitatively assess the onset of glycosaminoglycans accumulation in the murine IDS-KO, I examined Alcian blue/nuclear fast red stained liver tissue sections from IDS-KO and age-matched WT siblings at different stages. There was no evident GAGs storage in 1 week and 2 weeks'old KO mice liver samples, while at 9 months Alcian-blue stained regions were evident in all KO liver tissue samples (Fig. 78). It was possible to notice glycosaminoglycans accumulation in IDS-KO mice liver from 8-10 weeks (data not shown).

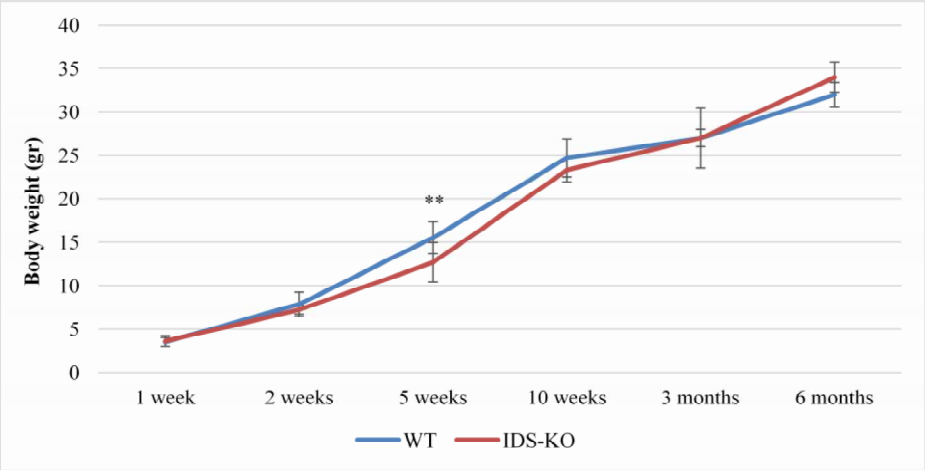

Figure 76: Ids-KO and WT mice body weight increases during development from 1 week to 6 months. At 5 weeks IDS-KO mice display a statistically significant lower weigh than WT siblings. (t-test **p<0,02).

	1 week		
	Mean (gr)	Standard deviation	p-value
WT	3,53	0,61	0,798
IDS-KO	3,59	0,48	

	2 weeks		
	Mean (gr)	Standard deviation	p-value
WT	7,83	0,50	0,122
IDS-KO	7,20	1,41	

	5 weeks		
	Mean (gr)	Standard deviation	p-value
WT	15,52	2,25	0,013
IDS-KO	12,68	1,85	

	10 weeks		
	Mean (gr)	Standard deviation	p-value
WT	24,71	1,31	0,182
IDS-KO	23,28	2,19	

	3 months		
	Mean (gr)	Standard deviation	p-value
WT	27,00	3,46	1,000
IDS-KO	27,00	1,00	

	6 months		
	Mean (gr)	Standard deviation	p-value
WT	32,00	1,73	0,152
IDS-KO	34,00	1,41	

Figure 77: Mean body weight of IDS-KO and WT mice at 1week (11 WT mice and 11 IDS-KO mice), 2weeks (14 WT mice and 16 IDS-KO mice), 5weeks (9 WT mice and 8 IDS-KO mice), 10weeks (6 WT mice and 8 IDS-KO mice), 3 months (3 WT mice and 3 IDS-KO mice) and 6months (3 WT mice and 4 IDS-KO mice).

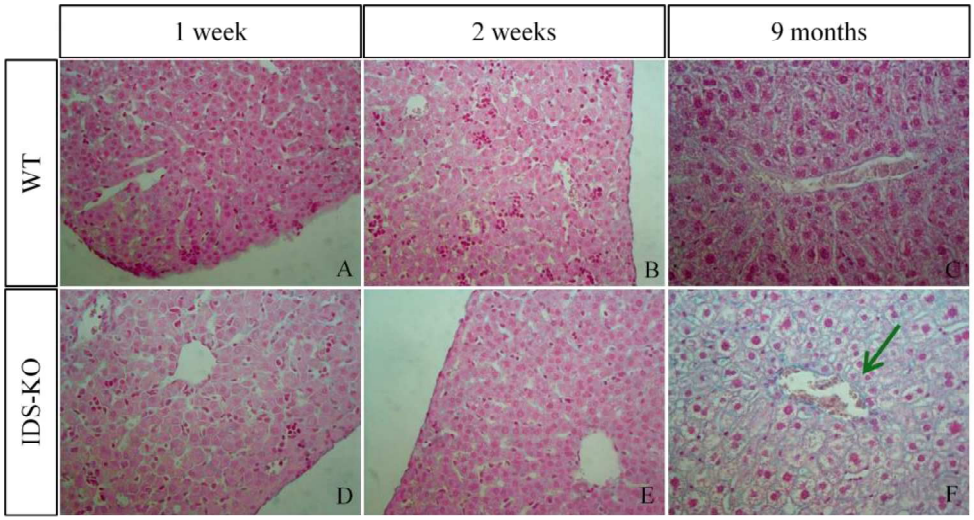

Figure 78: Alcian blue /nuclear fast red stained liver sections from IDS-KO and age-matched wild type mice. No GAGs accumulation was detectable in 1week (A-D) and 2weeks (B-E) old WT and knockout mice. Indeed 9 months old IDS-KO (F) show a large accumulation of glycosaminoglycans (arrow) in the liver which is not detectable in age-matched controls (C).

4.5.2 IDS-KO mice show altered early craniofacial development

To evaluate the onset of potential ossification defects in IDS-KO mice, I analyzed the skull conformation in 1 week and 2 weeks old IDS-KO and WT mice. One week old knockout mice displayed a flatter skull when compared to that of age-matched WT siblings (Fig. 79 and 81), while at 2 weeks the skull height was significantly increased when compared to age-matched controls (Fig. 80 and 81). The skull length was not different between knockout and WT mice at both ages (Fig. 81). Moreover, in two weeks old IDS-KO mice the skull was less vascularized when compared to that of age-matched WT mice (Fig. 80).

To evaluate differences in the rate of skull ossification, multiple Alcian blue/Alizarin Red stained samples from Ids-KO and WT mice were examined at different ages. Figure 82 shows the mouse skull organization, composed by frontal, parietal and interparietal bones that are intervened by metopic, coronal, sagittal and lamboid sutures (Fig. 82).

One day old Ids-KO mice showed increased Alcian blue staining in the cranial sutures that appeared also characterized by an irregular shape when compared to those of age-matched WT mice. Moreover, the interfrontal gap and lamboid sutures were wider in knockout mice when compared to those of WT controls (Fig. 83 A,B and 84 A,B).

At postnatal stages, i.e. at one 1 week and 2 weeks, IDS-KO mice exhibited more jagged skull sutures when compared with age-matched WT siblings (Fig. 83 C,D) (Fig. 84 C,D) (Fig. 83 E,F) (Fig. 84 E,F).

At 3 months and 6 months IDS-KO mice demonstrated persistent Alcian blue stained cranial sutures which were not detectable in age-matched WT skull samples (Fig. 85).

A skull size analysis was then performed in IDS-KO and WT mice at 1 day (4 WT mice and 6 IDS-KO mice), 1 week (5 WT mice and 5 IDS-KO mice), 2 weeks (6 WT mice and 7 IDS-KO mice), 3 months (3 WT mice and 3 IDS-KO mice) and 6 months (3 WT mice and 4 IDS-KO mice) of age, according to the previously described parameters (Kawakami et al., 2008) (Fig. 86).

Nasal length (NL): there were no differences during development between IDS-KO and WT mice (data not shown).

Frontal bone length (FL): from 1 day to 2weeks there were no differences between IDS-KO and WT mice, however at 3 months knockout mice showed a statistically significant reduction of this parameter while at 6 months a statistically significant increased FL was detected in KO mice when compared to the control one (Fig. 87 A and 88).

Parietal bone length (PL): there were no differences during development between IDS-KO and WT mice (data not shown).

Interparietal bone length (IL): IDS-KO mice showed a statistically significant reduction of this parameter at 1day compared to controls (Fig. 87 B).

Nasal bone width (NW): there were no differences during development between IDS-KO and WT mice (data not shown).

Distance between left and right anterolateral corner of the frontal bone (LR): IDS-KO mice displayed a statistically significant increase of this parameter at 6 months when compared to controls (Fig. 87 C and 88).

Frontal bone width (FW): there were no differences during development between IDS-KO and WT mice (data not shown).

Interparietal bone width (IW): IDS-KO mice demonstrated a statistically significant increase of this parameter at 6 months when compared to controls (Fig. 87 D).

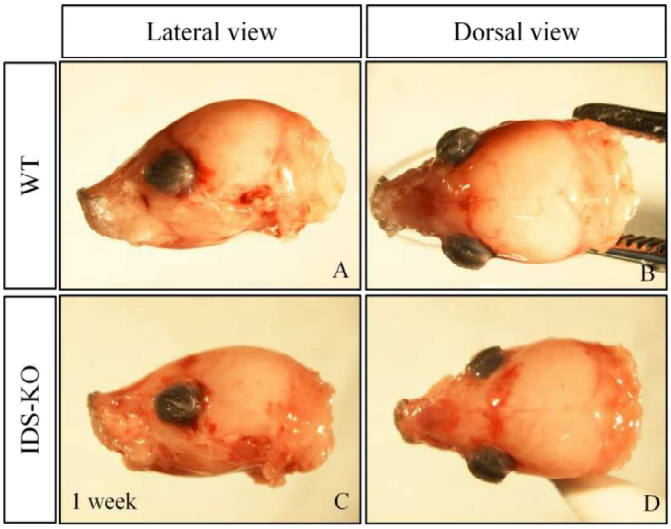

Figure 79: 1 week IDS-KO (C,D) and WT mice skull (A,B). Knockout mice display an altered skull shape when compared to the WT skull.

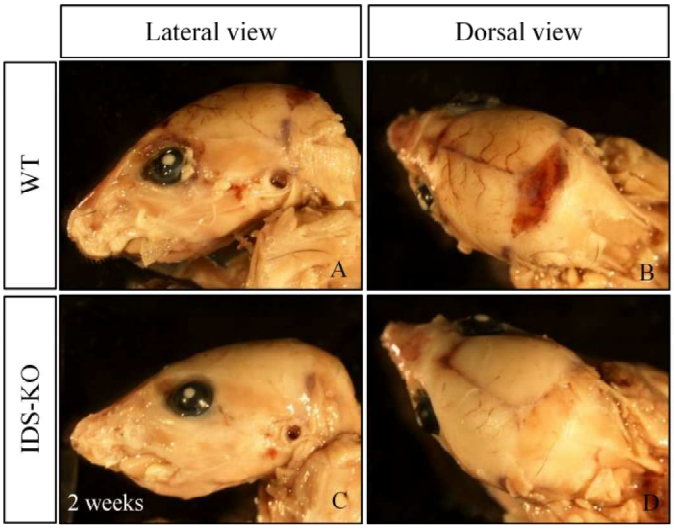

Figure 80: 2 weeks old IDS-KO (C,D) and WT (A,B) mice skull. IDS-KO mice skull (D) appears less vascularized when compared to the WT skull (B).

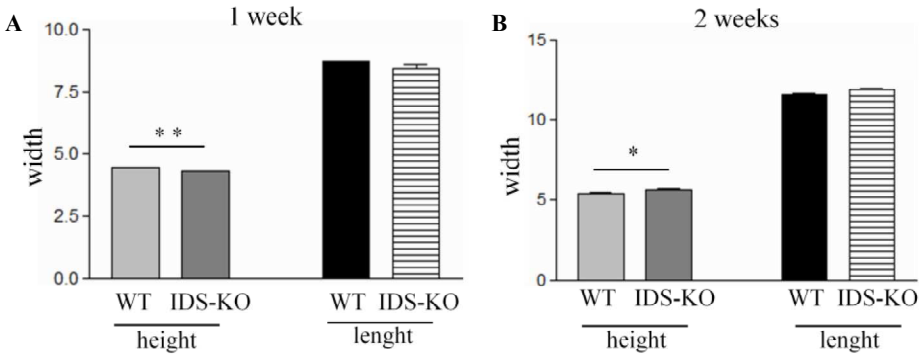

C	1 week	
	WT	IDS-KO
Mean height	4,42	4,29
Standard deviation	0,05	0,03
p value	0,018	
Mean lenght	8,72	8,42
Standard deviation	0,05	0,29
p value	0,157	

D	2 weeks	
	WT	IDS-KO
Mean height	5,36	5,63
Standard deviation	0,27	0,24
p value	0,026	
Mean lenght	11,62	11,89
Standard deviation	0,27	0,27
p value	0,054	

Figure 81: IDS-KO mice show a reduced skull height at 1 week (A) and an increased skull height at 2 weeks (B) when compared with age-matched controls (t test, *p<0,05; **p<0,02). 3 IDS-KO mice and 3 WT mice at 1 week and 10 IDS-KO mice and 10 WT mice at 2 weeks were been analyzed.

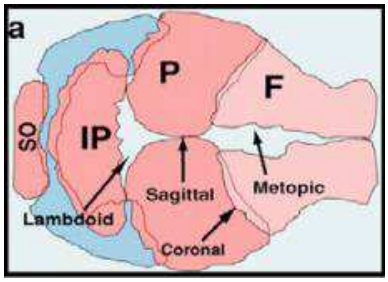

Figure 82: Schematic representation of a murine skull vault organization. It's formed by two frontal bones, two parietal bones and an interparietal bone. Bones are intervened by coronal, lambdoid, metopic and sagittal sutures. F: frontal bone, IP: interparietal bone; P: parietal bone. Image taken from (Deckelbaum et al., 2006)

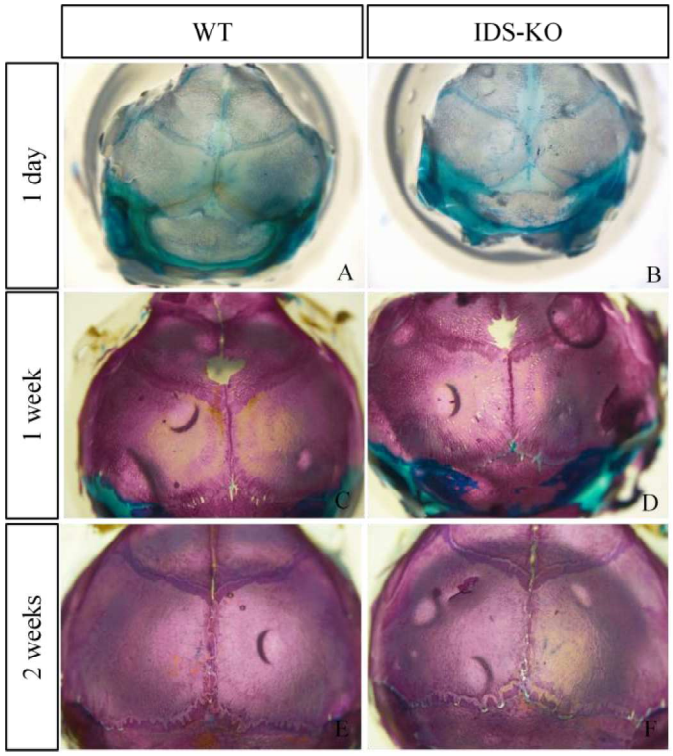

Figure 83: Alcian blue – Alizarin red stained skulls of 1 day (A,B), 1 week (C,D) and 2 weeks old (E,F) WT and IDS-KO mice. P0 knockout mice show wider gaps among sutures when compared to control skulls. 1 week and 2 weeks old IDS-KO mice display irregular shaped and incompletely closed skull sutures.

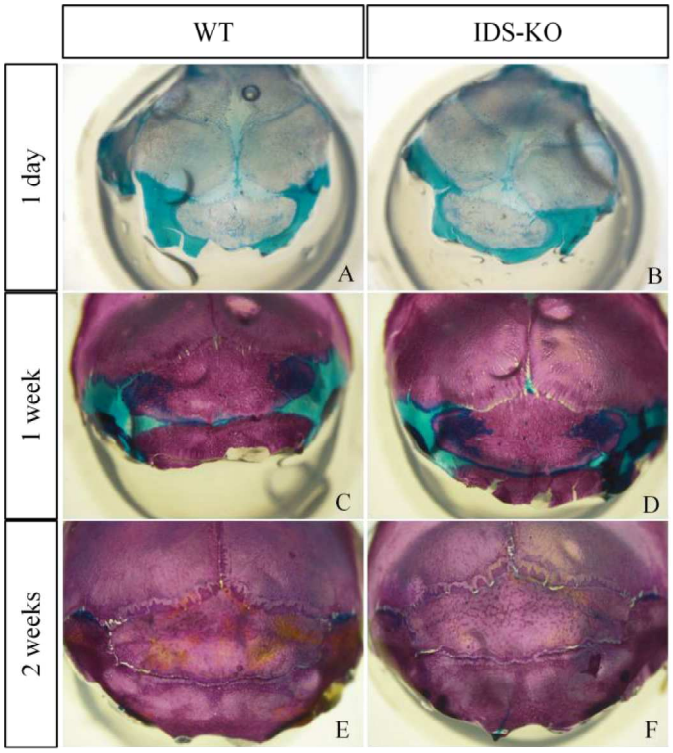

Figure 84: Alcian blue - Alizarin red stained skull samples of 1 day (A,B), 1 week (C,D) and 2 weeks (E,F) old WT and IDS-KO mice. More jagged shaped skull sutures in the interparietal bone and Alcian blue stained areas in the skull of knockout mice can be observed when compared to age-matched controls.

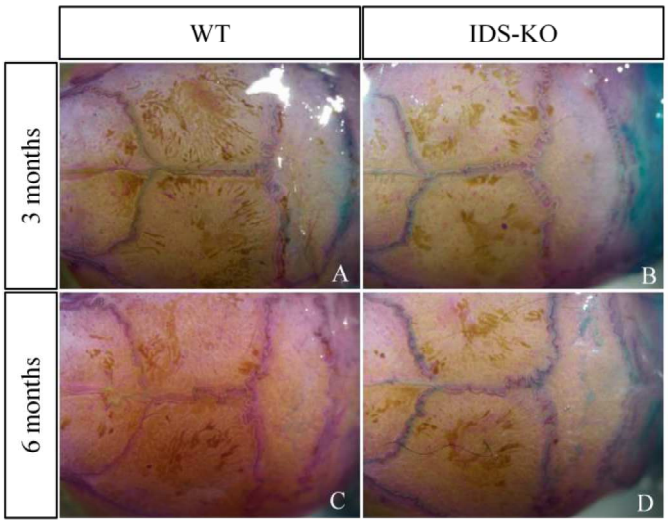

Figure 85: Alcian blue - Alizarin red stained skull samples of 3 months (A,B) and 6 months (C,D) old WT and IDS-KO mice. Marked Alcian blue staining is visible in IDS-KO mice skull sutures.

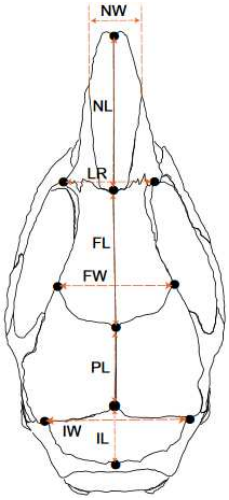

Figure 86: Schematic representation of linear measurements of the cranium. Image taken from (Kawakami et al., 2008)
NL: nasal bone length;
FL: frontal bone length;
PL: parietal bone length;
IL: interparietal bone length;
NW: nasal bone width;
LR: distance between left and right anterolateral corner of the frontal bone;
FW: frontal bone width;
IW: interparetal bone width.

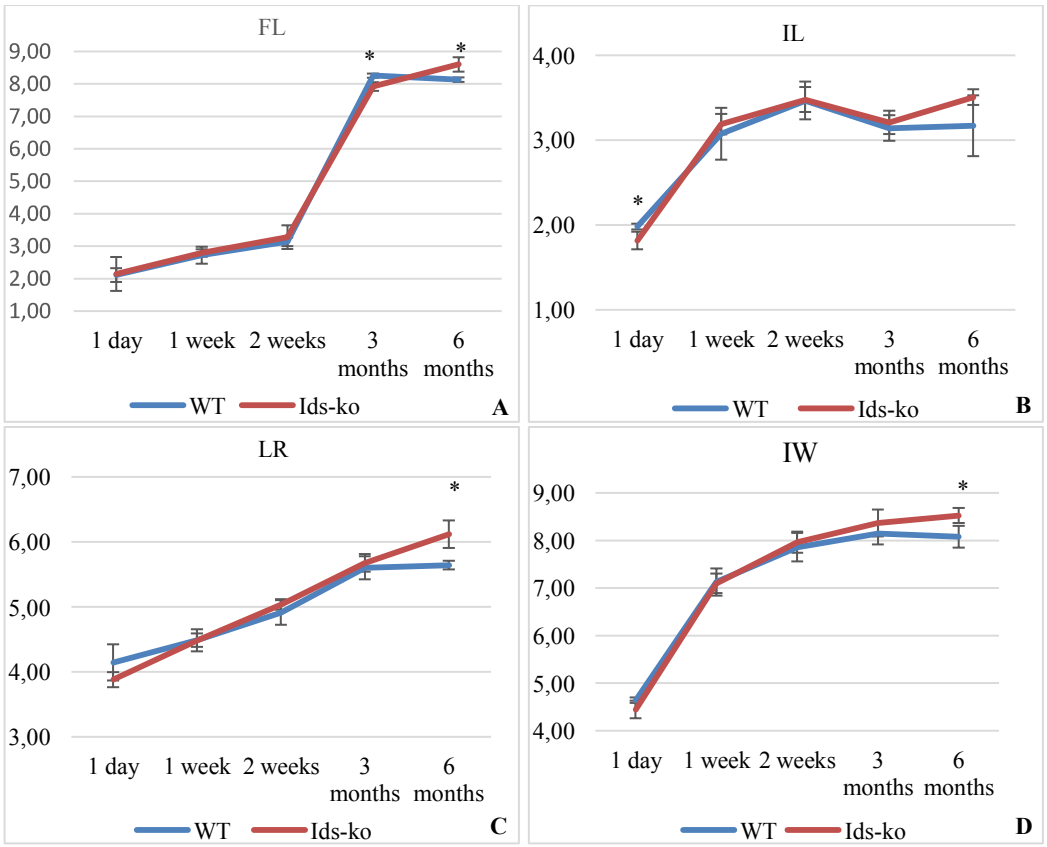

Figure 87: Graphical representation of measured skull bone parameters. For most measured parameters IDS-KO mice display a significant increase at 6 months of age. For only the IL parameter there is a statistically significant difference at 1 day post-partum between knockout and WT mice (t-test,*p<0,05). FL: frontal bone length; IL: interparietal bone length; LR: distance between left and right anterolateral corner of frontal bone; IW: interparietal width.

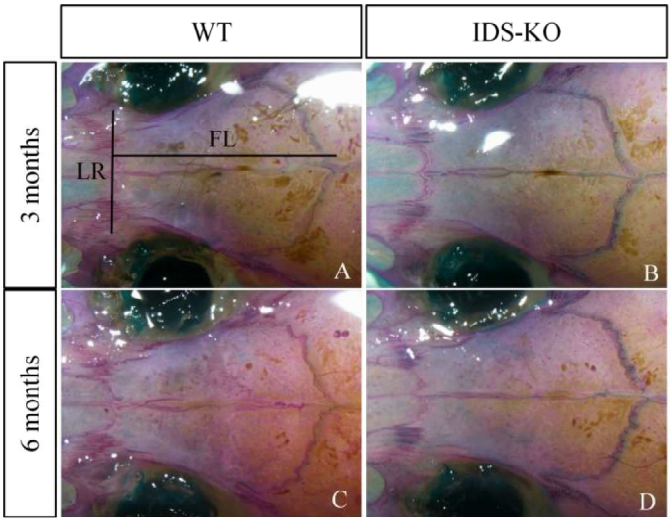

Figure 88: Alcian blue – Alizarin red stained skull samples of 3 months (A,B) and 6 months (C,D) WT and IDS-KO mice. FL (frontal bone length) and LR (distance between left and right anterolateral corner of the frontal bone) are indicated. Increased Alcian blue staining in knockout mice sutures is detectable when compared to WT mice.

4.5.3 IDS-KO mice show impaired long bones development

Long bones are particularly affected in Hunter syndrome patients, displaying short bone length and enlarged diaphysis. I, therefore, examined tibia and femur length in 1 day (4 WT mice and 6 IDS-KO mice), 1 week (5 WT mice and 5 IDS-KO mice), 2 weeks (6 WT mice and 7 IDS-KO mice), 3 months (3 WT mice and 3 IDS-KO mice) and 6 months (3 WT mice and 4 IDS-KO mice) Ids-KO and WT mice.

One day, 1 week and 2 weeks old knockout mice didn't exhibit any differences in tibia and femur length when compared with age-matched WT mice (Fig. 89) (Fig. 91) (Fig. 92) (Fig. 94). IDS-KO mice started to show reduced tibia and femur length at 3 months when compared with age-matched WT mice and the bone length difference became statistically significant at 6 months (Fig. 90) (Fig. 91) (Fig. 93) (Fig. 94).

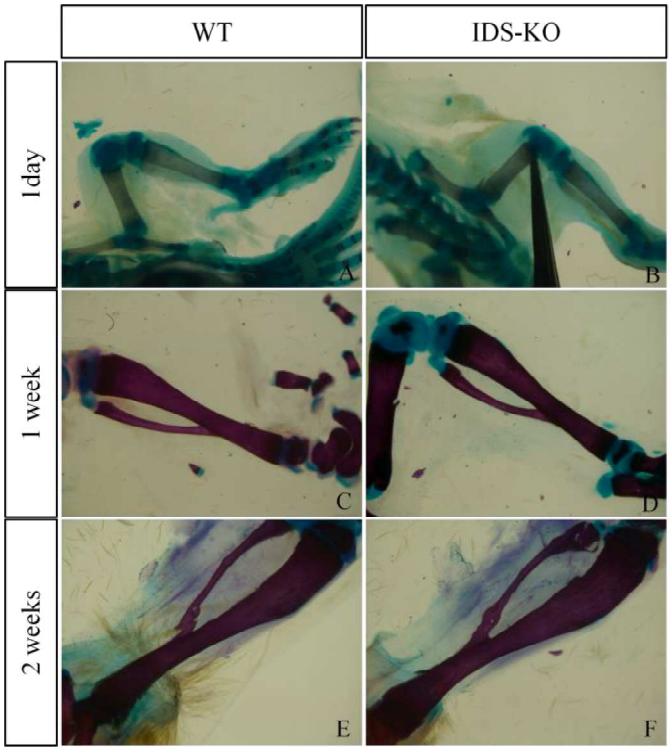

Figure 89: Representative tibial bone of 1 day (A,B), 1 week (C,D) and 2 weeks (E,F) IDS-KO and WT mice.

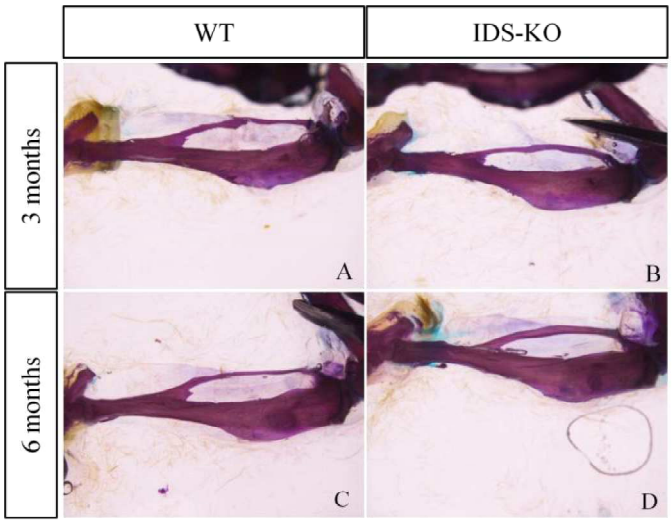

Figure 90: Representative tibial bone of 3 months (A,B) and 6 months (C,D) IDS-KO and WT mice.

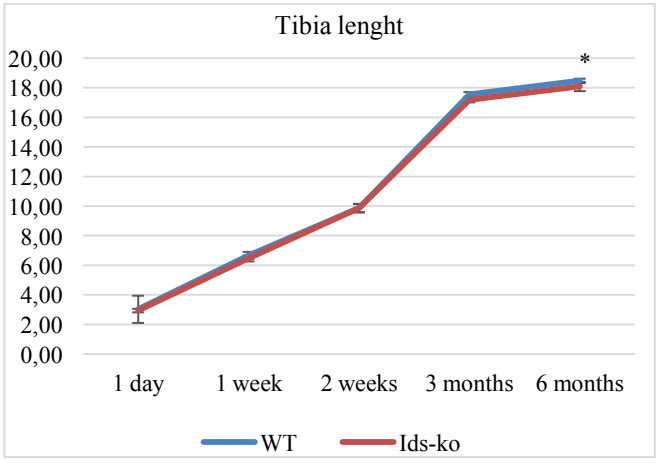

Figure 91: Tibia growth in IDS-KO and WT mice from 1day to 6 months. A statistically significant difference in tibia length is detectable at 6 months between IDS-KO and WT mice (t-test * $p<0,05$).

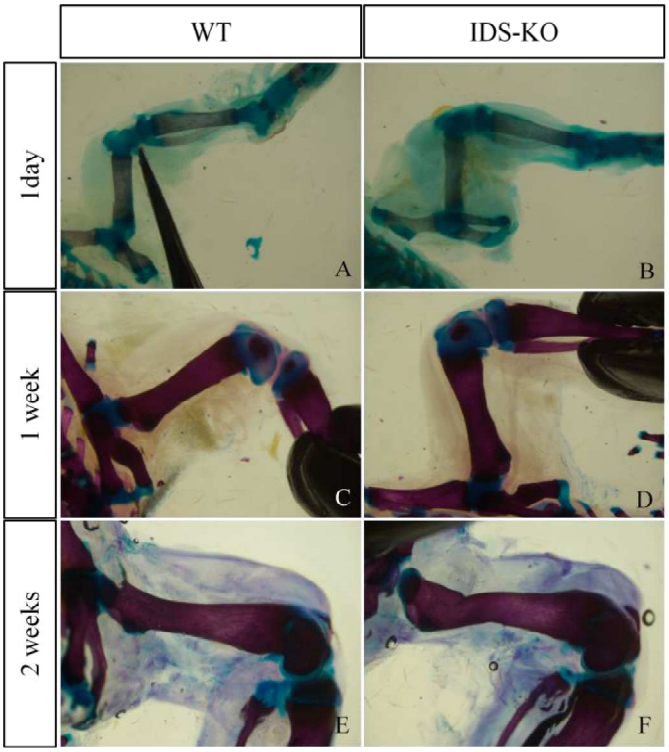

Figure 92: Representative femur bone of 1 day (A,B), 1 week (C,D) and 2 weeks (E,F) IDS-KO and WT mice.

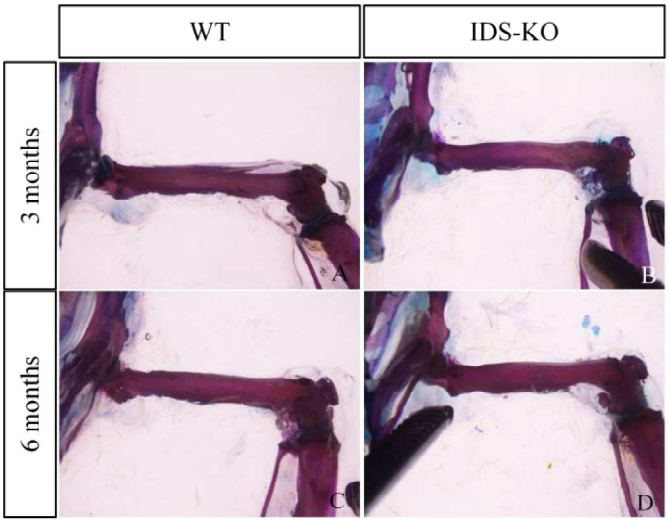

Figure 93: Representative femur bone of 3 months (A,B) and 6 months (C,D) IDS-KO and WT mice.

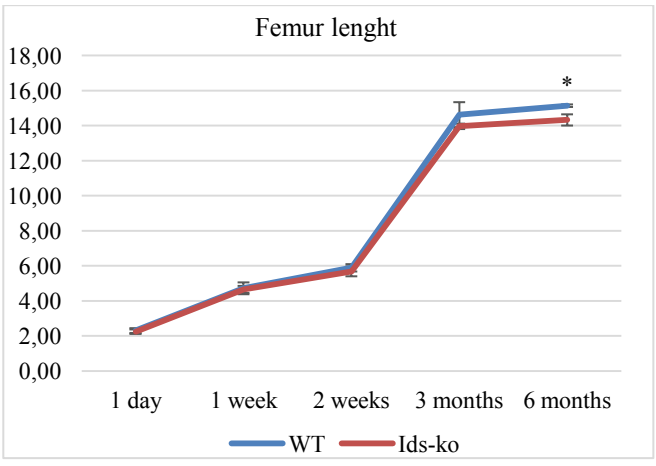

Figure 94: Femur growth in IDS-KO and WT mice from 1day to 6 months. A statistically significant difference in femur length is detectable at 6 months between IDS-KO and WT mice. (t-test * $p<0,05$).

4.5.4 IDS-KO mice show dysregulated expression of bone specific markers

To analyze whether IDS loss of function was affecting the expression of bone-related markers in mice at early life stages histochemical analysis for Collagen II and Osteocalcin (OCN) was carried out in tibial paraffin-embedded sections from 1 week and 2 weeks old Ids-KO and WT mice.

While an in silico-based quantitative analysis of immunopositive cells did not show obvious difference between Ids-KO and WT mice (Fig. 97), immunoreactive cell types were different between the two groups. In particular, Collagen II in Ids-KO mice was highly expressed in the proliferating region of both 1 week and 2 weeks old mice, while in WT mice Collagen II immunopositive cells were equally distributed among the proliferating, prehypertrophic and hypertrophic zones (Fig. 95 A,B and 96 A,B). When considering Osteocalcin in 1 week Ids-KO mice, more immunopositive cells were detected in the proliferating and hypertrophic zones, while in age-matched WT OCN-positivity was observed in proliferating, prehypertrophic and hypertrophic zones (Fig. 95 C,D). In two weeks old mice there was no difference in the distribution of immunopositive cells between WT and KO mice, as regards the three regions (Fig. 96 C,D).

To quantitatively assess differences in the expression levels of bone-related markers between WT and KO mice, I performed quantitative real time PCR in RNA extracts obtained from the cranial vault, femur epiphysis and femur diaphysis of 1 week and 2 weeks IDS-KO and WT mice. *Collagen II*, *Osteocalcin* and *Collagen X* were analyzed in pooled samples of the two groups. IDS-KO cranial vault samples showed a down-regulation of *Collagen X* expression at 1 week and a down-regulation of *Osteocalcin* at 1 week and 2 weeks, when compared to those of age-matched WT. No differences between in the expression of *Collagen 2* were detected between 1 week and 2 weeks old IDS-KO and WT mice cranial vault samples (Fig. 98 A,D) (Fig.99 A).

When considering the femur diaphysis, an up regulation of *Collagen II* and down regulation of *Collagen X* expression was seen in both 1 week and 2 weeks Ids-KO when compared with age-matched WT samples. A down regulation of *Osteocalcin* was observed only in 1 week IDS-KO mice samples when compared to wild type ones (Fig. 98 B, E) (Fig. 99 B). Femur epiphysis samples showed indeed a down regulation of *Collagen II* and *Osteocalcin* in 2 weeks old knockout mice samples when compared to age-matched controls (Fig. 98 F) (Fig. 99 C).

Since it is well known that activation of inflammatory pathway may contribute to the impaired bone development (Opoka-Winiarska et al., 2013), I analyzed the expression of *IL1β* and *TNFα* in all bone samples from the two groups.

As shown in Fig. 100 and 101, no differences in *TNFα* expression were measured in the cranial vault and epiphysis samples of both 1 week and 2 weeks old knockout mice when compared with age-matched control tissues. Indeed, diaphysis samples from 1 week and 2 weeks old IDS-KO mice showed a down-regulation of *TNFα* expression, when compared with age-matched WT mice diaphysis. No differences were detected in *IL1β* expression between WT and knockout mice for all bone samples, but in 1 week old IDS-KO mice diaphysis and epiphysis samples a significant decrease of *IL1β* was seen when compared with age-matched controls.

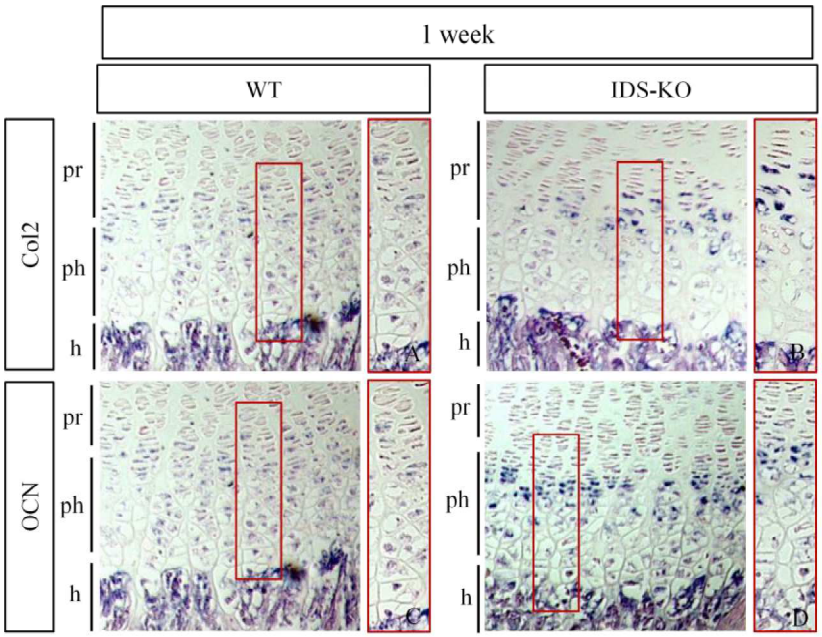

Figure 95: Representative immunohistochemistry analysis for collagen II (A,B) and osteocalcin (C,D) performed in tibia samples of 1 week old IDS-KO and WT mice . A different localization of immupositive cells is seen in Ids-KO mice when compared with controls. pr: proliferating zone, ph: prehypertrophic zone, h: hypertrophic zone.

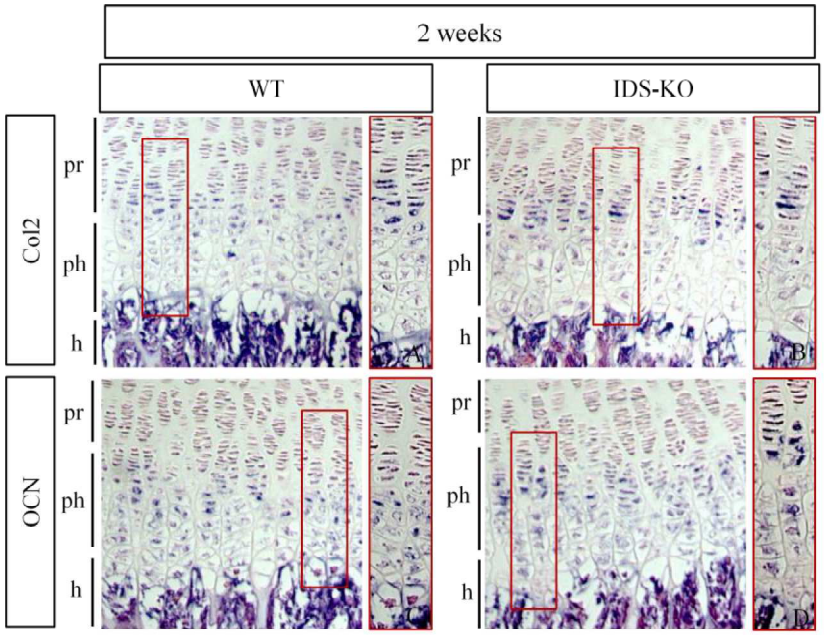

Figure 96: Representative immunohistochemistry analysis for collagen II (A,B) and osteocalcin (C,D) performed in tibia samples of 2 weeks old IDS-KO and WT mice. A different localization of immupositive cells is seen in IDS-KO mice when compared with controls. pr: proliferating zone, ph: prehypertrophic zone, h: hypertrophic zone

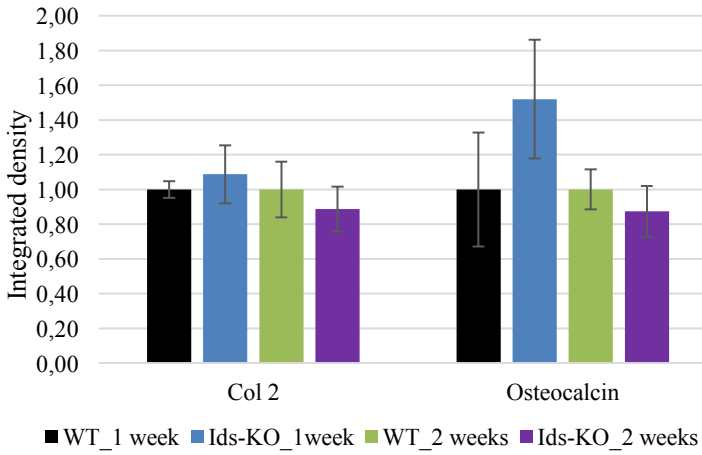

Figure 97: Integrated density quantification of collagen II and osteocalcin immunopositive cells in tibia sections. No statistically significant differences are detected between IDS-KO and WT mice.

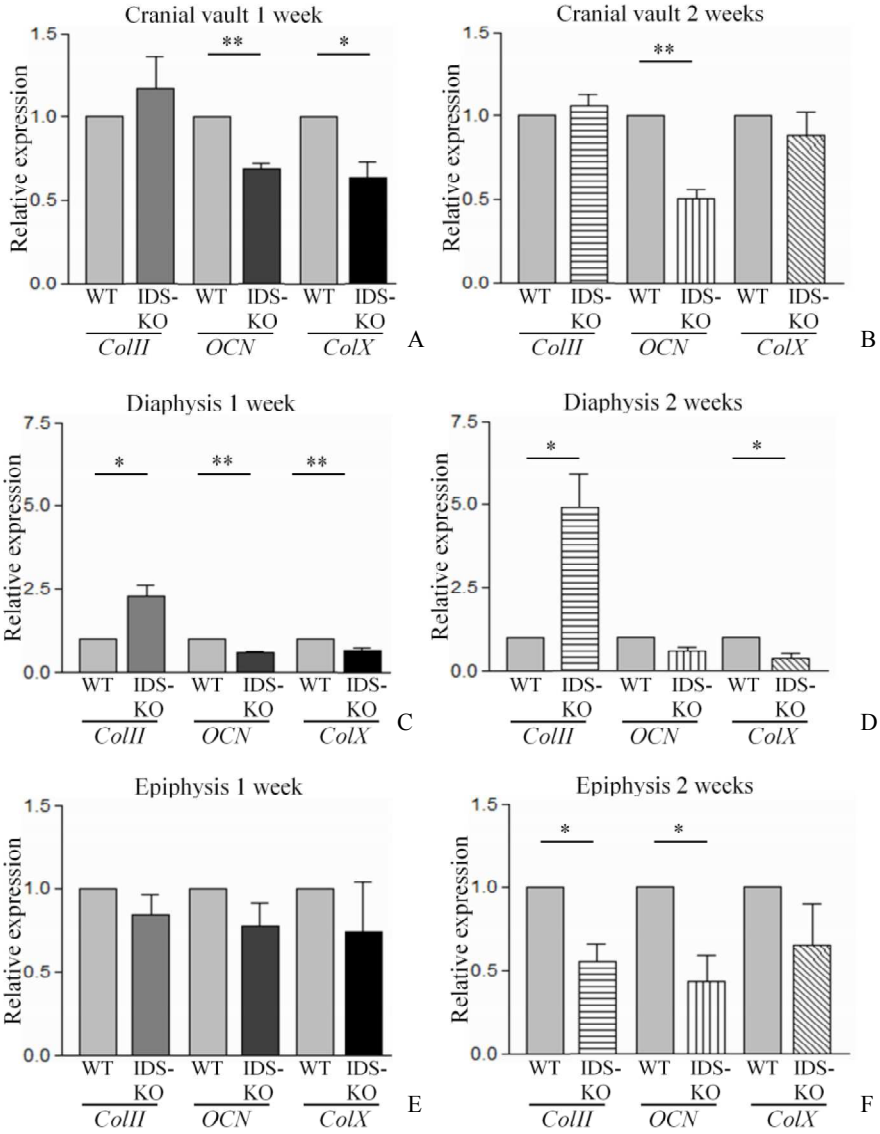

Figure 98: Quantitative real time PCR analysis in 1 week and 2 weeks IDS-KO and WT mice cranial vault (A-B), diaphysis (C-D) and epiphysis (E-F) samples for *Collagen II, Osteocalcin* and *Collagen X*. (t-test ;*p<0,05; **p<0,02).

Cranial vault				A
		Mean	Standard deviation	p value
WT		1	/	/
IDS-KO *ColII*	1 week	1,17	0,34	0,480
IDS-KO *OCN*	1 week	0,69	0,06	0,011
IDS-KO *ColX*	1 week	0,63	0,19	0,030
IDS-KO *ColII*	2 weeks	1,06	0,12	0,492
IDS-KO *OCN*	2 weeks	0,51	0,09	0,010
IDS-KO *ColX*	2 weeks	0,88	0,28	0,460

Diaphysis				B
		Mean	Standard deviation	p value
WT		1	/	/
IDS-KO *ColII*	1 week	2,28	0,67	0,032
IDS-KO *OCN*	1 week	0,58	0,08	0,011
IDS-KO *ColX*	1 week	0,65	0,14	0,015
IDS-KO *ColII*	2 weeks	4,89	2,02	0,031
IDS-KO *OCN*	2 weeks	1,06	0,23	0,088
IDS-KO *ColX*	2 weeks	0,33	0,24	0,045

Epiphysis				C
		Mean	Standard deviation	p value
WT		1	/	/
IDS-KO *ColII*	1 week	0,85	0,20	0,315
IDS-KO *OCN*	1 week	0,78	0,24	0,250
IDS-KO *ColX*	1 week	0,74	0,51	0,472
IDS-KO *ColII*	2 weeks	0,55	0,20	0,021
IDS-KO *OCN*	2 weeks	0,44	0,31	0,035
IDS-KO *ColX*	2 weeks	0,65	0,42	0,287

Figure 99: Quantitative real time PCR analysis in 1 week and 2 weeks old IDS-KO and WT mice cranial vault (A), diaphysis (B) and epiphysis (C) for *ColII*, *OCN* and *ColX* (t-test *p<0,05; **p<0,02).

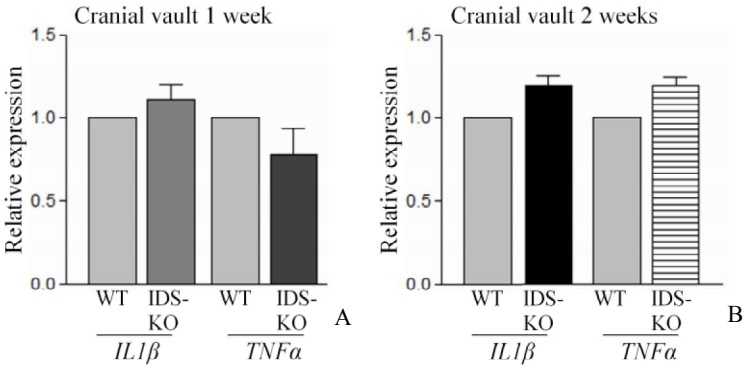

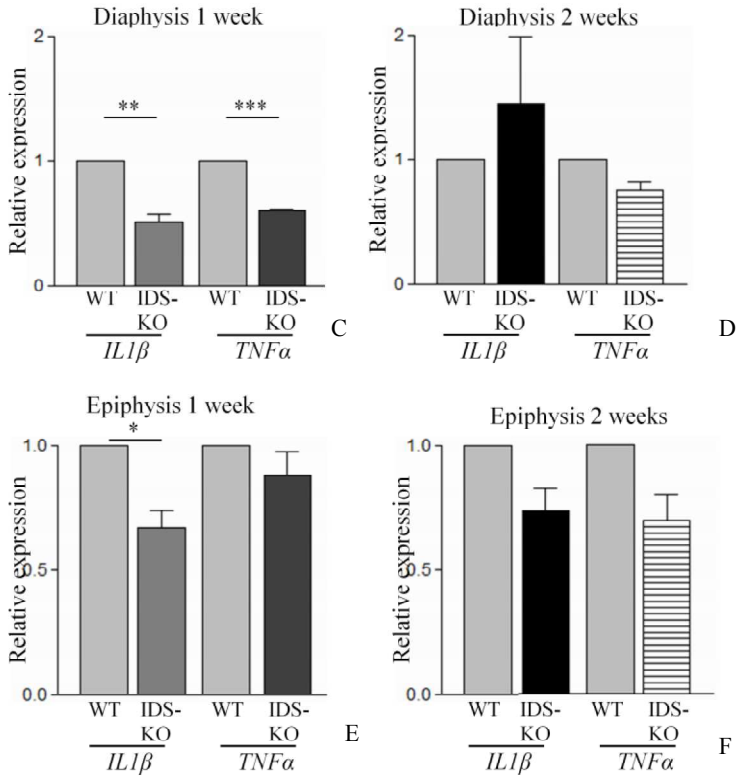

Figure 100: Quantitative real time PCR analysis in 1 week and 2 weeks old IDS-KO and WT mice cranial vault (A,B), diaphysis (C,D) and epiphysis (E,F) for IL1β and TNFα. (t-test *p<0,05; **p<0,02; ***p<0,002).

Cranial vault				**A**
		Mean	Standard deviation	p value
WT		1	/	/
IDS-KO *IL1β*	1 week	1,11	0,16	0,366
IDS-KO *TNFα*	1 week	0,78	0,27	0,287
IDS-KO *IL1β*	2 weeks	1,19	0,11	0,092
IDS-KO *TNFα*	2 weeks	1,19	0,09	0,064

Diaphysis				**B**
		Mean	Standard deviation	p value
WT		1	/	/
IDS-KO *IL1β*	1 week	0,51	0,1	0,013
IDS-KO *TNFα*	1 week	0,6	0,03	0,001
IDS-KO *IL1β*	2 weeks	1,45	1,07	0,558
IDS-KO *TNFα*	2 weeks	0,74	0,15	0,039

Epiphysis				**C**
		Mean	Standard deviation	p value
WT		1	/	/
IDS-KO *IL1β*	1 week	0,67	0,12	0,042
IDS-KO *TNFα*	1 week	0,88	0,17	0,325
IDS-KO *IL1β*	2 weeks	0,73	0,15	0,094
IDS-KO *TNFα*	2 weeks	0,7	0,21	0,063

Figure 101: Quantitative real time PCR analysis in 1 week and 2 weeks old IDS-KO and WT mice cranial vault (A), diaphysis (B) and epiphysis (C) for IL1β and TNFα (t-test *p<0,05; **p<0,02; ***p<0,002).

4.5.5 IDS-KO mice show altered FGF signaling

Given the impairment of FGF signaling activity detected in the fish model, I evaluated whether IDS-KO mice showed any deregulation of this pathway. Immunohistochemical analysis for PEA3 performed in tibia samples of Ids-KO and WT mice showed an overall decrease of PEA3 protein levels in 1 week old KO mice when compared with age-matched WT (Fig. 104). Moreover, 1 week old IDS-KO mice showed PEA3-immunopositivity in the prehypertrophic zones, while in WT mice immunopositive cells were detected in proliferating and prehypertrophic zones (Fig. 102). Concerning 2 weeks old IDS-KO and WT mice no differences in PEA3 expression were observed (Fig. 103).
To better quantify differences in FGF signaling activity I performed quantitative real time PCR analysis for *Pea3*, *Erk1* and *Dusp6* in cranial vault, femur diaphysis and femur epiphysis samples of 1 week and 2 weeks old IDS-KO and WT mice.
No differences in *Pea3* and *Dusp6* expression were detected in one week old cranial vault samples of IDS-KO and WT (Fig. 105 A) (Fig. 106 A). Similarly, no further significant discrepancies in terms of *Pea3*, *Erk1* and *Dusp6* expression were measured in cranial vault samples of the two groups at 2 weeks (Fig. 105 D) (Fig. 106 A). Indeed, one 1 week old KO-mice cranial vault samples showed a down-regulation of *Erk1* transcripts when compared with controls (Fig. 105 A) (Fig. 106 A).
As regards the diaphysis *Pea3*, *Erk1* and *Dusp6* expression was similar between both 1 week and 2 weeks old knockout and WT mice (Fig. 105 B, E) (Fig. 106 B).
Concerning the epiphysis a significant down-regulation of *Erk1* and *Dusp6* expression and *Pea3*, *Erk1* and *Dusp6* transcripts was observed, in 1 week and 2 weeks old KO mice, respectively, when compared with age-matched WT (Fig. 105 C, F) (Fig. 106 C).
To summarize, in all examined bone samples a significant decrease of FGF-related markers expression was detected in KO-mice, although with consistent differences according to the evaluated bone region.

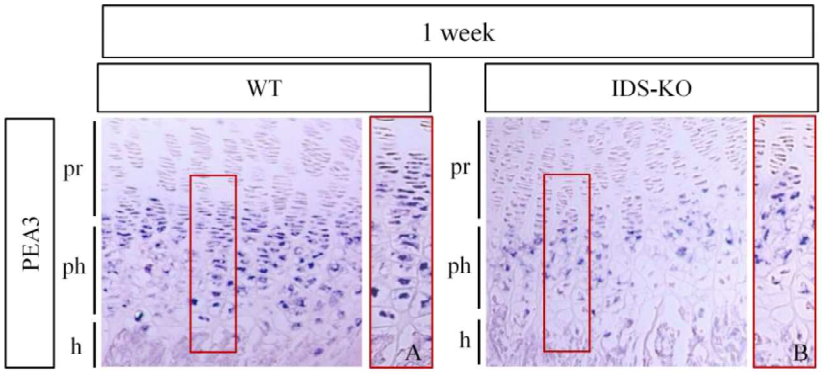

Figure 102: Representative immunohistochemistry for PEA3 in tibia samples of 1 week old IDS-KO and WT mice. A different signal distribution in detected in IDS-KO sections (B) when compared with controls (A). pr: proliferating zone, ph: prehypertrophic zone, h: hypertrophic zone.

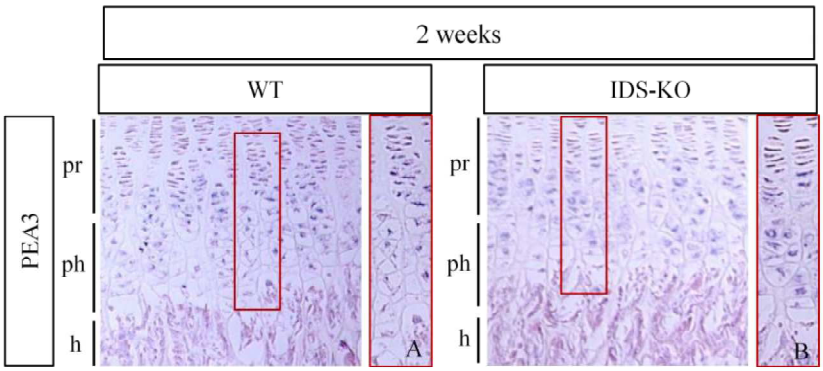

Figure 103: Representative immunohistochemistry for PEA3 in tibia samples of 2 weeks old IDS-KO and WT mice No differences are detected between IDS-KO (B) when compared with controls (A). pr: proliferating zone, ph: prehypertrophic zone, h: hypertrophic zone.

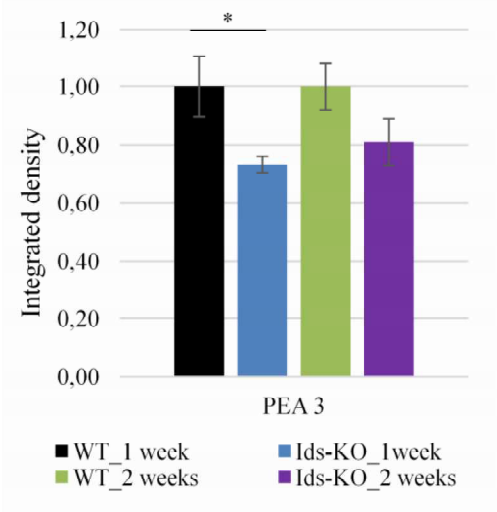

Figure 104: Integrated density quantification of PEA3 immunohistochemistry signal in tibia sections. Analysis were performed in 4 WT mice and 4 IDS-KO mice samples of 1 week and 2 weeks. A statistically significant reduction of PEA3 expression is seen in 1 week IDS-KO mice when compared with age-matched WT mice (t-test; *$p<0.05$).

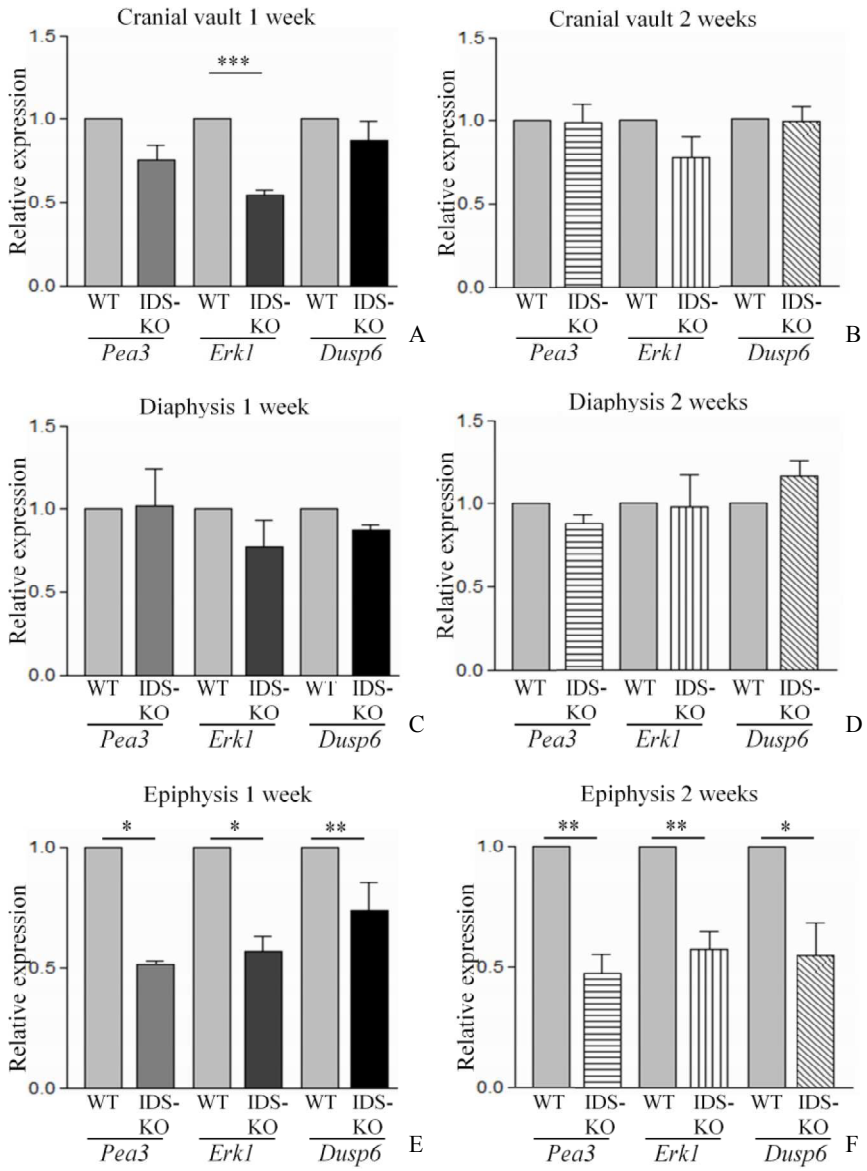

Figure 105: Quantitative real time PCR analysis in 1 week and 2 weeks Ids-KO and WT mice samples of cranial vault (A,B), diaphysis (C,D) and epiphysis (E,F) for *Pea3*, *Erk1* and *Dusp6* (t-test *p<0,05; **p<0,02; ***p<0,002).

Cranial vault		Mean	Standard deviation	p value	A
WT		1	/	/	
IDS-KO *Pea3*	1 week	0,75	0,17	0,063	
IDS-KO *Erk1*	1 week	0,55	0,05	0,001	
IDS-KO *Dusp6*	1 week	0,88	0,22	0,349	
IDS-KO *Pea3*	2 weeks	0,99	0,19	0,928	
IDS-KO *Erk1*	2 weeks	0,78	0,25	0,174	
IDS-KO *Dusp6*	2 weeks	0,99	0,17	0,914	

Diaphysis		Mean	Standard deviation	p value	B
WT		1	/	/	
IDS-KO *Pea3*	1 week	1,02	0,31	0,942	
IDS-KO *Erk1*	1 week	0,77	0,29	0,310	
IDS-KO *Dusp6*	1 week	0,87	0,06	0,057	
IDS-KO *Pea3*	2 weeks	0,88	0,11	0,112	
IDS-KO *Erk1*	2 weeks	0,98	0,39	0,917	
IDS-KO *Dusp6*	2 weeks	1,17	0,17	0,151	

Epiphysis		Mean	Standard deviation	p value	C
WT		1	/	/	
IDS-KO *Pea3*	1 week	0,52	0,02	0,020	
IDS-KO *Erk1*	1 week	0,57	0,10	0,017	
IDS-KO *Dusp6*	1 week	0,74	0,20	0,151	
IDS-KO *Pea3*	2 weeks	0,47	0,16	0,007	
IDS-KO *Erk1*	2 weeks	0,57	0,16	0,012	
IDS-KO *Dusp6*	2 weeks	0,55	0,27	0,043	

Figure 106: Quantitative real time PCR analysis in 1 week and 2 weeks old IDS-KO and WT mice cranial vault (A), diaphysis (B) and epiphysis (C) for *Pea3*, *Erk1* and *Dusp6* (t-test *p<0,05; **p<0,02; ***p<0,002).

4.6 Mucopolysaccharidosis type II patient fibroblasts

To understand whether an FGF signaling impairment could be a downstream effect due to IDS loss function in Hunter syndrome patients, I performed expression analysis of FGF-specific markers in fibroblasts retrieved from a selected cohort of patients. Anonymized samples were obtained from Biobank of Genova Institute G. Gaslini. Fibroblast cDNA samples from affected patients harboring different *iduronate 2-sulfatase* mutations were subjected to transcriptomic analysis and results were compared with those of healthy control samples (Table 10). All samples were grouped according to the type of mutation (non-sense mutation, missense mutation or deletion) and the localization of the *IDS* mutation (N-terminal or C-terminal) (Table 12).

Next some information related to the mutations characterizing the fibroblasts used for the analysis are reported:

P4Sfs: It's a frameshift micro insertion (c.10insT) and generates a premature stop codon in position X43, leading to a truncated protein (Lualdi et al., 2010).

R8X: This mutation causes the synthesis of a short polypeptide lacking the active site; however patients show a mild form of MPSII. It has been supposed that this stop codon may be occasionally skipped during transcription (Vafiadaki et al., 1998).

W12X: Produces a short N-terminal part of the protein that has not functional activity (Kato et al., 2005).

ΔS 117: It's an in-frame deletion c.472delTCC causing the loss of a serine residue in position 117. The skipping of this aminoacidic residue doesn't alter the enzyme maturation, so it has been supposed that the mutated polypeptide has an altered ability to reach the lysosome (Bonuccelli et al., 2001).

R88: Arginine 88 is highly conserved among sulfatases and human IDS structure analysis has revealed that this residue is important for the enzyme proper conformation. It is located near the active site residue Cystein 84 and it's part of the core of the major IDS domain. Mutations in this aminoacid can change the orientation of the secondary structure (Chkioua et al., 2011).

R88H: Arginine and Histidine aminoacids are both positively charged, but the presence of an imidazole group in the Histidine residue can alter the enzyme structure and function (Balzano et al., 1998).

R88P: The substitution of Arginine with a Proline residue can alter the stability of the protein because Proline has a larger and more hydrophobic conformation, but it doesn't directly affect enzyme activity. The protein instability causes altered IDS function leading to a severe form of the disease (Chkioua et al., 2011).

R443X: The truncated enzyme produced by this mutation has a residual enzymatic activity and decreased stability. This mutation is associated with an intermediate form of MPSII (Isogai et al., 1998).

C422R: This mutation affects a non-conserved residue among human sulfatases, but it can be associated with a severe form of the pathology (Moreira da Silva et al., 2001).

R468Q: This mutation could be a mutational hot spot because it is common in the Caucasian population (Isogai et al., 1998).

This aminoacid is adjacent to the positively charged active site residue K347, forming together a favorable electrostatic field for substrate entrance into the active site cavity (Koji & Koji, 2005). R468Q mutation has been found in several patients with severe or intermediate phenotype (Sukegawa-Hayasaka et al., 2006).

Patient	Mutation	Phenotype	Kind of mutation	Localization
Control	/	Healthy	/	/
H150	P4Sfs	Mild	Non-sense mutation	N-terminal
H147	R8X	Mild		
H122	W12X	Intermediate		
23-15	Q66X	Intermediate		
37-15	Q80X	Severe		
f23	Y103X	Intermediate		
614/14	ΔS117	Intermediate/Severe	Deletion	
616/14	N63D	Intermediate	Missense mutation	
15-15	R88H	Severe		
f48	R88P	Intermediate		
617/14	P120R	Intermediate		
12-15	L279X	Intermediate/Severe	Non-sense mutation	C-terminal
9-15	L359X	Mild		
1121-14	R443X	Intermediate		
H148	C422R	Mild/Intermediate	Missense mutation	
H162	C422R	Mild		
F24	P467L	Mild		
H8	R468Q	Severe		
13-15	R468Q	Severe		
1124-14	R468Q	Intermediate/Severe		
1122-14	R468Q	Severe		

Table 12: List of analyzed patients samples displaying different mutations (non-sense, missense or deletion) in N-terminal or C-terminal part of the *IDS* gene. The phenotypic classification of each patient (mild, intermediate or severe) is also reported.

Three FGF signaling-specific markers (*DUSP6, ERK1* and *PEA3*) were analyzed by RQ-PCR for each sample and results were compared to those obtained from healthy control samples.

Non-sense mutation N-terminal (Fig. 107):

Patient H150 (P4Sfs mutation) shows a down regulation of *DUSP6* and *ERK1* and an up-regulation of *PEA3* transcripts levels when compared with controls.

Patients H147 (R8X mutation) and f23 (Y103X mutation) display a down regulation of all markers when compared with control.

Patient H122 (W12X mutation) shows an up regulation of all markers expression when compared with control.

Patient 23-15 (Q66X mutation) displays an up regulation of *DUSP6* and *PEA3* and a down regulation of *ERK1* transcripts levels when compared with controls.

Patient 37-15 (Q80X mutation) shows a down regulation of *DUSP6* and *PEA3* transcripts levels when compared with controls.

Deletion N-terminal (Fig. 108):

Patient 614/14 (Δ117 mutation) displays a down regulation of *DUSP6* and *ERK1* and an up regulation of *PEA3* transcripts levels when compared with controls.

Missense mutation N-terminal (Fig. 109):

Patients 616/14 (N63D mutation) and 617/14 (P120R mutation) show a down regulation of *DUSP6* and *ERK1*and an up regulation of *PEA3* transcripts when compared with controls.

Patient f48 (R88P mutation) displays a down regulation of all markers expression when compared with controls.

Patient 15-15 (R88H mutation) show a down regulation of *DUSP6* and *PEA3* transcripts when compared with controls.

Non-sense mutation C-terminal (Fig. 110):

Patient 12-15 (L279X mutation) shows a down regulation of *DUSP6* transcripts when compared with controls.

Patient 9-15 (L359X mutation) displays a down regulation of *DUSP6* and *PEA3* transcripts expression when compared with controls.

Patient 1121-14 (R443X mutation) exhibits an up regulation of *DUSP6* transcripts when compared with controls .

Missense mutation C-terminal (Fig. 111):

Patients H148 (C422R mutation) and 1122-14 (R468Q mutation) display a down regulation of all markers when compared with controls.

Patient H162 (C422R mutation) shows a down regulation of *DUSP6* and *ERK1* and an up regulation of *PEA3* transcripts levels when compared with controls.

Patient F24 (P467L mutation) displays a down regulation of *DUSP6* and an up regulation of *PEA3* transcript levels when compared with controls.

Patients H8 (R468Q mutation) and 1124-14 (R468Q mutation) displays an up regulation of all markers expression when compared with controls

Patient 13-15 (R468Q mutation) shows an up regulation of *DUSP6* and *ERK1* transcripts when compared with controls.

Given the heterogeneous results detected when evaluating the same type of mutation, I tried to analyze the data considering patient phenotype (mild, intermediate and severe).

All patients displaying a mild form of the disease (H150, H147, 9-15, H162, F24) exhibited a general down regulation of FGF signaling markers.

Patient H148 that has a mild/intermediate form displayed a down regulation of all FGF signaling-related markers levels.

Patients with an intermediate form of the disease showed down regulation (f23, 616/14, f48, 617/14) or up regulation (H122, 23-15, 1121-14) of FGF signaling-related markers expression.

Among patients with the intermediate phenotype, all affected subjects displaying a down regulation of the FGF signaling markers were those harboring mutations in the N-terminal part of *IDS* gene: 616/14, f48 and 617/14 display a missense mutation, f23 has a non sense mutation with a stop codon after the active residue Cys84.

Among patients exhibiting an up regulation of the FGF signaling markers, H122 and 23-15 were characterized by a non-sense mutation and a stop codon before the active residue Cys84, respectively, while 1121-14 had a non sense mutation in the C-terminus.

Patients 614/14 and 1124-14 displaying an intermediate/severe phenotype showed a down regulation (614/14) and an up regulation (1124-14) of the analyzed markers.

Patients with a severe form of MPSII showed a down regulation (37-15, 15-15,1122-14) or an up regulation (H8, 13-15) of the analyzed FGF-signaling markers.

Among affected patients exhibiting a severe phenotype those characterized by a down regulation of the FGF signaling markers harbor mutations in the N-terminal part of the *IDS* gene (37-15 and 15-15) or a missense mutation in the C-terminus (1122-14), while patients displaying an up regulation of the same markers were characterized by missense mutations in the C-terminus.

Non-sense mutation N-terminal

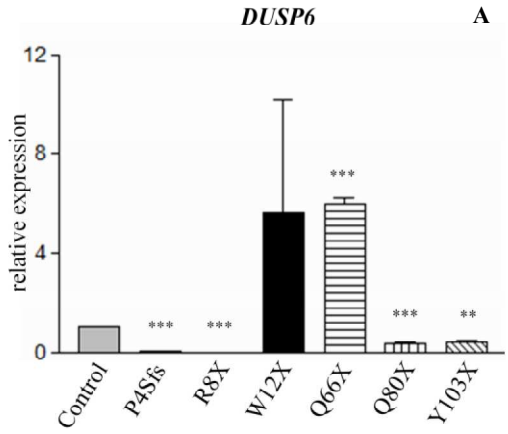

DUSP6				B
Sample	**Mutation**	**Mean**	**Standard deviation**	**p-value**
Control	/	1	/	/
H150	P4Sfs	0,03	0,00	4,02E-06
H147	R8X	0,00	0,00	6,17E-09
H122	W12X	5,64	10,12	0,364
23-15	Q66X	5,97	0,55	0,001
37-15	Q80X	0,34	0,08	0,001
f23	Y103X	0,41	0,13	0,003

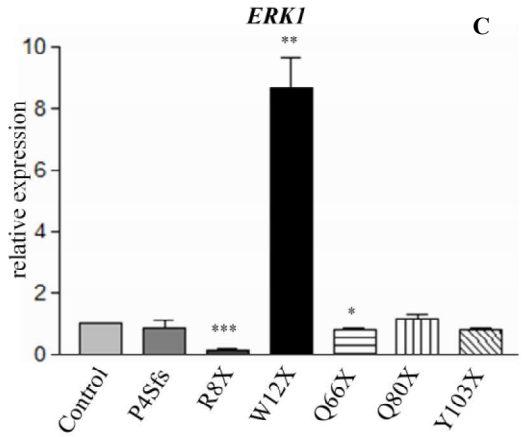

ERK1				D
Sample	**Mutation**	**Mean**	**Standard deviation**	**p-value**
Control	/	1	/	/
H150	P4Sfs	0,86	0,41	6,08E-01
H147	R8X	0,15	0,02	1,40E-04
H122	W12X	8,65	1,95	0,004
23-15	Q66X	0,76	0,12	0,028
37-15	Q80X	1,13	0,32	0,466
f23	Y103X	0,76	0,17	0,067

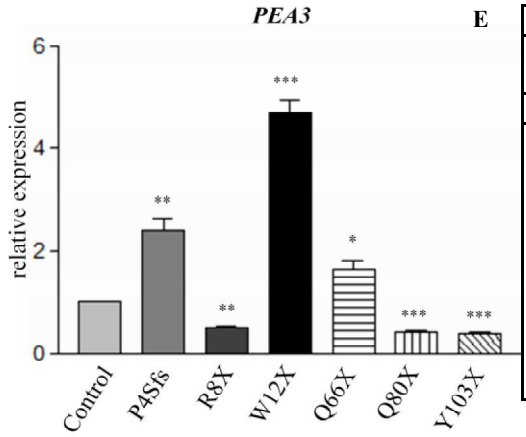

PEA3				F
Sample	**Mutation**	**Mean**	**Standard deviation**	**p-value**
Control	/	1	/	/
H150	P4Sfs	2,38	0,48	1,04E-02
H147	R8X	0,50	0,05	3,59E-03
H122	W12X	4,7	0,46	0,001
23-15	Q66X	1,65	0,35	0,035
37-15	Q80X	0,39	0,08	0,001
f23	Y103X	0,37	0,06	0,000

Figure 107: (B-D-F) Real time PCR analysis performed in patients with non-sense mutation in the N-terminal part of *IDS* gene, using *DUSP6*, *ERK1* and *PEA3* primers. The results were compared to unaffected control subjects. (A,C,E) Graphic representation of *DUSP6*, *ERK1* and *PEA3* expression in patients samples compared to unaffected subjects. Results are expressed as a mean ± SEM of four independent experiments. (* p<0,05; ** p<0,02; *** p<0,002; t-test).

Deletion N-terminal

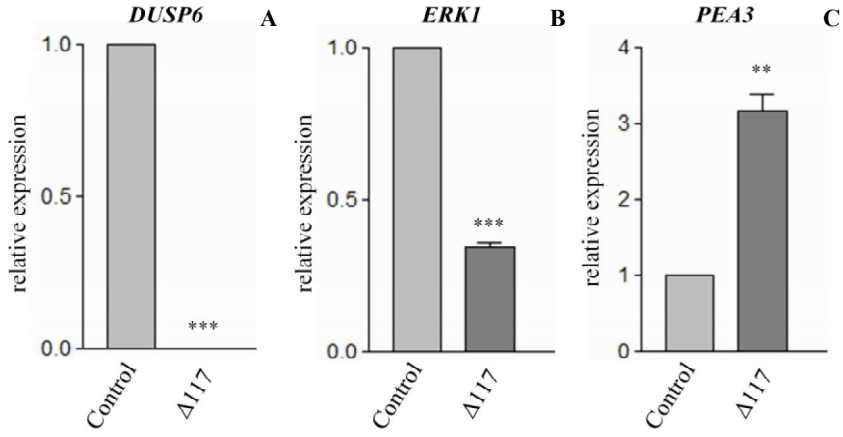

DUSP6				D
Sample	**Mutation**	**Mean**	**Standard deviation**	**p-value**
Control	/	1	/	/
614/14	ΔS117	0,00	0,00	8,10E-11

ERK1				E
Sample	**Mutation**	**Mean**	**Standard deviation**	**p-value**
Control	/	1	/	/
614/14	ΔS117	0,34	0,03	1,60E-05

PEA3				F
Sample	**Mutation**	**Mean**	**Standard deviation**	**p-value**
Control	/	1	/	/
614/14	ΔS117	3,16	0,43	2,00E-03

Figure 108: Real time PCR analysis performed in a patient with deletion Δ117 in the N-terminal part of *IDS* gene, using *DUSP6*, *ERK1* and *PEA3* primers. The results were compared to unaffected control subjects. (A,B,C) Graphic representation of *DUSP6*, *ERK1* and *PEA3* expression in patient samples compared to unaffected subjects. Results are expressed as a mean ± SEM of four independent experiments. (* p<0,05; ** p<0,02; *** p<0,002; t-test). (D,E,F) Expression mean, standard deviation and t test p-value.

Missense mutation N-terminal

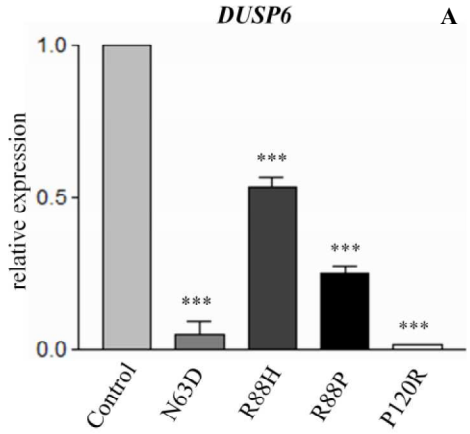

DUSP6				B
Sample	**Mutation**	**Mean**	**Standard deviation**	**p-value**
Control	/	1	/	/
616/14	N63D	0,05	0,09	0,001
15-15	R88H	0,54	0,05	0,001
f48	R88P	0,27	0,05	7,20E-05
617/14	P120R	0,01	0,00	1,40E-08

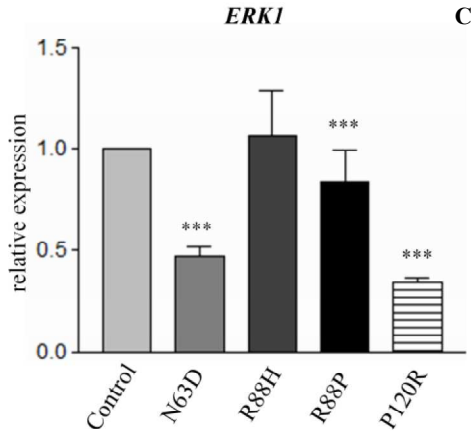

ERK1				D
Sample	**Mutation**	**Mean**	**Standard deviation**	**p-value**
Control	/	1	/	/
616/14	N63D	0,47	0,09	0,002
15-15	R88H	1,06	0,44	0,791
f48	R88P	0,84	0,35	3,63E-01
617/14	P120R	0,34	0,05	0,00E+00

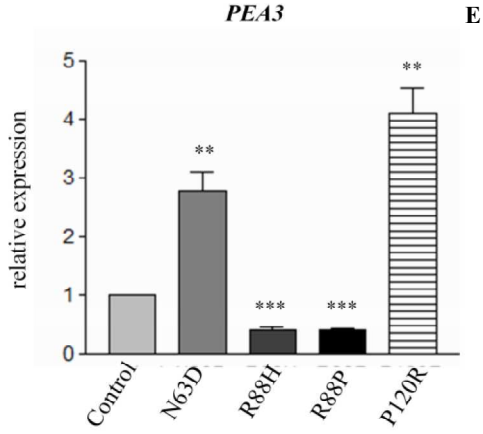

PEA3				F
Sample	**Mutation**	**Mean**	**Standard deviation**	**p-value**
Control	/	1	/	/
616/14	N63D	2,76	0,66	0,013
15-15	R88H	0,41	0,06	0,001
f48	R88P	0,38	0,06	1,00E-03
617/14	P120R	4,09	0,86	6,00E-03

Figure 109: (B,D,F) Real time PCR analysis performed in patients with missense mutation in the N-terminal part of *IDS* gene, using *DUSP6*, *ERK1* and *PEA3* primers. The results were compared to unaffected control subjects. (A,C,E) Graphic representation of *DUSP6*, *ERK1* and *PEA3* expression in patients samples compared to unaffected subjects. Results are expressed as a mean ± SEM of four independent experiments. (* p<0,05; ** p<0,02; *** p<0,002; t-test).

Non-sense mutation C-terminal

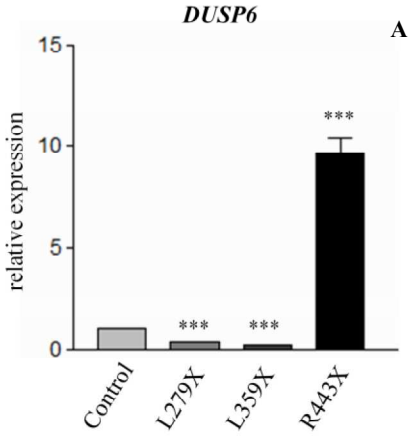

DUSP6				B
Sample	**Mutation**	**Mean**	**Standard deviation**	**p-value**
Control	/	1	/	/
12-15	L279X	0,33	0,07	0,001
9-15	L359X	0,20	0,06	8,90E-05
1121-14	R443X	9,63	1,53	0,002

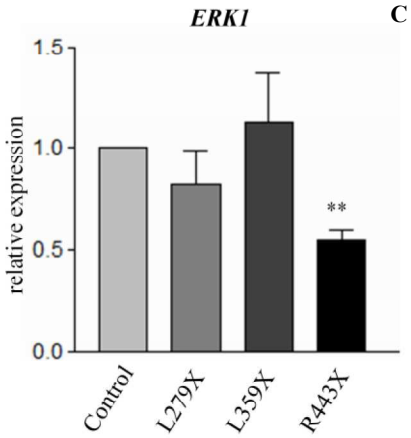

ERK1				D
Sample	**Mutation**	**Mean**	**Standard deviation**	**p-value**
Control	/	1	/	/
12-15	L279X	0,83	0,33	0,373
9-15	L359X	1,13	0,5	6,39E-01
1121-14	R443X	0,54	0,11	0,003

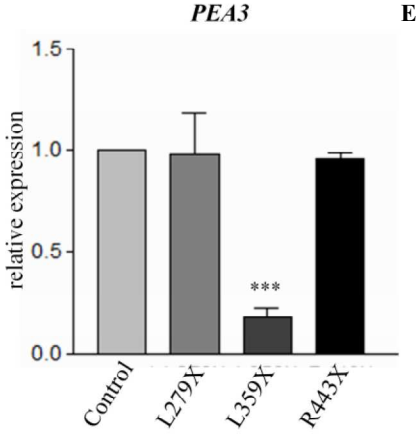

PEA3				F
Sample	**Mutation**	**Mean**	**Standard deviation**	**p-value**
Control	/	1	/	/
12-15	L279X	0,98	0,39	0,935
9-15	L359X	0,18	0,09	1,00E-03
1121-14	R443X	0,96	0,06	0,275

Figure 110: (B,D,F) Real time PCR analysis performed in patients with non-sense mutation in the C-terminal part of *IDS* gene, using *DUSP6*, *ERK1* and *PEA3* primers. The results were compared to unaffected control subjects. (A,C,E) Graphic representation of *DUSP6*, *ERK1* and *PEA3* expression in patients samples compared to unaffected subjects. Results are expressed as a mean ± SEM of four independent experiments. (* p<0,05; ** p<0,02; *** p<0,002; t-test).

Missense mutation C-terminal

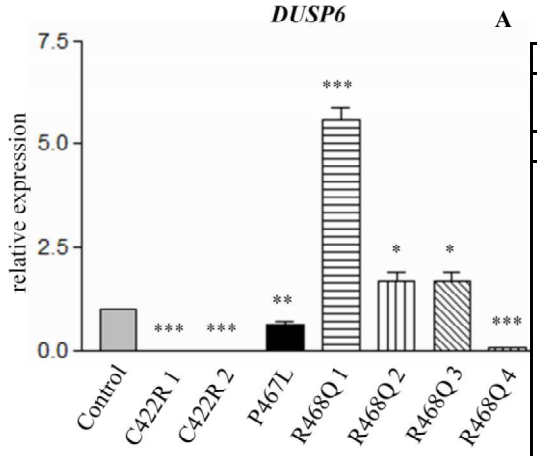

DUSP6				B
Sample	**Mutation**	**Mean**	**Standard deviation**	**p-value**
Control	/	1	/	/
H148	C422R 1	0,00	0,00	4,49E-09
H162	C422R 2	0,00	0,00	2,72E-08
f24	P467L	0,63	0,13	0,012
H8	R468Q 1	5,69	0,52	0,001
13-15	R468Q 2	1,67	0,55	0,031
1124-14	R468Q 3	1,68	0,57	0,033
1122-14	R468Q 4	0,05	0,00	2,60E-08

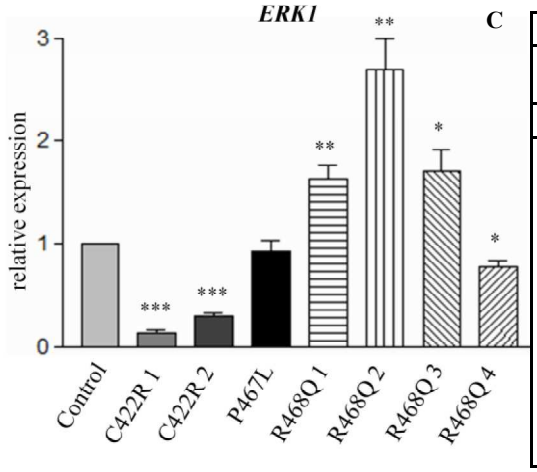

ERK1				D
Sample	**Mutation**	**Mean**	**Standard deviation**	**p-value**
Control	/	1	/	/
H148	C422R 1	0,13	0,04	7,98E-04
H162	C422R 2	0,30	0,05	1,51E-03
f24	P467L	0,92	0,22	0,527
H8	R468Q 1	1,63	0,26	0,016
13-15	R468Q 2	2,7	0,59	0,010
1124-14	R468Q 3	1,71	0,4	0,039
1122-14	R468Q 4	0,78	0,10	2,40E-02

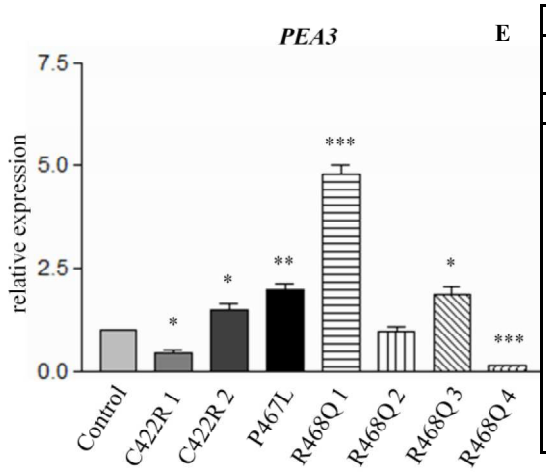

PEA3				F
Sample	**Mutation**	**Mean**	**Standard deviation**	**p-value**
Control	/	1	/	/
H148	C422R 1	0,42	0,15	2,24E-02
H162	C422R 2	1,50	0,32	2,50E-02
f24	P467L	1,98	0,27	0,005
H8	R468Q 1	4,78	0,48	0,001
13-15	R468Q 2	0,97	0,21	0,800
1124-14	R468Q 3	1,84	0,4	0,025
1122-14	R468Q 4	0,12	0,02	6,30E-06

Figure 111: (B,D,F) Real time PCR analysis performed in patients with missense mutation in the C-terminal part of the *IDS* gene, using *DUSP6*, *ERK1* and *PEA3* primers. The results were compared to unaffected control subjects. (A,C,E) Graphic representation of *DUSP6*, *ERK1* and *PEA3* expression in patients samples compared to unaffected

subjects. Results are expressed as a mean ± SEM of four independent experiments. (* p<0,05; ** p<0,02; *** p<0,002; t-test).

I examined the rate of dysregulation (down regulation, no change or up regulation) of each FGF signaling-marker (*DUSP6*, *ERK1* and *PEA3*) in patient samples.

DUSP6 is down regulated in the 67% of patients, up regulated in the 28% and has no change in its expression in the 5% of patients (Fig. 112).

ERK1 is down regulated in the 57% of patients, up regulated in the 24% and has no change in its expression in the 19% of patients (Fig. 113).

PEA3 is down regulated in the 38% of patients, up regulated in the 48% and has no change in its expression in the 14% of patients (Fig. 114).

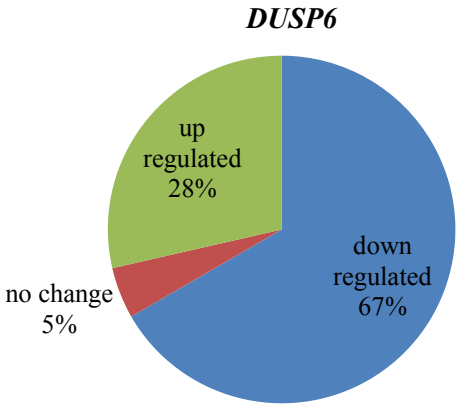

Figure 112: Percentage of *DUSP6* dysregulation (down regulation, up regulation or no change) in patients.

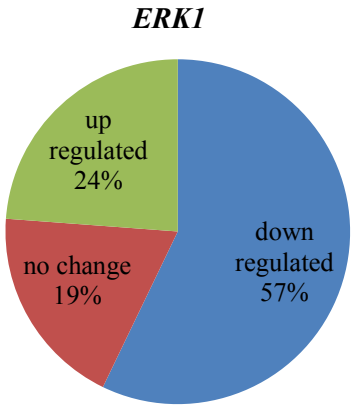

Figure 113: Percentage of *ERK1* dysregulation (down regulation, up regulation or no change) in patients.

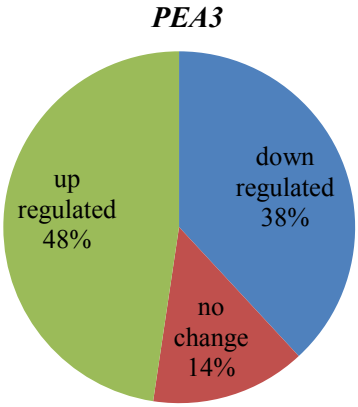

Figure 114: Percentage of *PEA3* dysregulation (down regulation, up regulation or no change) in patients.

5 DISCUSSION

Traditionally, the pathogenesis of Mucopolysaccharidosis type II has been attributed exclusively to the systemic accumulation of undegraded glycosaminoglycans and the consequent alterations in cellular processes.

However, considering the clinical heterogeneity of patients manifestations, this might be a simplistic view of a complex etiology. There is no correlation between enzymatic activity, that in patients is completely or almost completely depleted, and the degree of phenotypic severity. Moreover, patients with the same mutation may display different pathological manifestations (Martin et al., 2008). Despite IDS is an ubiquitously expressed enzyme, there is no correlation between MPSII severity and the extent of GAGs accumulation, organ involvement and tissue response to therapeutic treatments.

Moreover, the mouse model of another mucopolysaccharidosis, MPS I, displays a progressive worsening of symptoms irrespective of tissutal GAGs accumulation (Heppner et al., 2015).

These observations led my scientific group to hypothesize that alternative pathological mechanisms may occur in Hunter syndrome, together with GAGs storage.

Mucopolysaccharidosis type II is characterized by the involvement of many organs in which different cascades of molecular alterations may occur. To simplify the investigation of candidate molecular mechanisms underlying MPSII, I focused my research on the skeletal system.

It has been already shown in other MPSs that altered signaling pathways may be responsible for the skeletal manifestations: the MPS VI mouse model displays an enhanced TGFβ signaling causing osteopenia (Simonaro et al., 2005), and altered FGF signaling regulation has been detected in MPS I chondrocytes and MPS I mouse bones (Kingma et al., 2016).

However, it's not clear when the deregulation of signaling pathways and consequent bone alterations may occur. In the MPSI mouse model it has been demonstrated that alterations of skeletal development appear very early, before any histological change (Heppner et al., 2015). Moreover, ERT is completely unsuccessful in treating Hunter syndrome-related bone manifestations (Morini et al.,2010), suggesting that the only iduronate 2-sulfatase replacement is not sufficient to restore normal skeletal development and homeostasis.

In this work it has been hypothesized that IDS, beyond its GAGs catabolic role inside lysosomes, may have other molecular functions. It has been already demonstrated that

this enzyme is an important regulator of early developmental stages and that it controls the osteogenic process (Moro et al., 2010; Mandal et al., 2013).

For the comprehension of the molecular pathogenesis of Mucopolysaccharidosis type II, I took advantage of the zebrafish model, which allows to rapidly analyze signaling pathways and bone ossification defect in different life stages (Hammond & Moro, 2012).

Using the fish model, I first demonstrated that the IDS enzyme is highly expressed in bone regions with high osteogenic activity. In zebrafish the opercle, brachiostegal ray and ceratobranchial arches are neural crest-derived bones, while the cleithrum is of mesodermal origin (Kague et al., 2012). Immunohistochemical analysis at 5dpf showed that the IDS protein is particularly enriched in bones of neural crest origin, such as the opercle and brachiostegal ray, while it is weakly localized in the cleithrum.

I created different IDS loss of function zebrafish models using the morpholino technology and the Crispr/Cas9 technique. These animal models have been shown to be good to evaluate MPSII pathogenesis, because they display some typical Hunter patient manifestations such as hepatomegaly and defects in chondrogenesis and osteogenesis.

Using a translation initiation blocking morpholino for the fish Ids orthologue, I showed that fish morphants display an early down regulation of *sox10* expression, which is a marker of migrating cranial neural crest cells. The decrease of Sox10 was in turn associated with a dysregulation of bone markers expression together with cartilage and bone formation defects. The impaired expression of *sox10* and bone markers, appeared before any evident massive accumulation of GAGs, suggesting that other molecular mechanisms may have been implicated since early stages in the pathogenic process.

Interestingly, I found an up regulation of the FGF signaling in Ids-KD fish at 2dpf compared to age-matched controls, and this dysregulation was maintained during postnatal stages.

FGF signaling is a pathway involved in many developmental processes, including the skeletal embryonic development and postnatal growth (Ornitz et al., 2002). Therefore, I hypothesized that Ids deficiency may affect FGF signaling during early stages of development, thus leading to an impaired expression of genes involved in bone formation.

FGF signaling induces cranial neural crest (NCC) differentiation and regulates the expression and function of the Sox10 transcription factor (Dravis et al., 2015; Teven et al., 2014). *Sox10* is an important regulator of migrating NCCs, that differentiate into bone and cartilage, and it has been found to activate the *Col2a1* gene transcription (Suzuki et al., 2006). In Ids-KD morphant Sox10 appears to be down-regulated and morphant fish display defective *runx2b* and *collagenX* expression, in neural crest-derived bones

(opercle, brachiostegal ray, ceratobranchial arch). Moreover, FGF signaling is essential during early stages of endochondral and intramembranous ossification (Ornitz et al., 2002). In agreement with this, morphant fish showing alterations of the FGF pathway exhibited severe defects in chondrogenesis and osteogenesis.

To address the potential involvement of the FGF signaling in Ids loss of function models, I tested also a splicing site-blocking morpholino targeting a splice acceptor site of the *ids* exon2. While confocal microscopy and *in situ* hybridization analysis showed a down regulation of the FGF pathway similar results were not detected by quantitative real time PCR analysis. This discrepancy may be due to the fact that both confocal and *in situ* hybridization analysis allow the detection of tissue-specific differences of protein localization and gene expression, respectively. Indeed real time PCR analysis is generally performed on whole fish lysates.

In contrast to the up regulation of the FGF signaling detected in fish treated with the translation initiation-blocking morpholino, morphants generated by the Ids splicing site-blocking morpholino showed a mild FGF down-regulation. This further discrepancy may be due to the different targeting of the morpholinos: while the translation initiation-blocking one abrogates Ids synthesis from the ATG codon, the splicing site-blocking one leads to the generation of a truncated Ids peptide. It may be tempting to speculate that in some cases the complete abrogation of Ids function could trigger a boost of the FGF signaling, as a compensative mechanism. On the other hand, short Ids peptides, produced by premature stop codons, may act as dominant negative factors against the FGF pathway.

Nonetheless, both morphant models are characterized by a partial enzymatic deficiency which does not reflect the complete lack of IDS activity observed in Hunter patients. Moreover all morpholinos suffer from temporally-restricted activity, thus hampering analysis at late life stages.

To address these issues, by the Crispr/Cas9 technology I generated a stable zebrafish mutant which exhibited a complete loss of Ids activity.

Ids-KO fish at early stages of development showed a characteristic rapid bone mineralization process, which was associated with increased expression of bone-related markers up to 7dpf.

In mutant fish, the FGF pathway was shown to be down regulated, in agreement with the results obtained with the splicing-blocking morpholino. Since in the mutant a premature stop codon, due to an upstream deletion of five nucleotides was produced, the above mentioned hypothesis of a dominant-negative effect of a truncated Ids protein on FGF signaling activity cannot be ruled out.

Despite controversial studies describing the role of FGF signaling in bone formation, it has been already reported that reduced FGF signaling activity is associated with decreased proliferation of osteoprogenitor cells, while enhanced FGF signaling, is associated with increased osteoblast differentiation and apoptosis (Su et al., 2014; Ornitz & Marie, 2015).

Thus, the impaired FGF signaling-related osteogenic and chondrogenic process detected in the generated morphant and mutant Ids loss of function fish models represents a potential intriguing causative mechanism underlying the skeletal defects observed in Hunter patients.

To further support the results obtained with the fish models, I extended my investigation using an already established IDS knockout mouse model (Garcia et al., 2007). In particular, IDS-KO mice showed irregularly shaped Alcian blue-stained cranial sutures, suggesting a premature defective bone mineralization process. On the other hand, long bones of IDS-KO mice appeared normal at early stages of development, while at six months of age they start to become shorter when compared with age-matched WT mice. A detailed expression profile, revealed that IDS KO mice display a significant increase in the *col2a1* expression and decrease of bone-related markers (*collagen X* and *osteocalcin*), already at postnatal stages, when GAGs storage is negligible. More interestingly, the reduced expression of bone-related markers was not associated with increased transcription of cytokine genes (TNFα, IL1β), suggesting a defective osteoblast differentiation which was not related to an inflammatory process.

When evaluating FGF signaling markers, I found a substantial down regulation of FGF-related target genes, particularly in the epiphysis of long bones, supporting the evidence that secondary ossification centers appear more susceptible to the cell signaling defects. My observations are in agreement with the well-established role of FGF signaling in cranial suture premature closure and maintenance of proliferating osteogenic cells in the epiphyseal growth plate (Ornitz et al, 2002; Ornitz et al., 2015; Teven et al., 2014). It remains to be elucidated which of the different FGF ligands and receptors may be more affected in the long bones of IDS KO mice.

The use of different animal models confirmed the involvement of FGF signaling in the defective skeletal development occurring as a consequence of IDS loss of function. According to different variables, including the type of animal model, the degree of enzymatic dysfunction, the stage of development and analyzed tissue, a different FGF pathway dysregulation has been detected. In Hunter disease more than 300 different mutations have been so far characterized in the *IDS* gene (*www.hgmd.org*). Therefore, the animal models I used, do not perfectly resemble the wide spectrum of genetic alterations

underlying Hunter syndrome. Nonetheless, a convincing evidence of a direct link between IDS loss of function and FGF pathway deregulation might come from the analysis of patients fibroblasts harboring different IDS mutations. For this reason, I decided to analyze the expression of FGF pathway-related markers in isolated fibroblasts of a selected group of Hunter patients affected by well-defined mutations. All patients were characterized by different phenotypes (mild, intermediate or severe form) which were independent from the type and position of mutations in the *IDS* gene.

Despite heterogeneous results, all patients with a mild form of MPSII showed a general down regulation of FGF signaling markers.

In particular, most patients displayed a down regulation of *DUSP6* (67%) and *ERK1*(57%) markers when compared with healthy controls. *DUSP6* is a downstream target of FGF signaling and the activation of its transcription is regulated through the RAS/MAPK pathway in which ERK1 is a transducer (Znosko et al., 2010). Only 33% of the patients exhibited a down regulation of *PEA3,* which is a downstream target of FGF signaling and mediate the transcriptional response of the FGF pathway, activating directly *DUSP6* expression (Znosko et al., 2010). This result may suggest that other pathways may be implicated in the regulation of *PEA3* expression downstream to IDS loss of function.

Nevertheless, although the number of patients so far examined is limited, it might be plausible to conclude that at least in a significant proportion of Hunter patients a direct link between IDS deficit and FGF pathway deregulation does exist.

Which mechanisms may underlie the FGF pathway impairment due to IDS dysfunction remain to be clarified. It is possible that mutations altering lysosomal function may affect the endosomal/lysosomal system which controls the recycling of FGF receptors, or the transport of extracellular and membrane FGF pathway-associated proteins. Alternatively, since Iduronate 2-sulfatase participates to the catabolism of heparan and dermatan sulfate, alterations of its enzymatic activity may negatively impact on the amount, distribution and type of extracellular matrix components. In agreement with the latter hypothesis, other lysosomal storage disorders showed an impaired extracellular matrix remodeling (Ballabio & Gieselmann, 2009; Heppner et al, 2015). Since the extracellular matrix plays key roles in cell signaling modulation, its structural and functional impairment may affect the binding and diffusion of growth factors and signaling ligands. Moreover extracellular matrix components can enhance the interaction between cell-specific receptors and ligands or participate in signal transduction by directly activating cell signaling (Lu et al., 2011).

In particular, the ECM has been shown to have an important role in the regulation of FGF signaling activation, since heparan sulfate binding to FGF receptors and ligands is necessary to trigger the downstream pathway (Tumova et al., 2000). Alterations of GAGs distribution in the ECM may cause dysregulation of cell signaling pathways, including FGF signaling (Kingma et al., 2016).

Other mechanisms independent from the IDS enzymatic activity deficiency may be evoked. Intriguingly, as different mutations predicted to produce alternative IDS conformational structures have been shown to differently regulate the FGF pathway, it might be possible that the IDS enzyme itself may directly interact with key FGF-related cell signaling molecules.

In conclusion, this work showed that cell signaling alterations, earlier than substrate accumulation can be responsible for the skeletal manifestations in MPSII. A more complete knowledge of Hunter syndrome pathogenesis could contribute to the identification of novel therapies for the targeted treatment of MPSII bone defects.

6 BIBLIOGRAPHY

Aldenhoven M, Sakkers RJB, Boelens J, De Koning TJ, Wulffraat NM. Musculoskeletal manifestations of lysosomal storage disorders. *Ann Rheum Dis* 2009; 68:1659-1665

Al Sawaf S, Mayatepek E, Hoffmann B. Neurological findings in Hunter disease: Pathology and possible therapeutic effects reviewed. *J Inherit Metab Dis.* 2008 Aug;31(4):473-80.

Appelqvist H, Wäster P, Kågedal K, Öllinger K. The lysosome : from waste bag to potential therapeutic target. *J Mol Cell Biol.* 2013 Aug; 5(4):214-26.

Arya M, Shergill IS, Williamson M, Gommersall L, Arya N, Patel HRH. Basic principles of real-time quantitative PCR. *Expert Rev.Mol. Diagn.* 2005; 5(2):209-219.

Aszodi A, Bateman JF, Gustafsson E, Boot-Handford R, Fassler R. Mammalian skeletogenesis and extracellular matrix : What can we learn from knockout mice? *Cell Struct Funct.* 2000; 25:73–84.

Baek WY, Lee MA, Jung JW, Kim SY, Akiyama H, de Crombrugghe B, Kim JE. Positive regulation of adult bone formation by osteoblast-specific transcription factor osterix. *J Bone Miner Res*. 2009 Jun;24(6):1055-65.

Ballabio A, Gieselmann V. Lysosomal disorders : From storage to cellular damage. *Biochim Biophys Acta.* 2009 Apr;1793(4):684-96

Balzano N, Villani GR, Grosso M, Izzo P, Di Natale P. Detection of four novel mutations in the iduronate-2-sulfatase gene. *Hum Mutat.* 1998;11(4):333.

Behonick DJ, Werb Z. A bit of give and take : the relationship between the extracellular matrix and the developing chondrocyte. *Mech Dev.* 2003 Nov;120(11):1327-36.

Berkovits BD, Mayr C. Alternative 3' UTRs act as scaffolds to regulate membrane protein localization. *Nature.* 2015 Jun 18;522(7556):363-7.

Bonuccelli G, Regis S, Filocamo M, Corsolini F, Caroli F, Gatti R. A deletion involving exons 2-4 in the iduronate-2-sulfatase gene of a patient with intermediate Hunter syndrome. *Clin Genet.* 1998 Jun;53(6):474-7.

Bonuccelli G, Di Natale P, Corsolini F, Villani G, Regis S, Filocamo M. The effect of four mutations on the expression of iduronate-2-sulfatase in mucopolysaccharidosis type II. *Biochim Biophys Acta.* 2001 Nov 29;1537(3):233-8.

Boustany RN. Lysosomal storage diseases -- the horizon expands. *Nat Rev Neurol.* 2013 Oct;9(10):583-98.

Casari A, Schiavone M, Facchinello N, Vettori A, Meyer D, Tiso N, Moro E, Argenton F. A Smad3 transgenic reporter reveals TGF-beta control of zebrafish spinal cord development. *Dev Biol.* 2014 Dec 1;396(1):81-93.

Chen P, Cescon M, Zuccolotto G, Nobbio L, Colombelli C, Filaferro M, Vitale G, Feltri ML, Bonaldo P. Collagen VI regulates peripheral nerve regeneration by modulating macrophage recruitment and polarization. *Acta Neuropathol.* 2015 Jan;129(1):97-113.

Chkioua L, Khedhiri S, Ferchichi S, Tcheng R, Chahed H, Froissart R, Vianey-Saban C, Laradi S, Miled A. Molecular analysis of iduronate -2- sulfatase gene in Tunisian patients with mucopolysaccharidosis type II. *Diagn Pathol.* 2011 May 23;6:42.

Chistiakov DA, Kuzenkova LM, Savost'anov KV, Gevorkyan AK, Pushkov AA, Nikitin AG, Vashakmadze ND, Zhurkova NV, Podkletnova TV, Namazova-Baranova LS, Baranov AA. Genetic Analysis of 17 Children with Hunter Syndrome: Identification and Functional Characterization of Four Novel Mutations in the Iduronate-2-Sulfatase Gene. *J Genet Genomics.* 2014 Apr 20;41(4):197-203.

Clarke LA. Pathogenesis of skeletal and connective tissue involvement in the mucopolysaccharidoses : glycosaminoglycan storage is merely the instigator. *Rheumatology (Oxford).* 2011 Dec;50 Suppl 5:v13-8.

Clarke LA, Hollak CE. The clinical spectrum and pathophysiology of skeletal complications in lysosomal storage disorders. *Best Pract Res Clin Endocrinol Metab.* 2015 Mar;29(2):219-35.

Corallo D, Schiavinato A, Trapani V, Moro E, Argenton F, Bonaldo P. Emilin3 is required for notochord sheath integrity and interacts with Scube2 to regulate notochord-derived Hedgehog signals. *Development.* 2013 Nov;140(22):4594-601

Deckelbaum RA, Majithia A, Booker T, Henderson JE, Loomis CA. The homeoprotein engrailed 1 has pleiotropic functions in calvarial intramembranous bone formation and remodeling. *Development.* 2006 Jan;133(1):63-74.

Dravis C, Spike BT, Harrell JC, Johns C, Trejo CL, Southard-Smith EM, Perou CM, Wahl GM. Sox10 Regulates Stem / Progenitor and Mesenchymal Cell States in Mammary Epithelial Cells. *Cell Rep.* 2015 Sep 29;12(12):2035-48.

Felber K, Elks PM, Lecca M, Roehl HH. Expression of osterix Is Regulated by FGF and Wnt / β -Catenin Signalling during Osteoblast Differentiation. *PLoS One.* 2015 Dec 21;10(12):e0144982.

Flanagan-Steet H, Sias C, Steet R. Altered chondrocyte differentiation and extracellular matrix homeostasis in a zebrafish model for mucolipidosis II. *Am J Pathol*. 2009 Nov;175(5):2063-75.

Garcia AR, Pan J, Lamsa JC, Muenzer J. The characterization of a murine model of mucopolysaccharidosis II (Hunter syndrome). *J Inherit Metab Dis.* 2007 Nov;30(6):924-34.

Giugliani R, Federhen A, Rojas MV, Vieira T, Artigalás O, Pinto LL, Azevedo AC, Acosta A, Bonfim C, Lourenço CM, Kim CA, Horovitz D, Bonfim D, Norato D, Marinho D, Palhares D, Santos ES, Ribeiro E, Valadares E, Guarany F, de Lucca GR, Pimentel H, de Souza IN, Correa J Sr, Fraga JC, Goes JE, Cabral JM, Simionato J, Llerena J Jr, Jardim L, Giuliani L, da Silva LC, Santos ML, Moreira MA, Kerstenetzky M, Ribeiro M, Ruas N, Barrios P, Aranda P, Honjo R, Boy R, Costa R, Souza C, Alcantara FF, Avilla SG, Fagondes S, Martins AM. Mucopolysaccharidosis I , II , and VI : Brief review and guidelines for treatment. *Genet Mol Biol.* 2010 Oct;33(4):589-604.

Gökdoğan Ç, Altinyay Ş, Gökdoğan O, Tutar H, Gündüz B, Okur İ, Tümer L, Kemaloğlu YK. Audiologic evaluations of children with mucopolysaccharidosis. *Braz J Otorhinolaryngol.* 2016 May-Jun;82(3):281-4.

Hammond CL, Schulte-merker S. Two populations of endochondral osteoblasts with differential sensitivity to Hedgehog signalling. *Development*. 2009 Dec; 136(23):3991-4000.

Hammond CL, Moro E. Using transgenic reporters to visualize bone and cartilage signaling during development in vivo. *Front Endocrinol (Lausanne).* 2012 Jul 18;3:91.

Harada S, Rodan GA. Control of osteoblast function and regulation of bone mass. *Nature.* 2003 May 15;423(6937):349-55.

Heppner JM, Zaucke F, Clarke LA. Extracellular matrix disruption is an early event in the pathogenesis of skeletal disease in mucopolysaccharidosis I. *Mol Genet Metab.* 2015 Feb;114(2):146-55.

Inoue D, Wittbrodt J. One for All — A Highly Efficient and Versatile Method for Fluorescent Immunostaining in Fish Embryos. *PLoS One.* 2011;6(5):e19713.

Isogai K, Sukegawa K, Tomatsu S, Fukao T, Song XQ, Yamada Y, Fukuda S, Orii T, Kondo N. Mutation analysis in the iduronate-2-sulphatase gene in 43 Japanese patients with mucopolysaccharidosis type II (Hunter disease). *J Inherit Metab Dis.* 1998 Feb;21(1):60-70.

Jao L, Wente SR, Chen W. Efficient multiplex biallelic zebra fi sh genome editing using a CRISPR nuclease system. *Proc Natl Acad Sci U S A.* 2013 Aug 20 ; 110(34): 13904-9.

Kague E, Gallagher M, Burke S, Parsons M, Franz-Odendaal T, Fisher S. Skeletogenic Fate of Zebrafish Cranial and Trunk Neural Crest. *PLoS One.* 2012;7(11):e47394.

Kato T, Kato Z, Kuratsubo I, Tanaka N, Ishigami T, Kajihara J, Sukegawa-Hayasaka K, Orii K, Isogai K, Fukao T, Shimozawa N, Orii T, Kondo N, Suzuki Y. Mutational and structural analysis of Japanese patients with mucopolysaccharidosis type II. *J Hum Genet.* 2005;50(8):395-402.

Kawakami M, Yamamura K. Cranial bone morphometric study among mouse strains. *BMC Evol Biol.* 2008 Feb 29;8:73

Kingma SD, Wagemans T, IJlst L, Bronckers AL, van Kuppevelt TH, Everts V, Wijburg FA, van Vlies N.Altered interaction and distribution of glycosaminoglycans and growth factors in mucopolysaccharidosis type I bone disease. *Bone.* 2016 Jul;88:92-100.

Kirby BB, Takada N, Latimer AJ, Shin J, Carney TJ, Kelsh RN, Appel B. In vivo time-lapse imaging shows dynamic oligodendrocyte progenitor behavior during zebrafish development. *Nat Neurosci.* 2006 Dec;9(12):1506-11.

Korzh S, Pan X, Garcia-Lecea M, Winata CL, Pan X, Wohland T, Korzh V, Gong Z. Requirement of vasculogenesis and blood circulation in late stages of liver growth in zebrafish. *BMC Dev Biol.* 2008 Sep 16;8:84.

Lieschke GJ, Currie PD. Animal models of human disease : zebrafish swim into view. *Nat Rev Genet.* 2007 May;8(5):353-67.

Lin SM, Lin HY, Chuang CK, Lin SP, Chen MR. Cardiovascular abnormalities in Taiwanese patients with mucopolysaccharidosis. *Mol Genet Metab.* 2014 Apr;111(4):493-8.

Lu P, Takai K, Weaver VM, Werb Z. Extracellular Matrix Degradation and Remodeling in Development and Disease. *Cold Spring Harb Perspect Biol.* 2011 Dec 1;3(12).

Lualdi S, Di Rocco M, Corsolini F, Spada M, Bembi B, Cotugno G, Battini R, Stroppiano M, Gabriela Pittis M, Filocamo M. Identification of nine new IDS alleles in mucopolysaccharidosis II . Quantitative evaluation by real-time RT-PCR of mRNAs sensitive to nonsense-mediated and nonstop decay mechanisms. *Biochim Biophys Acta.* 2006 Apr;1762(4):478-84.

Lualdi S, Tappino B, Di Duca M, Dardis A, Anderson CJ, Biassoni R, Thompson PW, Corsolini F, Di Rocco M, Bembi B, Regis S, Cooper DN, Filocamo M. Enigmatic in vivo iduronate-2-sulfatase (IDS) mutant transcript correction to wild-type in Hunter syndrome. *Hum Mutat.* 2010 Apr;31(4):E1261-85.

Mackay EW, Apschner A, Schulte-Merker S. A bone to pick with zebrafish. *Bonekey Rep.* 2013 Nov 13;2:445.

Mandal C, Baek MN, Jung KH, Chai JC, Lee YS, Chai YG. Gene expression profile associated with the reversine-mediated transdifferentiation of NIH-3T3 fibroblast cells into osteoblasts. *BioChip Journal*, *7*(3), 278–287.

Martin R, Beck M, Eng C, Giugliani R, Harmatz P, Muñoz Vand Muenzer J. Recognition and diagnosis of mucopolysaccharidosis II (Hunter Syndrome). *Pediatrics*. 2008; 121:377-386.

McKeehan WL, Wang F, Luo Y. The fibroblast growth factor (FGF) signaling complex. *Handbook of Cell Signaling*, 2nd ed; Volume I, Chapter 38. New York: Academic/Elsevier Press; 2009. pp. 253–259.

Mitchell RE, Huitema LF, Skinner RE, Brunt LH, Severn C, Schulte-Merker S, Hammond CL. New tools for studying osteoarthritis genetics in zebrafish. *Osteoarthritis Cartilage*. 2013 Feb;21(2):269-78.

Molina G,Vogt A, Bakan A,Dai W, Queiroz de Oliveira P, Znosko W, Smithgall TE, Bahar I, Lazo JS, Day BW, Tsang M. Zebrafish chemical screening reveals an inhibitor of Dusp6 that expands cardiac cell lineages. *Nat Chem Biol*. 2009 Sep; 5(9): 680–687.

Moreira da Silva I, Froissart R, Marques dos Santos H, Caseiro C, Maire I, Bozon D. Molecular basis of Mucopolysaccharidosis type II in Portugal : identification of four novel mutations. *Clin Genet.* 2001 Oct;60(4):316-8.

Morini SR, Steiner CE, Gerson LB. Mucopolysaccharidosis type II : skeletal – muscle system involvement. *J Pediatr Orthop B*. 2010 Jul;19(4):313-7.

Moro E, Tomanin R, Friso A, Modena N, Tiso N, Scarpa M, Argenton F. A novel functional role of iduronate-2-sulfatase in zebrafish early development. *Matrix Biology* 2010; *29*(1), 43–50.

Moro E, Ozhan-Kizil G, Mongera A, Beis D, Wierzbicki C, Young RM, Bournele D, Domenichini A, Valdivia LE, Lum L, Chen C, Amatruda JF, Tiso N, Weidinger G, Argenton F. In vivo Wnt signaling tracing through a transgenic biosensor fish reveals novel activity domains. *Dev Biol*. 2012 Jun 15;366(2):327-40.

Moro E, Vettori A, Porazzi P, Schiavone M, Rampazzo E, Casari A, Ek O, Facchinello N, Astone M, Zancan I, Milanetto M, Tiso N, Argenton F. Generation and application of signaling pathway reporter lines in zebrafish. *Mol Genet Genomics*. 2013 Jun;288(5-6):231-42.

Muenzer J. The mucopolysaccharidoses: a heterogeneous group of disorders with variable pediatric presentations. *J Pediatr.* 2004 May;144(5 Suppl):S27-34.

Opoka-Winiarska V, Jurecka A, Emeryk A, Tylki-Szymańska A. Osteoimmunology in mucopolysaccharidoses type I , II , VI and VII . Immunological regulation of the

osteoarticular system in the course of metabolic inflammation. *Osteoarthritis Cartilage.* 2013 Dec;21(12):1813-23.

Ornitz DM, Marie PJ. FGF signaling pathways in endochondral and intramembranous bone development and human genetic disease. *Genes Dev.* 2002 Jun 15;16(12): 1446-65.

Ornitz DM, Marie PJ. Fibroblast growth factor signaling in skeletal development and disease. *Genes Dev.* 2015 Jul 15;29(14):1463-86.

Patel P, Suzuki Y, Maeda M, Yasuda E, Shimada T, Orii KE, Orii T, Tomatsu S. Growth charts for patients with Hunter syndrome. *Mol Genet Metab Rep*. 2014;1:5-18.

Petrey AC, Flanagan-Steet H, Johnson S, Fan X, De la Rosa M, Haskins ME, Nairn AV, Moremen KW, Steet R. Excessive activity of cathepsin K is associated with cartilage defects in a zebrafish model of mucolipidosis II. *Dis Model Mech.* 2012 Mar;5(2):177-90.

Polgreen LE, Thomas W, Fung E, Viskochil D, Stevenson DA, Steinberger J, Orchard P, Whitley CB, Ensrud KE. Low bone mineral content and challenges in interpretation of dual-energy X-ray absorptiometry in children with mucopolysaccharidosis types I, II, and VI. *J Clin Densitom.* 2014 Jan-Mar;17(1):200-6.

Shen G. The role of type X collagen in facilitating and regulating endochondral ossification of articular cartilage. *Orthod Craniofac Res.* 2005 Feb;8(1):11-7.

Schilling TF. Genetic analysis of craniofacial development in the vertebrate embryo. *Bioessays.* 1997 Jun;19(6):459-68.

Settembre C, Fraldi A, Medina DL, Ballabio A. Signals from the lysosome : a control centre for cellular clearance and energy metabolism. *Nat Rev Mol Cell Biol.* 2013 May;14(5):283-96.

Simonaro CM, D'Angelo M, Haskins ME, Schuchman EH.. Joint and Bone Disease in Mucopolysaccharidoses VI and VII : Identification of New Therapeutic Targets and BioMarkers Using Animal Models. *Pediatr Res.* 2005 May;57(5 Pt 1):701-7.

Spoorendonk KM, Peterson-Maduro J, Renn J, Trowe T, Kranenbarg S, Winkler C, Schulte-Merker S. Retinoic acid and Cyp26b1 are critical regulators of osteogenesis in the axial skeleton. *Development*. 2008 Nov;135(22):3765-74.

Su N, Jin M, Chen L. Role of FGF/FGFR signaling in skeletal development and homeostasis: learning from mouse models. *Bone Res.* 2014 Apr 29;2:14003.

Sukegawa-Hayasaka K, Kato Z, Nakamura H, Tomatsu S, Fukao T, Kuwata K, Orii T, Kondo N. Effect of Hunter disease (mucopolysaccharidosis type II) mutations on

molecular phenotypes of iduronate-2-sulfatase : Enzymatic activity , protein processing and structural analysis. *J Inherit Metab Dis.* 2006 Dec;29(6):755-61.

Suzuki T, Sakai D, Osumi N, Wada H, Wakamatsu Y. Sox genes regulate type 2 collagen expression in avian neural crest cells. *Dev Growth Differ.* 2006 Oct;48(8):477-86.

Teven CM, Farina EM, Rivas J, Reid RR. Fibroblast growth factor (FGF) signaling in development and skeletal diseases. *Genes Dis.* 2014 Dec 1;1(2):199-213.

Tomatsu S, Alméciga-Díaz CJ, Montaño AM, Yabe H, Tanaka A, Dung VC, Giugliani R, Kubaski F, Mason RW, Yasuda E, Sawamoto K, Mackenzie W, Suzuki Y, Orii KE, Barrera LA, Sly WS, Orii T. Therapies for the bone in mucopolysaccharidoses. *Mol Genet Metab.* 2015 Feb;114(2):94-109

Tsang KY, Cheung MC, Chan D, Cheah KS. The developmental roles of the extracellular matrix : beyond structure to regulation. *Cell Tissue Res.* 2010 Jan;339(1):93-110.

Tumova S, Woods A, Couchman JR. Heparan sulfate proteoglycans on the cell surface : versatile coordinators of cellular functions. *Int J Biochem Cell Biol.* 2000 Mar;32(3):269-88.

Vafiadaki E, Cooper A, Heptinstall LE, Hatton CE, Thornley M, Wraith JE. Mutation analysis in 57 unrelated patients with MPS II (Hunter ' s disease). *Arch Dis Child.* 1998 Sep;79(3):237-41.

Wraith JE. Lysosomal disorders. *Paediatrics and Child Health*. 2011 Feb; 21(2:) 76–79.

Wraith JE, Scarpa M, Beck M, Bodamer OA, De Meirleir L, Guffon N, Meldgaard Lund A, Malm G, Van der Ploeg AT, Zeman J. Mucopolysaccharidosis type II (Hunter syndrome): a clinical review and recommendations for treatment in the era of enzyme replacement therapy. *Eur J Pediatr.* 2008 Mar;167(3):267-77.

Znosko WA, Yu S, Thomas K, Molina GA, Li C, Tsang W, Dawid IB, Moon AM, Tsang M. Overlapping functions of Pea3 ETS transcription factors in FGF signaling during zebra fi sh development. *Dev Biol.* 2010 Jun 1;342(1):11-25.